

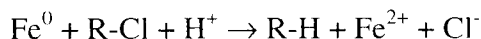
AN ABSTRACT OF THE THESIS OF

Lisa Jean Graham for the degree of Doctor of Philosophy in Chemical Engineering, presented on December 10, 1998. Title: Dechlorination of *p*-Chlorophenol on Bimetallic Pd/Fe Catalyst in a Magnetically Stabilized Fluidized Bed; Experiment and Theory.

Abstract approved: _____
Redacted for privacy
✓ ✓ Goran Jovanovic _____

The implementation of a Pd/Fe catalytic dechlorination reaction for dechlorination of chlorinated aromatic hydrocarbons, in an applied engineering process, effectively treats liquid and sludge type wastes. In this work we a) studied the chemical kinetics of dechlorination of *p*-chlorophenol, a chlorinated aromatic hydrocarbon, on the Pd/Fe catalyst including the characterization of factors governing catalyst preparation, reusability, and deactivation effects and we b) investigated the mass transfer phenomena related to the technological application of the Pd/Fe catalyst for potential remediation of contaminated liquids and sludges within the Magnetically Stabilized Fluidized Bed (MSFB).

The dechlorination process consists of many steps with the following overall reaction:



The pseudo-first order rate with respect to the chlorinated hydrocarbon (*p*-chlorophenol) concentration was found to be the most appropriate kinetic model in a batch reactor.

$$-\frac{d(vC_A)}{dt} = (kW)C_A^a = k^* C_A^a$$

$$-\frac{da}{dt} = k_d a^n$$

To account for the passivation effects on the Pd/Fe surface, an activity term, a , is integrated into the reaction kinetics as shown above. This term accounts for the decrease in catalyst activity caused by the loss of dechlorination sites. This kinetic model was investigated in a laboratory batch system consisting of a 400 [ml] batch reactor. Careful preparation of the catalyst including acid pretreatment of the iron, Fe, and the palladium, Pd, solution concentration for the palladization reaction are deemed important for reproducible reaction kinetics. The presence of O₂, solution pH and surface coverage of Fe⁰ by Pd play an important role in the catalyst activity for the dechlorination reaction.

The normalized reaction rate constant, k [m³/s·kg_{catalyst}], and the deactivation rate constant, k_d [1/s], were obtained over a range of pH (3-6) and catalyst weights for freely suspended Pd/Fe catalyst. The k and k_d values for the catalyst (0.188 [w/w%] Pd/Fe) as a function of pH over the pH range (3-6) are given as follows:

$$k = -0.025 [pH] + 0.161 \quad [\text{m}^3/\text{s} \cdot \text{kg}_{\text{catalyst}}] \quad \text{pH range 3 to 6} \quad R^2 = 0.94$$

$$k_d = 0.091 [H^+] \quad [1/\text{s}] \quad \text{pH range 3 to 6} \quad R^2 = 0.99$$

The relationship describing the reaction rate coefficient, k^* [m³/s], over a range of Pd catalyst weights, W , (Pd/Fe: 2-6 [g]; 0.188 [w/w%] Pd) at pH=5.8 is given as:

$$k^* = 0.0126 [W] \quad [\text{m}^3/\text{s}] \quad R^2 = 0.99 \quad (\text{Pd/Fe: 2-6 [g]; 0.188 [w/w\%] Pd})$$

The deactivation rate constant remains independent of the amount of catalyst at a constant pH and is given as $k_d = 1.8 \times 10^{-4} \pm 2.1 \times 10^{-6}$ [1/s] (pH = 5.8 ± 0.087)

The fluidization particles used in the MSFB are composite ferromagnetic particles which are prepared from a mixture of sodium alginate and the Pd/Fe catalyst powder. The alginate beads (nominal diameter: 2 [mm]) consist of 88% alginate (1.5% algin, 98.5% DI H₂O) and 12% catalyst with 0.188 Pd/Fe [w/w%]. The overall dechlorination process encompasses 5 steps: 1) desorption of chlorinated hydrocarbons from solid particles found in sludges, 2) bulk mixing, 3) convective transport of the chlorinated hydrocarbon to the alginate bead, 4) diffusion through the alginate bead, and 5) reaction and deactivation on the Pd/Fe surface within the alginate bead. Steps 1-3 occur in series and steps 4 and 5 occur in parallel. The system parameters including the diffusion coefficient, D_e , the mass transfer coefficient, k_l , the normalized reaction rate constant, k , and the deactivation rate constant, k_d , are determined from two different experimental approaches. First, the parameters are determined separately from independent, controlled experiments or from existing correlations. These parameters are in very good agreement with those obtained from experimental data in the MSFB. From this data, all four parameters, D_e , k_l , k , and k_d are evaluated with the help of an optimization routine (IMSL).

Dechlorination of *p*-Chlorophenol on Bimetallic Pd/Fe Catalyst in a Magnetically
Stabilized Fluidized Bed; Experiment and Theory

by

Lisa Jean Graham

A Thesis Submitted
to
Oregon State University

In Partial Fulfillment of
the requirements for the
degree of

Doctor of Philosophy

Presented December 10th, 1998
Commencement June 1999

Doctor of Philosophy thesis of Lisa Jean Graham presented December 10, 1998

Approved:

Redacted for privacy

Major Professor, representing Chemical Engineering

Redacted for privacy


Head of Department of Chemical Engineering

Redacted for privacy

Dean of Graduate School

I understand that my thesis will become part of the permanent collection of Oregon State University libraries. My signature below authorizes release of my thesis to any reader upon request.

Redacted for privacy

 Lisa Jean Graham, Author

Acknowledgment

I wish to express my grateful appreciation to my advisor, Dr. Goran Jovanovic, to whom I owe very much in many respects. His excellent instruction during my graduate studies and professional guidance have helped me to begin a successful career. I will miss working with him on the WERC project which provided me with great leadership experience while working with students on many environmental projects.

I must also thank Dr. Ali Hassan for his great patience with me in learning numerical methods and computer programming. He was of great support when I worked to develop my mathematical modeling skills which were crucial for the completion of my thesis.

I would also like to recognize Dr. Shoichi Kimura for his assistance in my modeling efforts as well as his insistence on academic excellence.

I am truly grateful for the unwavering support provided by my family during this challenging time. Special thanks go to my parents, Ron and Lin Clement, as well as my brother, Ron Clement, Jr., for welcoming me into their home to avoid the long commute to Wilsonville. I will miss being with you. To my husband, Jeremy, thank you for being an endless reservoir of help, understanding and love during the ups and downs. For this, my love goes to you.

Contribution of Authors

Dr. Goran Jovanovic was involved in the design, analysis of experimental data, and editing of the manuscript. The experiments were performed in the laboratory of Dr. Goran Jovanovic. Scanning electron microscopy pictures were taken in Dr. Al Soeldner's laboratory.

Table of Contents

1. INTRODUCTION	1
1.1 Introduction	1
1.2 Magnetically Stabilized Fluidized Bed (MSFB) Technology	11
1.3 Thesis Intent	16
2. THEORETICAL DEVELOPMENT	18
2.1 Dechlorination of Chlorinated Hydrocarbons	18
2.1.1 Reaction Stoichiometry	21
2.1.2 Determination of the Rate Equation for Dechlorination Chemical Kinetics on Powder Pd/Fe Catalyst	23
2.2 Modeling Diffusion and Dechlorination of <i>p</i> -Chlorophenol in Alginate Beads With Entrapped Pd/Fe Catalyst	27
2.2.1 Diffusion Through Beads Without Reaction and Without External Mass Transfer Resistance	40
2.2.2 Diffusion Through Beads Without Reaction and With External Mass Transfer Resistance	42
2.2.3 Diffusion Through Beads With Reaction and Without External Mass Transfer Resistance	44
2.3 Modeling <i>p</i> -Chlorophenol Desorption From Contaminated Soil	46
2.4 Modeling of <i>p</i> -Chlorophenol Dechlorination of Contaminated Soil Using Entrapped Pd/Fe Catalyst in Alginate Beads	46
2.5 MSFB Technology	52

Table of Contents, Continued

3. EQUIPMENT, MATERIALS, AND METHODS	60
3.1 Equipment	60
3.1.1 Chemical Kinetic Apparatus	60
3.1.2 Alginate Bead Generator	60
3.1.3 MSFB Apparatus	63
3.2 Materials	63
3.2.1 <i>p</i> -Chlorophenol and Phenol Properties	63
3.2.2 Pd/Fe Catalyst	65
3.2.3 Alginate	67
3.2.4 Soil Properties/Contaminant Interaction	67
3.3 Methods for Dechlorination	68
3.3.1 Pd/Fe Catalyst Preparation	68
3.3.2 Repeatability and Reusability of Pd/Fe Catalyst	77
3.3.3 Pd/Fe Entrapment/ Particle Design Flexibility	80
3.3.4 Determination of <i>p</i> -Chlorophenol and Phenol Concentrations	81
3.3.5 Absorption of <i>p</i> -Chlorophenol to Alginate Beads	82
3.3.6 Soil Adsorption and Desorption of <i>p</i> -Chlorophenol	83
3.3.7 <i>p</i> -Chlorophenol Dechlorination Experimental Procedure for Freely Suspended Pd/Fe Catalyst	88
3.3.8 Diffusion Coefficient of <i>p</i> -Chlorophenol into Alginate	88
3.3.9 <i>p</i> -Chlorophenol Dechlorination Experimental Procedure for Alginate Entrapped Pd/Fe Catalyst	91

Table of Contents, Continued

4. EXPERIMENTAL RESULTS	92
4.1 Aqueous Solution Dechlorination of <i>p</i> -Chlorophenol on Powdered Catalyst	92
4.1.1 Overall Mass Balance in the Dechlorination Reaction System	92
4.1.2 Formation of $\text{Fe}(\text{OH})_2$ and $\text{Fe}(\text{OH})_3$	94
4.1.3 Acidic Conditions With Varied Mixer Speed	98
4.1.4 Dechlorination of <i>p</i> -Chlorophenol at Various pH	99
4.1.5 Dechlorination With Varied Amounts of Pd/Fe Catalyst	100
4.2 Aqueous Solution Dechlorination of <i>p</i> -Chlorophenol on Alginate Entrapped Catalyst	102
4.3 Soil/Liquid Solution Dechlorination of <i>p</i> -Chlorophenol on Alginate Entrapped Catalyst	107
5. DATA INTERPRETATION AND MODELING	109
5.1 Results of <i>p</i> -Chlorophenol Dechlorination on Powdered Catalyst	109
5.2 Determination of the Diffusion Coefficient, D_e , in Alginate Beads	115
5.3 Results of <i>p</i> -Chlorophenol Dechlorination on Alginate Entrapped Pd/Fe Catalyst	116
5.4 Results of <i>p</i> -Chlorophenol Dechlorination on Alginate Entrapped Catalyst in Soil/Liquid System	120

Table of Contents, Continued

6. CONCLUSIONS AND RECOMMENDATIONS	122
6.1 Conclusion	122
6.2 Recommendations	125
REFERENCES	126
APPENDICES	132

List of Figures

<u>Figure</u>	<u>Page</u>
1.1 Magnetically Stabilized Fluidized Bed schematic (MSFB).	13
1.2 Particle fluidization with and without an applied gradient magnetic field.	15
2.1 Illustration of multistep dechlorination reaction on the Pd/Fe catalyst surface.	25
2.2 Iron hydroxide and/or H ₂ (g) bubble formation on the Pd/Fe catalyst surface.	26
2.3 Model 1 schematic: Plug Flow (PF).	28
2.4 Model 2 schematic: Continuously Stirred Tank Reactor (CSTR).	31
2.5 Mass balance on the dechlorination system for scenario 4.	37
2.6 Comparison of the CSTR and PF models.	39
2.7 Mass balance on the dechlorination system for scenario 1.	40
2.8 Mass balance on the dechlorination system for scenario 2.	42
2.9 Mass balance on the dechlorination system for scenario 3.	44
2.10 SEM pictures of Willamette Valley type soil (54-104 [μm]) a) 1000x soil particle, b) 3000x rough surface, c) 3000x smooth surface, d) 30,000x showing negligible porosity.	49
2.11 Overall mechanism for dechlorination of <i>p</i> -chlorophenol from soil particles.	51
2.12 Effect of the magnetic field on fluidized particles within the MSFB.	54
2.13 Enhancement of the mass transfer coefficient, k_t , in the MSFB (Al-Mulhim, 1995).	55
2.14 Effect of magnetic field strength on bed voidage.	57

List of Figures, Continued

<u>Figure</u>	<u>Page</u>
3.1 Chemical kinetic apparatus.	61
3.2 Alginate bead generator.	62
3.3 MSFB lab apparatus.	64
3.4 Scanning electron microscopy pictures: a) Acid pretreated Fe particles, b) Palladized Fe particles.	66
3.5 Addition of H^+ ions to maintain pH as a result of iron dissolution.	70
3.6 H^+ consumption on the Pd/Fe surface as a function of Pd/Fe catalyst available for reaction.	70
3.7 Effect of the acid strength during Fe pretreatment on <i>p</i> -chlorophenol dechlorination.	71
3.8 Effect of palladium concentration during catalyst preparation on reaction rate.	72
3.9 SEM pictures of Pd/Fe catalyst with: a) high palladium solution concentration, b) low palladium solution concentration.	74
3.10 Varied surface coverage of iron by palladium (Pd/Fe [w/w%]) a) 0.048 [w/w%], b) 0.188 [w/w%], c) 0.67 [w/w%], d) 0.75 [w/w%]	75
3.11 Repeatability of Pd/Fe catalyst preparation for <i>p</i> -chlorophenol dechlorination.	77
3.12 Reusability of Pd/Fe catalyst with loss from iron dissolution reaction.	78
3.13 SEM pictures of the Pd/Fe catalyst showing extent of recoverability a) Freshly prepared Pd/Fe b) Reacted Pd/Fe.	79

List of Figures, Continued

<u>Figure</u>	<u>Page</u>
3.14 <i>p</i> -Chlorophenol absorption isotherm on alginate beads.	83
3.15 Adsorption isotherm for <i>p</i> -chlorophenol onto Willamette Valley type soil.	85
3.16 Desorption of <i>p</i> -chlorophenol from Willamette Valley type soil.	87
3.17 Diffusion of <i>p</i> -chlorophenol through alginate beads with varied polymerization times (Nominal bead size: 2 [mm]).	90
4.1 a) Volatilization check on phenol, b) Volatilization check on <i>p</i> -chlorophenol.	93
4.2 Overall mass balance on the dechlorination reaction.	94
4.3 pH change during dechlorination reaction under oxygenated conditions.	96
4.4. Development of a hydroxide layer on the Pd/Fe catalyst a) Freshly prepared Pd/Fe, b) Pd/Fe surface with hydroxide layer.	97
4.5 Dechlorination of <i>p</i> -chlorophenol under varied mixing conditions.	98
4.6 Effect of pH on dechlorination of <i>p</i> -chlorophenol.	100
4.7 Effect of Pd/Fe to chlorine ratio on overall rate of dechlorination.	101
4.8 Dechlorination of <i>p</i> -chlorophenol with alginate entrapped Pd/Fe catalyst.	103
4.9 Entrapped Pd/Fe <i>p</i> -chlorophenol dechlorination without an applied field.	104
4.10 Entrapped Pd/Fe <i>p</i> -chlorophenol dechlorination with an applied field.	105
4.11 Comparison of dechlorination rates with the MSFB enhancement.	106
4.12 Dechlorination of contaminated soil in the MSFB.	108

List of Figures, Continued

<u>Figure</u>	<u>Page</u>
5.1 Dechlorination of <i>p</i> -chlorophenol at pH=3.8 with an optimized model.	110
5.2 Dechlorination of <i>p</i> -chlorophenol at pH=4.5 with an optimized model.	111
5.3 Dechlorination of <i>p</i> -chlorophenol at pH=5.8 with an optimized model.	111
5.4 a) Effect of pH on the normalized reaction rate constant, k [$\text{m}^3/\text{s}\cdot\text{kg}_{\text{catalyst}}$]. b) Effect of $[\text{H}^+]$ on the deactivation rate constant, k_d [$1/\text{s}$].	112
5.5 Loss of catalyst activity with time over the pH range.	113
5.6 Reaction rate constant, k^* , as a function of catalyst weight at $\text{pH}=5.8\pm0.087$.	114
5.7 Determination of the deactivation rate constant, k_d , as a function of catalyst weight.	114
5.8 Determination of the effective diffusion coefficient, D_e , for <i>p</i> -chlorophenol into alginate beads (Nominal size: $d_p=2$ [mm]).	116
5.9 Applied dechlorination model for dechlorination within Pd/Fe entrapped alginate beads with catalyst passivation.	118
5.10 Applied soil <i>p</i> -chlorophenol dechlorination model for alginate entrapped Pd/Fe catalyst.	121

List of Tables

<u>Table</u>	<u>Page</u>
1.1 Technological Overview for Organic Contaminant Removal	5
1.2 Literature Review of Experimental Investigations	8
3.1 Chemical Properties of <i>p</i> -Chlorophenol and Phenol	65
3.2 Particle Characteristics	81
5.1 Comparison of Values Without an Applied Field	119
5.2 Comparison of Values for an Applied Field	119
5.3 Soil Dechlorination with Applied Model Parameters	120

List of Appendices

<u>Appendix</u>	<u>Page</u>
A. Supplemental information for the dechlorination investigations	134
B. Analytical development for Model 1 and Model 2	143
C. HPLC analysis: Standard curves for phenol and <i>p</i> -chlorophenol	150
D. Alginate bead production procedure	152
E. Determination of organic carbon fraction, f_{oc} , of Willamette Valley type soil	154
F. Determination of the K_{ow} and K_{om} values for K_d determination	156
G. MSFB flowrate calibration and field gradient	157
H. Calculation of <i>p</i> -chlorophenol aqueous diffusivity	160
I. Numerical solution for the partial differential equation for dechlorination of <i>p</i> -chlorophenol on alginate bead entrapped Pd/Fe catalyst	162
J. FORTRAN/IMSL: Reaction/ deactivation rate kinetics; k_r and k_d	164
K. FORTRAN/IMSL routine to determine D_e , k_r and k_d and k_{la}	165
L. Concentration in a solid-fluid network/ mixture	166

List of Appendix Figures

<u>Figure</u>	<u>Page</u>
C.1 Standard curve for HPLC analysis of phenol concentrations.	150
C.2 Standard curve for HPLC analysis for <i>p</i> -chlorophenol concentration.	151
C.3 Chromatograph of phenol and <i>p</i> -chlorophenol peaks.	151
G.1 Calibration curve for MSFB flowrate over full pumping range.	158
G.2 Linear portion of calibration curve for flowrate determination in the MSFB.	158
G.3 MSFB applied magnetic field gradient.	159

List of Appendix Tables

<u>Table</u>	<u>Page</u>
D.1 Alginate and Pd/Fe Properties	152
E.1 Calibration of Dohrmann DC-80 Total Carbon Analyzer	154
E.2 Raw Data From Dohrmann DC-80 Total Carbon Analyzer	155
E.3 Calculated Total Organic Carbon Fractions	155
G.1 MSFB Flowrate Data	157
H.1 Estimated D_{AB} Values for <i>p</i> -Chlorophenol	161

Nomenclature

A	Cross-sectional area of the reactor, m
a	Catalyst activity [-]
a'	External bead surface area/unit bulk liquid volume, m^2/m^3
C_A	Concentration of <i>p</i> -chlorophenol, mol/m^3
$C_{A,0}$	Initial concentration of <i>p</i> -chlorophenol, mol/m^3
C_b	Bulk concentration, mol/m^3
$C_{b,0}$	Initial bulk concentration, mol/m^3
C_b'	Bulk concentration inside plug flow reactor, mol/m^3
$C_{b,e}$	Equilibrium bulk concentration, mol/m^3
C_l	Alginate bead liquid concentration, mol/m^3
C_H	Concentration of H^+ in solution, mol/m^3
C_{H^*}	Concentration of H^* in solution (reactive intermediate), mol/m^3
C_s	Concentration of <i>p</i> -chlorophenol on Willamette Valley type soil, mol/kg soil
D_{AB}	Diffusivity of a solute, A, in water, B, m^2/s
D_e	Diffusion coefficient for <i>p</i> -chlorophenol in alginate beads, m^2/s
d_p	Diameter of alginate bead, m
d_c	Diameter of catalyst particle, μm
F	Liquid flowrate, m^3/s
F_b	Bouyancy force exerted on the particle, N
F_d	Drag force exerted on the particle, N

Nomenclature, Continued

F_g	Gravitational force exerted on the particle, N
f_{oc}	Fraction of organic carbon, [-]
f_{om}	Fraction of organic matter, [-]
$[H^+]$	Concentration of hydrogen ions in solution, moles/m ³
H	Magnetic field intensity, A/m
H_0	Characteristic field strength, A/m
k_l	Liquid-solid mass transfer coefficient in MSFB ($H \neq 0$), m/s
$k_{l,0}$	Liquid-solid mass transfer coefficient in conventional bed ($H=0$), m/s
$K_{d,s}$	Solid water distribution ratio, moles/kg soil/ (moles/m ³ bulk liquid)
$k_{l,s}$	Mass transfer coefficient from soil particles to bulk liquid, m/s
k	Reaction rate coefficient for <i>p</i> -chlorophenol dechlorination, m ³ /kg _{catalyst} s
k_r	Reaction rate coefficient for <i>p</i> -chlorophenol dechlorination, 1/s
k'	Reaction rate coefficient for <i>p</i> -chlorophenol dechlorination, m ⁶ /mol·kg _{catalyst} s
k^*	Reaction rate coefficient for <i>p</i> -chlorophenol dechlorination, m ³ /s
k_d	Deactivation rate coefficient for H ₂ (g) passivation, 1/s
k_{ds}	Mass transfer coefficient for <i>p</i> -chlorophenol desorption from soil, 1/s
K_d	Solid-water distribution ratio, mol/kg soil/ (mol/ L H ₂ O)
K_b	Gel solid-water distribution ratio, mol/kg bead/(mol/L H ₂ O)
K_{om}	Organic matter- water distribution ratio, kg/kg organic matter/ (kg/ L H ₂ O)

Nomenclature, Continued

K_{ow}	Octanol-water distribution ratio, kg/L Octanol/ (kg/ L H ₂ O)
m	$(\Delta\epsilon/\Delta H)$; Change of bed voidage with magnetic field intensity, m/A
n'	Solenoid turns, turns/m
n	Deactivation order
r	Bead radius, mm
Re	Reynolds number, [-]
Sc	Schmidt number, [-]
Sh	Sherwood number, [-]
t	Time, s
u_o	Liquid superficial velocity, m/s
u_{int}	Liquid interstitial velocity, m/s
V	Volume of reactor liquid, m ³
V_0	Initial volume of reactor liquid, m ³
v	Rate of volume addition of acid, m ³ /min
W	Weight of catalyst Pd, g
x_{wt}	Mass fraction of ferromagnetic powder in beads, [-]

Nomenclature, Continued

Greek symbols

α Constant

ε Reactor voidage in magnetically stabilized fluidized bed ($H \neq 0$), [-]

ε_0 Reactor voidage in conventional fluidized bed ($H=0$), [-]

ε_m Average bed voidage in the stabilized regime, [-]

ε_p Average bed voidage in the random motion regime, [-]

ΔP Pressure drop across the fluidized bed, Pa

μ_l Liquid viscosity, Pa-s

ν_l Liquid kinematic viscosity, m^2/s

ρ_l Liquid density, kg/m^3

ϕ Fraction of gel solid within the alginate bead

Dechlorination of p-Chlorophenol on Bimetallic Pd/Fe Catalyst in a Magnetically Stabilized Fluidized Bed; Experiment and Theory

CHAPTER 1 INTRODUCTION

Never doubt that a small group of thoughtful, committed citizens can change the world; indeed it is the only thing that ever has.

--Margaret Mead, Anthropologist

1.1 Introduction

The rate at which we are increasing pollution is still much greater than the rate of recovery. Our world today is overwhelmed with the responsibility of cleaning up the polluted waters and soils of the past while preventing further pollution and environmental deterioration. Due to the complete disregard for subsurface cleanliness from the "out of sight, out of mind" concept, we are facing contaminated sites having a conglomeration of organic compounds, metals and radionuclides. Chlorinated organics in the form of pesticides, pharmaceuticals, solvents and dielectric fluids have been released from industrial, commercial and agricultural sources only to be persistent in the soils we build our houses upon and in the waters from which we drink. From a global perspective, the remediation of these sites is essential not only for the current human population but also for the health and safety of future generations. Our planet is facing a growing population which is pushing the boundaries of civilization to new limits. As a result, we must take care of the land upon which future generations will be forced to build their houses and grow their food. According to the article published in *Chemistry and Industry* (Kovalick,

Jr., 1995), major public and private resources are being committed in an integrated effort to begin restoring the contaminated environment. Government efforts include the creation of environmental laws such as the Comprehensive Environmental Resource and Conservation Liability Act (CERCLA), or Superfund, and the Resource Conservation and Recovery Act (RCRA). These are aimed towards remediating industrial sites as well as elimination of all tanks storing toxic chemicals and highly polluted media.

Besides addressing current waste issues, we must begin the transformation into a functioning sustainable society which integrates all human activity into the cycles of nature so that resources can be continually reused within society or nature. As originally developed by the Swedish organization Det naturliga steget /The Natural Step and published by the Natural Step Newsletter, the "four system conditions" to classify a behavior as being a sustainable activity are:

1. "Substances from the earth's crust must not be systematically increased in nature."
2. "Substances produced by society must not systematically increase in nature."
3. "The physical basis for the productivity and diversity of nature must not be systematically diminished."
4. "We must be fair and efficient in meeting basic human needs."

From a chemical engineering perspective, our knowledge of chemical reactions, mass and energy balances, and overall design principles, gives us the ability to actively work to clean up the environment as well as to incorporate the necessity of sustaining the ecology while maintaining a strong economy. The application of our knowledge and

understanding can effectively be used to develop state of the art technologies to begin to clean up the waste left by our predecessors. Accepting the "four system conditions" of nature and developing innovative methods that will change current technologies and chemical processes is essential for restoring the environment.

There are many technologies currently being evaluated for effective remediation of chlorinated organics in liquids, soils, or sludges including bioreremediation, soil vapor extraction, activated carbon sorption, vitrification, and catalytic processes. The use of bioremediation for removing chlorinated contaminants from soil or sludges is one possible process being investigated. However, while this method has advantages of in-situ performance and use of indigenous organisms, high contaminant concentration can be lethal to the organisms and a change from anaerobic to aerobic conditions may be necessary to completely dechlorinate compounds (Klasson *et. al*, 1996). A final concern lies in long bioremediation times usually necessary to reach required concentration levels (Klasson *et. al*, 1996). However, this method is often the only viable way of dealing with the problem.

Another remediation technique used is soil vapor extraction (SVE) which takes advantage of the relatively high vapor pressures of the organic compounds for their separation from polluted media (McCann *et. al*, 1994). However, any application such as soil vapor extraction, which removes the chlorinated organics from soil, must still address the issue of destroying these substances. A soil vapor extraction approach coupled with activated carbon for the off gas only changes the media to which the chlorinated

compound is attached. The possibility of incineration of the activated carbon for regeneration is limited due to formation of toxic dioxins during the process (Williams, 1990). Polychlorinated dibenzo-p dioxins, or dioxins (PCDD), and polychlorinated dibenzofurans, or furans (PCDF), are found as combustion products which are highly toxic to humans at trace levels (ppt) (Williams, 1990). Incinerator plants in 6 countries of the world, including the United States, Germany, Canada, Sweden, the Netherlands, and Belgium, have emissions ranging from 500 [ng/m³] to over 10,000 [ng/m³] of dioxins depending upon the age and care of the facility (Williams, 1990). Knowledge of health risks and the emission levels should result in an effort to find an improved method of converting chlorinated compounds to non-halogenated compounds prior to incineration.

To avoid dealing with the issue of chlorinated compound destruction in mixed waste, some technologies like vitrification are used to reduce contaminated soil volume but leave a solid mass which must eventually be dealt with. Table 1.1 is a concise summary of potential technologies and their advantages and disadvantages which must be considered before choosing a specific remediation approach. Emerging new technologies are required to be integrated with present solutions while being more efficient. These include the integration of several functions which include the introduction of new operating principles and flexibility in capacity and applications while remaining economically feasible.

Table 1.1: Technological Overview for Organic Contaminant Removal

Technology	Media	Advantages	Disadvantages	Reference
Vitrification	Soil	<ul style="list-style-type: none"> • Addresses mixed waste sites; • High reduction in soil volume; 	<ul style="list-style-type: none"> • Must address final disposal issue; • Land may not be usable; 	Caruana, 1996
Soil Vapor Extraction	Soil	<ul style="list-style-type: none"> • Works well with relatively high vapor pressure compounds; • In-Situ or ex-situ application; 	<ul style="list-style-type: none"> • Must address final disposal issue; • Low vapor pressure compounds challenging; 	McCann <i>et. al.</i> , 1994
Activated Carbon Sorption	Liquid	<ul style="list-style-type: none"> • High adsorption capacity for chlorinated and non-chlorinated organics; • Excellent trace concentration removal; 	<ul style="list-style-type: none"> • Must address final disposal issue; • Regeneration by incineration a potential hazard for dioxin formation; 	Raghaven <i>et. al.</i> , 1996
Biological Remediation	Soil Sludge	<ul style="list-style-type: none"> • In-Situ or ex-situ application; • Use of indigenous organisms; 	<ul style="list-style-type: none"> • Complete dechlorination may require both aerobic and anaerobic conditions; • Possible toxicity from high contaminant concentration; • Long degradation times; 	Klasson <i>et. al.</i> , 1996
Catalytic Dechlorination	Liquid Soil Sludge	<ul style="list-style-type: none"> • Completely dechlorinates a variety of aromatic and straight-chain compounds; • Fast dechlorination rates for both high and low initial contaminant conc.; 	<ul style="list-style-type: none"> • Must address lifetime of catalyst and cost; • Deactivation effects present; 	Muftikian <i>et. al.</i> , 1995 Sivavec <i>et. al.</i> , 1997
Soil Washing	Soil	<ul style="list-style-type: none"> • Hydrophilic organics readily removed; • Removes a wide variety of compounds; 	<ul style="list-style-type: none"> • Highly hydrophobic compounds may require a surfactant; • Must address final disposal issue of secondary waste stream; 	Gombert, 1995
Thermal Desorption	Soil	<ul style="list-style-type: none"> • In-situ application; • Works well with volatile and semi-volatile compounds; • Applicable to a variety of soils including low permeability clays and of heterogeneous nature; 	<ul style="list-style-type: none"> • Must address final disposal issue; • Slow desorption from recalcitrant fraction; 	Vinegar, 1998 Uzgiris <i>et. al.</i> , 1995

A new possibility for removal of chlorinated organics which would address these issues includes the catalytic destruction of the chlorine constituents. This would ultimately result in non-halogenated organics which could easily adsorbed by activated carbon for direct incineration without the potential hazards of dioxin formation (Raghaven *et. al*, 1996). Investigation into the chemical kinetics for dechlorination has focused on two catalyst types; zero valent iron alone, Fe^0 , (Matheson and Tratnyek, 1994) or palladized substrates, Pd/Fe, Pd/Ni or Pd/Carbon (Muftikian, *et. al*, 1995; Sivavec, *et. al*, 1997; Johnson, *et. al*, 1996; Cheng *et. al*, 1997).

As evident from the literature over the past 3-5 years, limitations on dechlorination by Fe^0 has changed the focus to a variety of palladized substrates for complete dechlorination of conjugated straight chain and aromatic compounds (Muftikian *et. al*, 1995; Wang and Zhang, 1997; Johnson *et. al*, 1996; Graham and Jovanovic, 1997). However, comparison of the rates of dechlorination is challenging as the laboratory conditions have differed between investigators. An important factor has been the inconsistency in the actual properties of the catalyst. As a heterogeneous reaction, surface area is usually an important parameter (Gillham and O' Hannelsin, 1994; Grittini *et. al*, 1995; Boronina *et. al*, 1995). The catalysts utilized range from nano-size particles to iron filings and even include the use of iron wire or palladized electrodes. Further, the chlorinated compounds studied, their relative concentrations and percentage of Pd palladized on the Fe surface and the reaction vessel have widely varied. Further, in depth modeling efforts have not been applied to the kinetics of dechlorination. Also, the effects

by parameters such as oxide layers and pH on the kinetics have not been explored. Further, no engineering approach to utilize catalytic destruction of the chlorine constituents on organic contaminants besides "the underground iron barrier" has been envisioned or applied.

Table 1.2 gives an overview of investigations into dechlorination of chlorinated organics while Appendix A gives more detailed information for each study.

Dechlorination of these toxic compounds would be justifiable on the grounds for both steps 2 and 3 of the "four system conditions". These synthetic compounds were created by man and thus their presence in the environment is systematically increased and must be removed and their inherent toxicity interferes with the natural element of productivity and diversity.

Table 1.2: Literature Review of Experimental Investigations

Compounds Treated	Resulting Products	Catalyst Properties	Reactor Properties	Reference
Carbon tetrachloride Chloroform, dichloromethane	Methylene chloride	Fe 100 mesh Fe, degreased iron filings, iron turnings; 3% HCl pretreated (1 hr)	Batch system $C_0=100-800 \mu\text{M}$	Matheson and Tratnyek, 1994
Lindane, chloroform 1,1,1-trichloroethane Trichloroethylene Chlorobenzene	Benzene, methane methylene chloride trichloroethylene chlorobenzene	Fe, Al, Zn, Mg 0.2-0.4 mm particles Fe/Cu, Al/Cu, Mg/Cu	Packed bed, $C_0=8-14 \mu\text{M}$ Deoxygenated solution pH=5.0, Buffer	Schlimm and Heitz, 1996
Carbon tetrachloride, Methylene chloride	Chloroform Dichloromethane Methane CO_2	Sn Cryo particles: 2000 Angstroms SA= $30 \text{ m}^2/\text{g}$ Granular: SA= $<1 \text{ m}^2/\text{g}$ Zn Cryo particles: 450 Angstroms SA= $60 \text{ m}^2/\text{g}$ Dust: SA $<1 \text{ m}^2/\text{g}$ Mg Ribbon	Batch system $C_0=10 \mu\text{M}$, $T=25^\circ\text{C}$ Deoxygenated solution Argon atmosphere	Boronina <i>et. al</i> , 1995
14 different chlorinated methanes, ethanes, ethenes	Dichloromethane	Fe 100 mesh Fe and ground iron pyrite SA= $0.287 \text{ m}^2/\text{g}$	Batch system: Mixer: 2 rpm Packed bed $C_0=700-3600 \mu\text{g/L}$	Gillham and O-Hannesin, 1994
Trans and cis- DCE Vinyl chloride	Vinyl chloride, ethane, acetylene ethylene	Fe 40 mesh: SA= $0.7 \text{ m}^2/\text{g}$ Zn 30 mesh: SA= $0.035 \text{ m}^2/\text{g}$	Batch system; $C_0=200 \mu\text{M}$ Mixer: 4-30 rpm	Roberts <i>et. al</i> , 1996
Trichloroethylene	Ethene, ethane, dichloroethene, vinyl chloride	Fe 100 mesh	Packed bed, $C_0=1.3-6 \text{ ppm}$	Orth and Gillham, 1995

C_0 = Initial Concentration SA: Surface area

DCB- 2,2'-dichlorobiphenyl TCB-2,5,2'-Trichlorobiphenyl and 2,3,2' Trichlorobiphenyl

DCE- Dichloroethylene

DSS-Dihexyl sulfosuccinate surfactant

Table 1.2: (continued)

Compounds Treated	Resulting Products	Catalyst Properties	Reactor Properties	Reference
Carbon tetrachloride	Chloroform	Fe 100 mesh electrolytic power Granular: SA= 0.005-0.038 m ² /g Turnings: SA= 0.9-1.0 m ² /g	Batch system: Mixer: 36 rpm	Johnson <i>et. al</i> , 1996
Carbon tetrachloride	Chloroform	Fe Rotating iron disk electrode SA= 0.071 cm ² Turnings: 20-32 mesh SA= 0.019 m ² /g	Batch, Mixer: 3000 rpm pH=8.4 with buffer C ₀ = 85μM Mixer: 30 rpm Deoxygenated solution T=4-45 °C	Scherer <i>et. al</i> , 1997
Trichloroethylene, 1,1-dichloroethylene 1,2-dichloroethylene Carbon tetrachloride Chloroform, Dichloromethane	Ethane, butane, hexane (10μm Pd/Fe) Methane (Pd/Fe)	Fe Iron filings, 10 μm iron particles, 40 mesh iron filings; 6M HCl pretreated Pd/Fe 0.0375-0.05 w% Pd/Fe	Batch system, C ₀ =20 ppm	Muftikian <i>et. al</i> , 1995
Trichloroethylene	Ethane, cis-DCE Vinyl chloride	Pd/Ni -8+50 mesh granular iron filings 0.50 mol % relative to Fe ⁰	Packed bed, C ₀ =2.1-3.3 ppm	Sivavec <i>et. al</i> , 1997
Trichloroethylene	Vinyl chloride Ethane	Fe 40 mesh Fe filings Pd/Fe 0.05 wt% Pd; 40 mesh Fe filings	Batch system/Packed bed C ₀ =2 ppm 2% DSS, 2% ethanol, isopropanol cosolvents	Gu <i>et. al</i> , 1997
2,3,2',5'-tetrachlorobiphenyl	DCB, TCB, Biphenyl	Pd/Fe 0.1 wt% Pd; 100-200 mesh Fe filings	Batch system/Packed bed C ₀ =1.2 ppm 2% DSS, 2% ethanol, isopropanol cosolvents	Gu <i>et. al</i> , 1997

C₀ = Initial Concentration SA: Surface area

DCB- 2,2'-dichlorobiphenyl TCB-2,5,2'-Trichlorobiphenyl and 2,3,2' Trichlorobiphenyl

DSS-Dihexyl sulfosuccinate surfactant

DCE- Dichloroethylene

Table 1.2: (continued)

Compounds Treated	Resulting Products	Catalyst Properties	Reactor Properties	Reference
4-Chlorophenol	Phenol	Pd/Carbon cloth; Pd/Graphite electrode Pd/2 mm Fe wire; Pt/Carbon cloth	Batch system	Cheng <i>et. al</i> , 1997
2,3-Dichlorophenol	Phenol	Pd/Fe 0.2 wt% Pd; < 40 mesh Fe	Batch system, C ₀ =0.08mM Mixer: 40 rpm	Agrawal, 1997
Trichloroethylene PCB: Aroclor 1254	Aroclor 1254 Biphenyl	Fe 10 μ m SA= 0.9 m ² /g Nano Fe 1-100 nm SA=33.5 m ² /g Pd/Fe Nano Pd/Fe	Batch system Rotary shaker: 30 rpm C ₀ =20 ppm (TCE) C ₀ =200 μ g/L (PCB) Ethanol cosolvent T= 22 \pm 1.0 °C	Wang and Zhang, 1997
PCBs: Aroclor 1254 Aroclor 1260	Biphenyl	Pd/Fe 10 μ m SA= 0.9 m ² /g	Batch system, C ₀ =20 ppm Wrist shaker Methanol, acetone cosolvents Ambient temperature	Grittini <i>et. al</i> , 1995
PCB: Aroclor 1260	Aroclor 1260	Fe 10 μ m SA= 0.9 m ² /g		
PCBs: Aroclor 1221 Aroclor 1254	Biphenyl (T >400°C)	Fe 100 mesh electrolytic power, 95.63%	Batch system, C ₀ =0.56 mg/ml Temperature: 200-600 °C	Chuang <i>et. al</i> , 1995

C₀ = Initial Concentration SA: Surface area

DCB- 2,2'-dichlorobiphenyl TCB-2,5,2'-Trichlorobiphenyl and 2,3,2' Trichlorobiphenyl

DSS-Dihexyl sulfosuccinate surfactant

DCE- Dichloroethylene

1.2 Magnetically Stabilized Fluidized Bed (MSFB) Technology

Magnetically Stabilized Fluidized Beds (MSFBs) have found many applications including bubble suppression in gas fluidization (Rosensweig, 1979) and solids filtration through layers of ferromagnetic particles (Kwauk *et. al*, 1992). Specifically, liquid-solid MSFBs have been applied in new wastewater treatment processes, chromatography techniques, and high rate chemical and biochemical processes (Terranova and Burns, 1991; Burns and Graves, 1985; Sada *et. al*, 1981). The Magnetically Stabilized Fluidized Bed (MSFB) is an innovative combination of the best characteristics of fluidized and packed beds necessary for future technologies to effectively treat liquid and sludge type wastes contaminated by chlorinated organics. Fixed bed reactors typically require excess catalyst to lengthen batch time before regeneration of bed solids is required (Rosensweig, 1995). Further, fixed beds tend to become difficult to operate due to high pressure drop as small bead sizes are approached when one desires greater efficiency from increased surface area. To eliminate clogging, a fluidized bed can be used but lower mass transfer is a negative effect. As a new unit operation, the MSFB combines the excellent efficiency of the fixed bed including mass transfer between fluid and solid particles with the best characteristics of the fluidized bed, like low pressure drop and the ability to handle particulates without clogging due to sediment buildup. Table 1.3 compares the operating characteristics of a packed bed, fluidized bed, and the MSFB. The enhanced mass transfer efficiency gives the MSFB a distinct advantage while having good particle design flexibility. Particle design flexibility involves the capacity to entrap a variety of active substances such as activated carbon, crystalline silico titanate (CST), biomaterial,

reactive catalysts and ion exchange resins (Graham and Jovanovic, 1996). For the objectives of this study, it is particularly important to consider entrapment of the Pd/Fe catalyst as described in Chapters 2 and 3.

Table 1.3: MSFB, Packed bed, and Fluidized Bed Performance Characteristics

	MSFB	Packed Bed	Fluidized Bed
Surface to volume ratio	+	-	+
Continuous operation	+	-	+
ΔP , pressure drop	+	-	+
Reaction efficiency	+	+	-
Ability to process sludges	+	-	+
Mass transfer efficiency	+	+	-
Particle design flexibility	+	+	+

The implementation of a Pd/Fe catalytic dechlorination reaction for dechlorination of organic compounds in an applied engineering process requires development and testing of a robust reactor. For treating solid laden streams, the MSFB provides two possible modes of operation. The first is to mobilize and extract reactants from the sludge type system and then treat the extracted liquid within the fluidized bed. The liquid is typically recycled to the extracting unit until the concentration in the sludge reaches a permissible level (Figure 1.1).

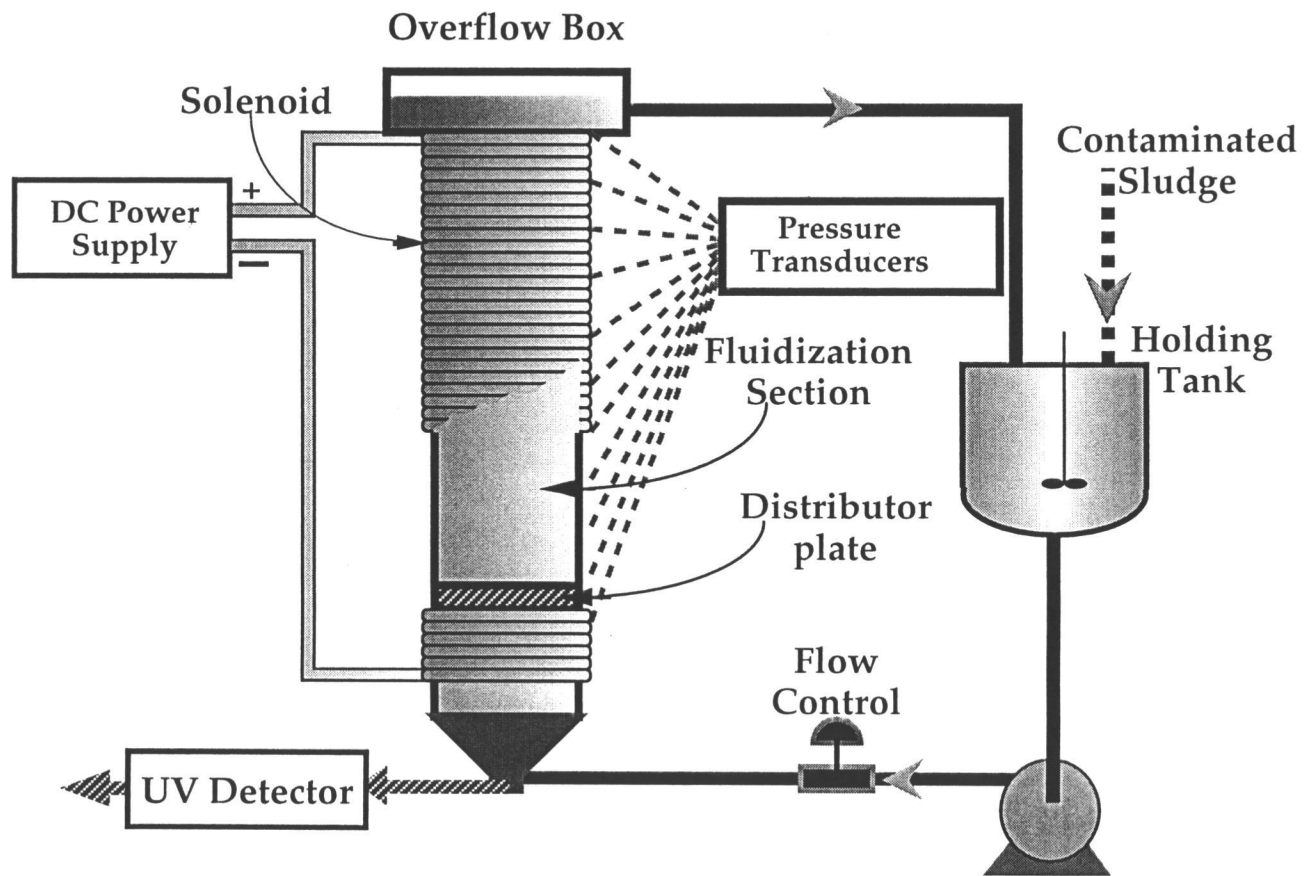
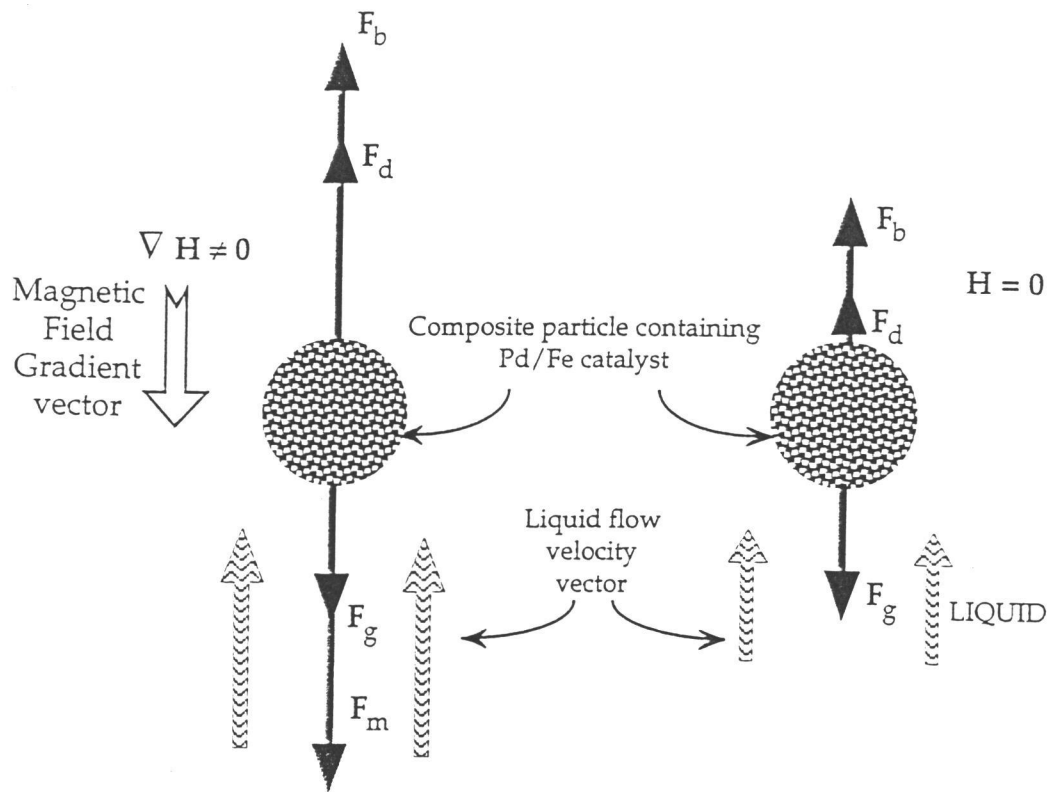


Figure 1.1: Magnetically Stabilized Fluidized Bed schematic (MSFB).

The second method of treatment involves direct pumping of particle laden streams through the MSFB. The use of the magnetic field in a system containing beads susceptible to the applied field offers the advantage of maintaining the active beads within the fluidized bed while the slurry is processed. Further, the transfer of the chlorinated compound from the bulk of the slurry to the active bead for dechlorination is substantially enhanced (Al-Mulhim, 1995; Jovanovic and Al-Mulhim, 1995; Rhee, 1998).

Mass transfer of the chlorinated aromatic compounds from the sludge to the bead's surface and subsequent diffusion through the alginate beads are limiting factors as the chemical reaction in itself is fast. The MSFB greatly enhances the convective mass transfer by allowing higher relative velocity between liquid or sludge and beads than is otherwise achieved in an ordinary fluidized bed.

Mass transfer is enhanced simply through the application of a new force, f_m , which can be used to compensate the fluid drag force acting upon the active particle. Thus, when the interstitial fluid velocity is increased, the mass transfer between the particles and fluid is also increased (Figure 1.2a and 1.2b) (Al-Mulhim, 1995; Jovanovic and Al-Mulhim, 1995). Further, the magnetic force allows the use of smaller bead diameters thus reducing diffusion resistance through the beads.



a) Fluidization in MSFB; $\nabla H \neq 0$ b) Ordinary Fluidization; $H=0$

Figure 1.2: Particle fluidization with and without an applied gradient magnetic field.

1.3 Thesis Intent

The goal of this work is to create a flexible and robust reaction system which can be implemented in dechlorination of chlorinated aromatic compounds. It is evident that appropriate development of the catalyst and its integration into a viable engineering reactor platform must take place. Investigation into the reaction kinetics provides important knowledge of the catalyst's unique reaction properties as well as insight into the overall process kinetics. Acquired experimental information provides a foundation of knowledge for better insight into the dechlorination chemical reaction of which we currently have limited understanding. While experimental data provides a wide base of information, the mathematical model provides integration of the acquired knowledge. Thus, extensive effort went into modeling of the complete system including such parameters as diffusion through beads, liquid/solid mass transfer, chemical reaction kinetics, deactivation kinetics, adsorption and desorption.

The main objective of this work is divided into two specific investigations. First, the chemical kinetics of the dechlorination of p-chlorophenol on the Pd/Fe catalyst is explored. This investigation includes the examination of factors governing catalyst preparation, reusability of the catalyst and deactivation effects. Second, the technological application of the Pd/Fe catalyst in the MSFB for potential remediation of contaminated liquids, soils and sludges has been explored. This investigation included modeling of the important steps in the overall dechlorination process.

Chapter 2 proceeds to detail supporting theory for the chemical reaction including the proposed mechanism and chemical rate equation. Entrapment of the Pd/Fe catalyst into alginate beads along with descriptive modeling for diffusion and reaction is also proposed. Important fluidization characteristics of the MSFB are expressed as well as the mass transfer correlations utilized. Chapter 3 provides the description of the laboratory equipment and materials used as well as the methods incorporated for experimental work. Chapter 4 presents the experimental data obtained for a variety of situations and Chapter 5 demonstrates the modeling effort as applied to the experimental data. Chapter 6 completes this work with conclusions and recommendations. All detailed experimental methods and numerical approximations used in the modeling are included in the appropriate appendices.

CHAPTER 2 THEORETICAL DEVELOPMENT

2.1 Dechlorination of Chlorinated Hydrocarbons

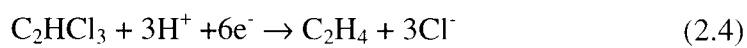
A specific application of the MSFB technology is envisioned and proposed in the area of selective dechlorination of chlorinated hydrocarbons in liquids and sludges (Graham and Jovanovic, 1998b). Currently, several researchers are investigating the chemistry behind reductive dechlorination of chlorinated hydrocarbons using metal surfaces. These developments include a wide range of commonly found environmental contaminants including tetrachloroethylene (PCE), trichloroethylene (TCE), chloroform, lindane, pentachlorophenol, and polychlorinated biphenyls (PCBs). Previous research focused on degrading chlorinated hydrocarbons by utilizing the metal surfaces of magnesium, zinc, tin and iron (Boronina and Klabunde, 1995; Matheson and Tratnyek, 1994; Gillham and O'Hannesin, 1994; Schlimm and Heitz, 1996). The dechlorination process with zero-valent metal in aqueous solutions follows the process of chemical corrosion of the metal by the chlorinated compound (Schlimm and Heitz, 1996).



While zinc, tin, and iron successfully dechlorinated several compounds, oxidation by water was an undesirable competing reaction. Reactions with magnesium, in particular,

were found to be overwhelmed by the competing process of metal oxidation by water (Boronina *et. al.* 1995).

According to research done by Matheson and Tratnyek (1994), iron sequentially dehalogenates an aliphatic chlorinated hydrocarbon such as carbon tetrachloride with an initial pseudo-first-order kinetics in substrate. Hence, the Fe^0 metal system quickly degrades the heavily chlorinated hydrocarbon while gradually slowing with each sequential dechlorination step. Matheson and Tratnyek (1994) propose the following overall reaction for the dechlorination of trichloroethylene, C_2HCl_3 , with zero-valent iron:



Other experiments include the dechlorination of lindane and chloroform in which over 99% conversion was achieved in 1-2 hours using a zinc surface (Schlimm and Heitz, 1996). However, the successful implementation of Fe^0 and Zn^0 is limited to saturated, aliphatic chlorinated hydrocarbons. Unfortunately, straight chain conjugated compounds such as PCE require significant time before visible degradation can take place and produce low concentrations of DCE isomers which are persistent (Gillham and O'Hannesin, 1994).

Unfortunately, these metals are unable to satisfactorily dechlorinate conjugated or aromatic compounds and all of their congeners. As a result, the idea of utilizing specially prepared bi-metallic surfaces using palladium or nickel coupled with iron in treatment of these difficult to dechlorinate compounds has been explored (Muftikian *et. al*, 1995; Sivavec *et. al*, 1997). Recently, the $\text{Fe}^0\text{-Pd}^0$ bimetallic system has been shown to dechlorinate aromatic hydrocarbons including chlorophenols and PCBs (Agrawal, 1997; Gu *et. al*, 1997; Wang and Zhang, 1997; Grittini *et. al*, 1995). One important characteristic of an $\text{Fe}^0\text{-Pd}^0$ bimetallic system is its ability to thoroughly dechlorinate all compounds present without leaving chlorinated side-products. For example, the $\text{Fe}^0\text{-Pd}^0$ surface dechlorinated all PCB congeners within the Aroclor 1260 and Aroclor 1254 mixtures at ambient temperatures (Grittini *et. al*, 1995). This reaction took between 5 and 10 minutes with biphenyl as the only remaining product. Also, complete dechlorination was reported for 2,3-dichlorophenol in the presence of an $\text{Fe}^0\text{-Pd}^0$ surface (Agrawal, 1997).

Importantly, the preparation of the $\text{Fe}^0\text{-Pd}^0$ surface is a fairly straightforward procedure and requires a low percentage of Pd as compared to the amount of Fe present (Grittini *et. al*, 1995). Recently, an X-ray photoelectron spectra of the palladium-iron bimetallic surface was performed (Muftikian *et. al*, 1996). This analysis included the important aspect of restoring the $\text{Fe}^0\text{-Pd}^0$ surface to its original reactivity after it had been used in a dechlorination reaction. Fortunately, the bimetallic surface was nearly completely restored through washing with 3 [M] HCl and no loss of Pd was detected

during any experiment (Muftikian *et. al*, 1996). This is a favorable indication of recycling the metal for further dechlorination in the MSFB. However, it must be noted that the experimental apparatus used by some investigators involved a high catalyst weight/chlorinated solvent volume ratio with low initial chlorinated solvent concentrations at neutral pH thus setting up extremely favorable conditions which avoided the intrusion of undesirable effects on the Pd/Fe catalyst (Muftikian *et. al*, 1995). However, under certain conditions, such as low pH and long reaction time, the iron base for the palladium islets can be attacked through dissolution reactions thus affecting the lifetime of the Pd/Fe catalyst. This is an important factor which is discussed in the following section.

2.1.1 Reaction Stoichiometry

Two key areas not previously addressed or reported in the open literature are explored in this investigation. The chemical kinetics of the dechlorination reaction have been determined under varying Pd/Fe ratios relative to the solute concentration and pH conditions. As in many other solid catalyzed reactions the pseudo-first order rate kinetics with respect to the chlorinated hydrocarbon (*p*-chlorophenol) concentration is found to be the most agreeable kinetic model. As discussed by Graham and Jovanovic (1998b), the chemical reactions involved have three separate factors contributing to the overall dechlorination reaction which include various *surface reactions*, *solution reactions*, and the actual *chlorine removal reaction*.

The surface reactions include the dissolution of iron from the zero-valent state and the consumption of hydrogen ion on both the iron and palladium surfaces as represented by Equations 2.5, 2.6 and 2.7, respectively. The abundance of hydrogen, H^+ , is controlled by its formation from the solution reactions (Equations 2.8 and 2.9) and its removal by Fe to form H_2 (g) (Equation 2.6) or Pd to form the intermediate reactive hydrogen, H^* (Equation 2.7) (Matheson and Tratnyek, 1994; Plonski, 1997; Westall, 1998). The electrons produced in the iron dissolution reaction are utilized by the palladium surface to form the highly reactive intermediate, H^* , which is used in the dechlorination reaction (Equation 2.10). Coupling these steps together from Equations 2.5, 2.7, 2.8, and 2.10, one can obtain the overall reaction in Equation 2.11.

Surface Reactions:



Solution Reactions:



Dechlorination Reaction:



Overall Reaction (Equations 2.5, 2.7, 2.8 and 2.10):



Grittini *et. al* (1997) and Graham and Jovanovic (1998b) discuss how this reaction can be visualized as a series of steps as shown in Figure 2.1. Several important operating parameters became apparent in developing an understanding of the kinetics of this overall reaction. These included the ratio of Pd/Fe interfacial area to the amount of chlorine to be removed, system pH, dissolved O_2 , the extent of the Pd/Fe interfacial area, and the extent of palladization or Pd/Fe weight ratio. Also, formation of $\text{Fe}(\text{OH})_2$ and $\text{Fe}(\text{OH})_3$ and hydrogen gas bubbles, which are dependent on the various operating parameters, were studied. Figure 2.2a and 2.2b illustrate the effect of these resistances on the overall reaction. Both of these passivation/deactivation mechanisms can be controlled by adjusting pH in a deoxygenated environment.

2.1.2 Determination of the Rate Equation for Dechlorination Chemical Kinetics on Powder Pd/Fe Catalyst

As a heterogeneous reaction, the disappearance of the chlorinated solvent, A, depends on the concentrations of A and H^* as well as the amount of catalyst, W (Equation 2.12). The concentration of H^* from H^+ on the palladized surface as expressed in Equation 2.7 was assumed constant at constant pH. This results in a pseudo first order in C_A rate

expression (Equation 2.12) (Note that catalyst deactivation/passivation effects are not yet taken into account). If a constant pH is maintained, the constant H^* value may be combined with the k' to give k which was further combined with catalyst weight, W , to give an overall rate constant, k^* (Equations 2.13 and 2.14).

$$-\frac{1}{W} \frac{d(VC_A)}{dt} = k' C_A C_{H^*} \quad (2.12)$$

$$-\frac{d(VC_A)}{dt} = (Wk) C_A = k^* C_A \quad (2.13)$$

$$\text{Therefore, } k^* = k' WC_{H^*} \quad (2.14)$$

To account for the passivation effects on the Pd/Fe surface, an activity term, a , is integrated into the reaction kinetics as shown in Equation 2.15. This term accounts for the decrease in active surface area and other similar effects compounded by the loss of dechlorination sites (Levenspiel, 1999). Levenspiel (1999) discusses several possible deactivation models for fluid-solid catalytic reactions. Catalyst passivation due to H_2 (g) bubble or hydroxide formation clearly falls into the category describing parallel reaction/deactivation kinetics as suggested by Levenspiel (1999). The activity of the catalyst is further described by Equation 2.16 for an n^{th} order deactivation process.

$$-\frac{d(VC_A)}{dt} = (kW) C_A^a = k^* C_A^a \quad (2.15)$$

$$-\frac{da}{dt} = k_d a^n \quad (2.16)$$

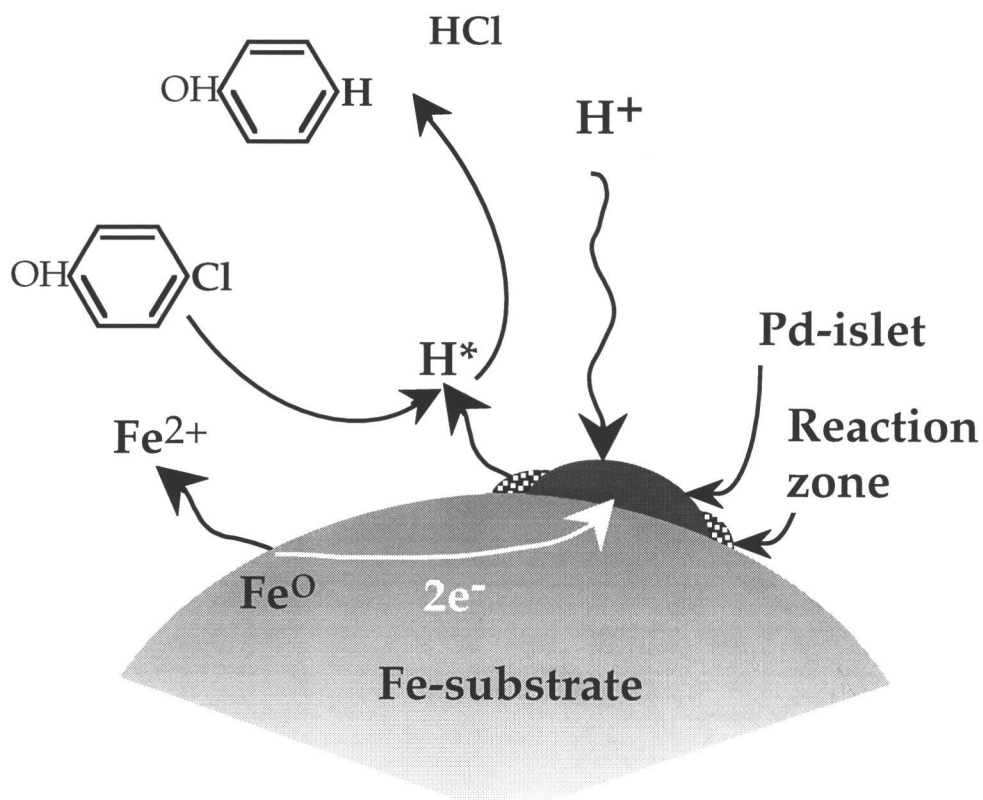


Figure 2.1: Illustration of multistep dechlorination reaction on the Pd/Fe catalyst surface.

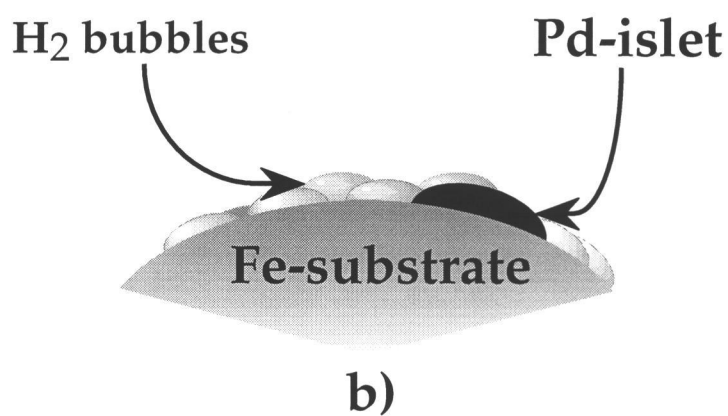
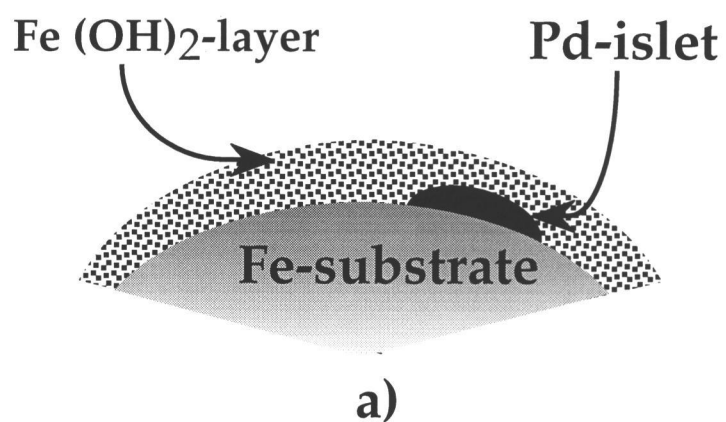


Figure 2.2: Iron hydroxide and/or H₂(g) bubble formation on the Pd/Fe catalyst surface.

2.2 Modeling Diffusion and Dechlorination of *p*-Chlorophenol in Alginate Beads With Entrapped Pd/Fe Catalyst

There are two feasible models which can be used in this study to evaluate the experimental system.

Model 1: This model presumes that the experimental reaction system is schematically represented by Figure 2.3. System boundary 1 represents the fluid volume of the system (including the overflow box, connecting pipes, pump, etc.) with no particles present. A well-mixed volume is assumed with a constant $C_b(t)$. System boundary 2 envelops the volume in which particles are in contact with the chlorinated organic, *p*-chlorophenol, where mass transfer, reaction and deactivation are occurring.

Model assumptions include:

1. The adsorbate concentration, C_b , within system boundary 1 is uniform. No reaction is occurring in the bulk liquid.
2. The adsorbate concentration from the fluidized bed inlet through the fluidized bed is not changing substantially. Hence, it is a quasi-steady state assumption as used by other investigators in model development with short bed heights (Al-Mulhim, 1995; Tang, 1990). Maximum bed height reached in our experiments is 40 [cm] with a fluid superficial velocity of 5 [cm/s]. This indicates that a maximum of 8 seconds is required for an element of fluid to pass once through the bed.
3. The fluid flows in plug flow through the fluidized bed.

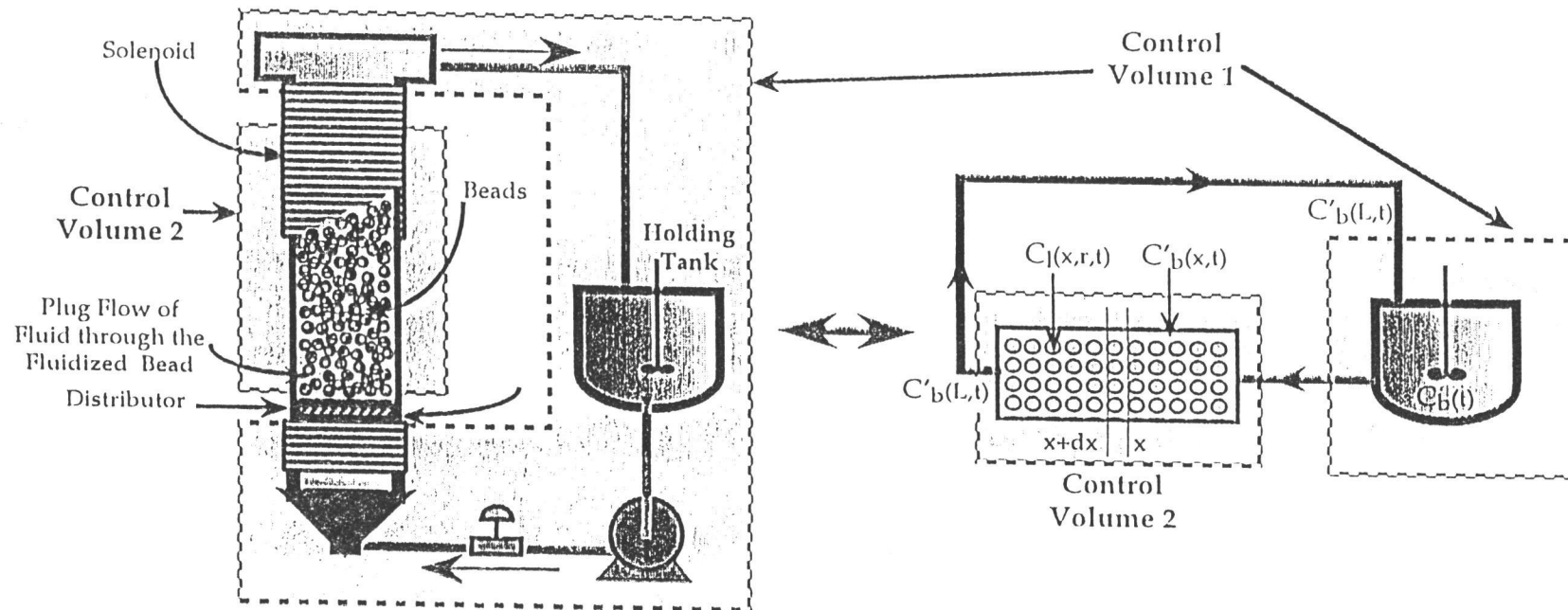


Figure 2.3: Model 1 schematic: Plug Flow (PF).

Model 2: This model presumes that the particles and the adsorbate are in contact with each other throughout the whole volume of the system as if the experimental system is a well mixed agitated tank (Figure 2.4). Model 2 has been used to measure liquid-particle mass transfer coefficients in well agitated vessels by many investigators including McKay (1983) and Furusawa and Smith (1973).

There are two approaches to demonstrate equality of Model 1 and Model 2 under certain experimental conditions. First, an additional assumption can be made which neglects interparticle diffusion resistance since the internal volume is readily accessible to the adsorbate. Several investigators also neglected the interparticle diffusion resistance in their model development with justification (Furusawa and Smith, 1973; McKay, 1983; Silem *et. al*, 1993; Al-Mulhim, 1995). The analytical solution for both models is derived in Appendix B with the useful form of the solutions represented by:

Model 1:

$$\ln \left\{ \frac{C_b(l + mK_b) - C_{b,0}}{C_{b,0}(l + mK_b) - C_{b,0}} \right\} = - \frac{l + mK_b}{mK_b} \frac{F}{V} (e^{-\alpha k_l} - 1)t \quad (2.17)$$

where $\alpha = \frac{a'AL}{F} = \frac{a'V}{F}$ (2.18)

Model 2:

$$\ln \left\{ \frac{C_b(1 + mK_b) - C_{b,0}}{C_{b,0}(1 + mK_b) - C_{b,0}} \right\} = - \frac{1 + mK_b}{mK_b} (k_l a) t \quad (2.19)$$

with the variables defined as:

- A Cross-sectional area of the reactor, m
- a' External bead surface area/unit bulk liquid volume, m²/m³
- C_b Bulk concentration, mol/m³
- C_{b,0} Initial bulk concentration, mol/m³
- F Liquid flowrate, m³/s
- H Magnetic field intensity, A/m
- k_l Liquid-solid mass transfer coefficient in MSFB (H≠0), m/s
- K_b Gel solid-water distribution ratio, mol/kg bead/(mol/L H₂O)
- m (Δε/ΔH); Change of bed voidage with magnetic field intensity, m/A
- t Reaction time (s)
- V Volume of reactor liquid, m³
- ε Reactor voidage in magnetically stabilized fluidized bed (H≠0), [-]

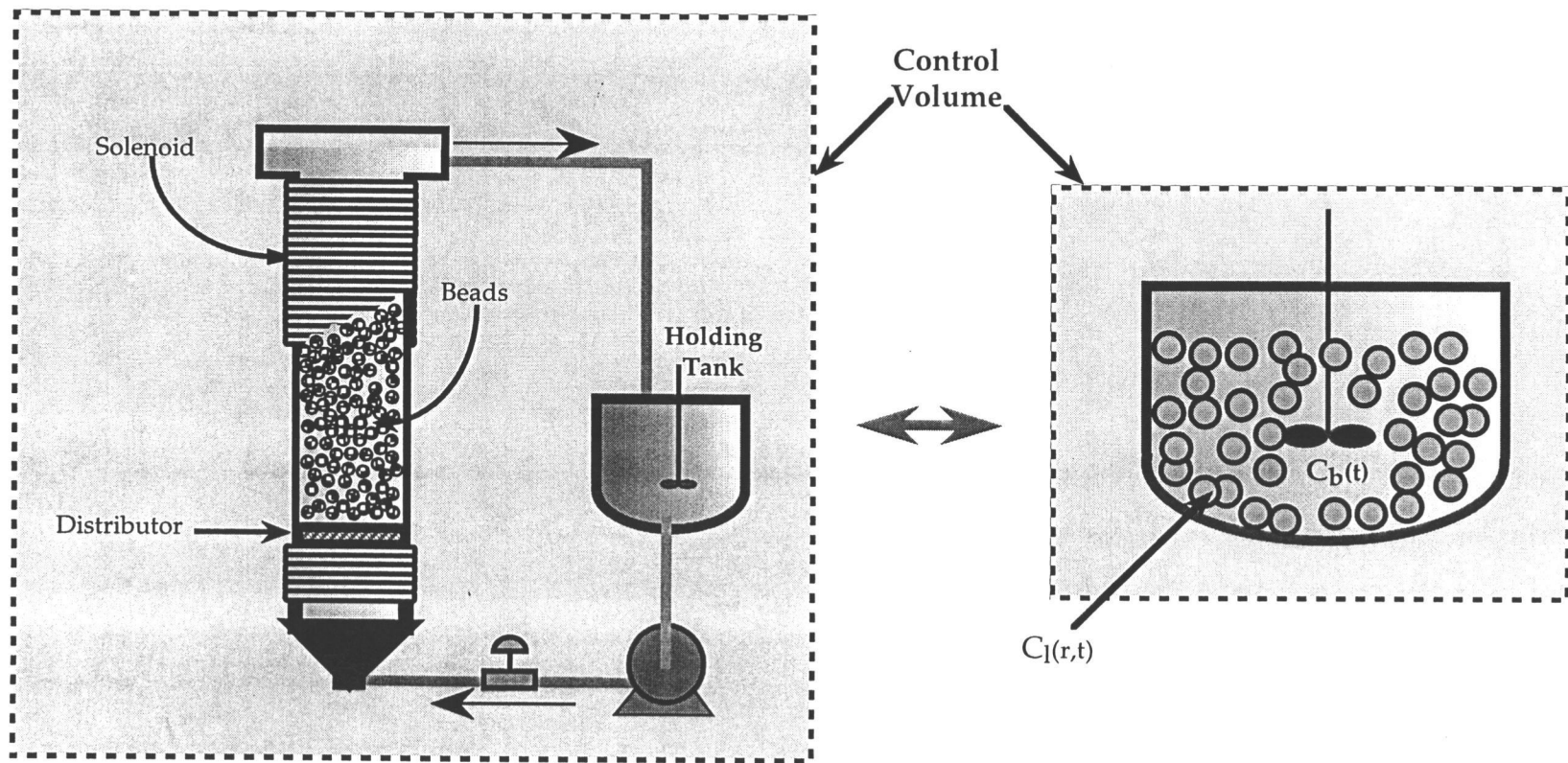


Figure 2.4: Model 2 schematic: Continuously Stirred Tank Reactor (CSTR).

Model 1 and model 2 can be simplified further if the assumption that the equilibrium concentration, $C_{b,e}$, is zero at the beginning of the experiment as detailed in Appendix B (Al-Mulhim, 1995).

Model 1:

$$\text{Ln}\left(\frac{C_b}{C_{b,0}}\right) = \frac{F}{V}(e^{-\alpha k_i} - 1)t \quad (2.20)$$

Model 2:

$$\text{Ln}\left(\frac{C_b}{C_{b,0}}\right) = -k_i at \quad (2.21)$$

The initial condition for both models is given as:

$$t=0 \quad C_b = C_{b,0}$$

Model 1 can be mathematically shown to simplify to model 2 if the volume of liquid outside the fluidized bed can be neglected or if a high liquid inlet velocity is present. In other words, if the ratio of V/F is small. If this condition is satisfied, $e^{-\alpha k}$ term in Equation 2.20 is reduced to $(1-\alpha k)$ thus resulting in the equality of the two expressions.

However, this development is for a case in which intraparticle diffusion is considered negligible. A second approach does not neglect interparticle diffusion and includes a

reaction and deactivation term which represents our specific case. This produces an analytical situation which is more complicated and must be solved numerically for each model in order to demonstrate that the two models are equivalent under our experimental conditions.

The following possible scenarios can be envisioned in either reactor configuration.

1. Diffusion into alginate gel beads is accounted for without a dechlorination reaction and without external mass transfer resistance at the outer boundary of the alginate bead.
2. Diffusion into alginate gel beads is accounted for without a dechlorination reaction but including external mass transfer resistance at the outer boundary of the alginate bead.
3. Diffusion into alginate gel beads is accounted for with the dechlorination reaction and without external mass transfer resistance at the outer boundary of the alginate bead.
4. Diffusion into alginate gel beads is accounted for with the dechlorination reaction and external mass transfer resistance at the outer boundary of the alginate bead.

For comparison of the two reactors, scenario #4 is modeled for each reactor configuration with the following important assumptions:

1. The alginate gel beads are of equal size and are uniform spheres of radius, r .
2. A constant effective diffusion coefficient, D_e , exists throughout the gel beads.

Hence, the tortuosity effect on the aqueous diffusion coefficient is not changing from the surface of the alginate bead to the center. This assumption implies that alginate gel beads are homogeneously polymerized or cross-linked.
3. No reaction is occurring in the completely mixed bulk liquid as the Pd/Fe catalyst is entrapped within the gel beads and not permitted into the bulk liquid.
4. The Pd/Fe catalyst is homogeneously entrapped within the gel bead thus ensuring a uniform reaction surface throughout the gel bead.
5. The gel bead liquid is defined as a volume fraction of the total bead volume. The symbol, ϕ , represents the fraction of bead occupied by gel and/or entrapped substance.
6. The gel bead “open flux area for diffusion” is defined as a fraction of the total surface area and is dependent upon the fraction of bead surface occupied by gel.

Model 1:

Utilizing the model depicting a plug flow scenario with a constant reactor volume (Figure 2.3), the following equations represent the system.

System Boundary 1:

$$FC'_b - FC_b = V \frac{dC_b}{dt} \quad (2.22)$$

$$F(C'_b - C_b) = V \frac{dC_b}{dt} \quad (2.23)$$

The initial condition and boundary conditions to solve Equation 2.23 are:

$$t=0 \quad C_b = C_{b,0} \quad (2.24)$$

$$t=t \quad C_b = C_b \quad (2.25)$$

System Boundary 2 (using quasi-steady state assumption):

For bulk fluid:

$$(FC'_b)_x - (FC'_b)_{x+\Delta x} - k_l(C'_b - C_l(R, t))a' A \Delta x = 0 \quad (2.26)$$

where $a = a'V$ and a' is the area of particles per volume of column.

This gives:

$$F(C'_{b,x+\Delta x} - C'_{b,x}) = -k_l(C'_b - C_l(R, t))a' A \Delta x \quad (2.27)$$

Taking the limit of Equation as $\Delta x \rightarrow 0$ leads to:

$$F \frac{dC'_b}{dx} = -k_l a' A (C'_b - C_l(R, t)) \Rightarrow F \frac{dC'_b}{(C'_b - C_l(R, t))} = -k_l a' A dx \quad (2.28)$$

The boundary conditions to solve Equation 2.28 are:

$$x=0 \quad C'_b = C_b \quad (2.29)$$

$$x=H \quad C'_b = C'_b \quad (2.30)$$

By taking a differential balance of the adsorbate within the particle, we obtain:

$$\frac{\partial C_l(r, t)}{\partial t} = D_e \left(\frac{\partial^2 C_l(r, t)}{\partial r^2} + \frac{2}{r} \frac{\partial C_l(r, t)}{\partial r} \right) - \frac{k^*}{V} C_l(r, t) a^n \quad (2.31)$$

The boundary conditions used in solving Equations 2.31 are:

$$D_e \frac{\partial C_l(R, t)}{\partial t} = k_l \left(C'_b - \frac{C_l(R, t)}{K_b} \right) \quad (2.32)$$

$$\left(\frac{\partial C_l(r, t)}{\partial t} \right)_{r=0} = \text{finite} \quad (2.33)$$

Model 2:

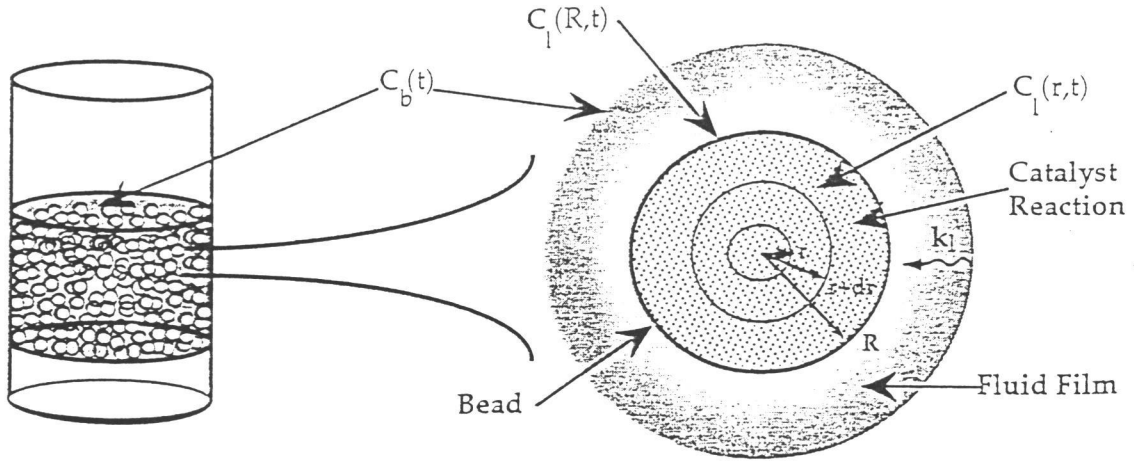


Figure 2.5: Mass balance on the dechlorination system for scenario 4.

A mass balance on alginate bead liquid including both reaction and deactivation mechanisms for Figure 2.4 (CSTR) is given as:

$$\frac{\partial C_l(r,t)}{\partial t} = D_e \left(\frac{\partial^2 C_l(r,t)}{\partial r^2} + \frac{2}{r} \frac{\partial C_l(r,t)}{\partial r} \right) - \frac{k^*}{V} C_l(r,t) a^n \quad (2.34)$$

with last term in Equation 2.34 is representing the disappearance of the chlorinated organic as discussed in the previous section.

However, if the fluid-particle mass transfer resistance cannot be neglected as a controlling factor, then the boundary condition at $r=R$ for the alginate bead becomes:

$$D_e \frac{\partial C_l(R, t)}{\partial r} = k_l \left[C_b(t) - \frac{C_l(R, t)}{K_b} \right] \quad (2.35)$$

A mass balance on the bulk liquid concentration, $C_b(t)$, is related to the diffusion at the outer boundary and is given by:

$$\varepsilon V \frac{dC_b(t)}{dt} = -Vk_l a \left[C_b(t) - \frac{C_l(R, t)}{K_b} \right] \quad (2.36)$$

The initial conditions of the bulk and bead liquid as well as the boundary condition for the center of the bead, respectively are:

$$\text{Bead Liquid: } C_l(r, t=0) = C_{l,0} \quad (2.37)$$

$$\text{Bulk Liquid: } C_b(t=0) = C_{b,0} \quad (2.38)$$

$$\text{At the center of the bead for all time: } \left. \frac{\partial C_l(r, t)}{\partial r} \right|_{r=0} = 0 \quad (2.39)$$

Figure 2.6 shows the output bulk concentration of *p*-chlorophenol as a function of time from both models. As discussed previously, the two models can be shown to be equivalent either analytically as in Equations 2.20-2.21 with a simplifying assumption or numerically at a high inlet velocity. As the flowrate was increased in the plug flow model (Model 1) to achieve the flowrate used in the experimental setup, the rate of dechlorination of *p*- chlorophenol increased until no further change was observed. At this

point, the plug flow model output for a recycle plug flow reactor became equivalent to the CSTR model output (Figure 2.6).

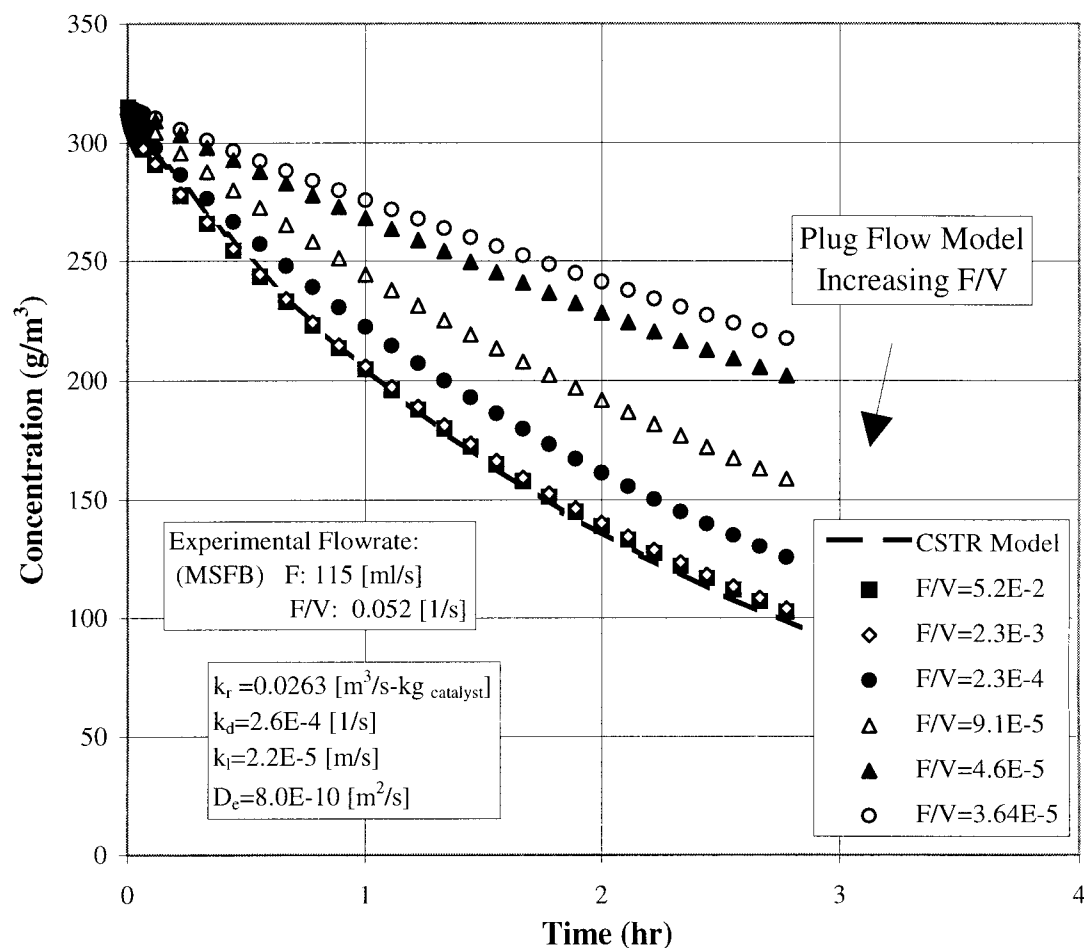


Figure 2.6: Comparison of the CSTR and PF models.

Scenarios #1-3 discussed previously which include interparticle diffusion, and/or reaction and mass transfer are modeled in the following sections.

2.2.1 Diffusion Through Beads Without Reaction and Without External Mass Transfer Resistance

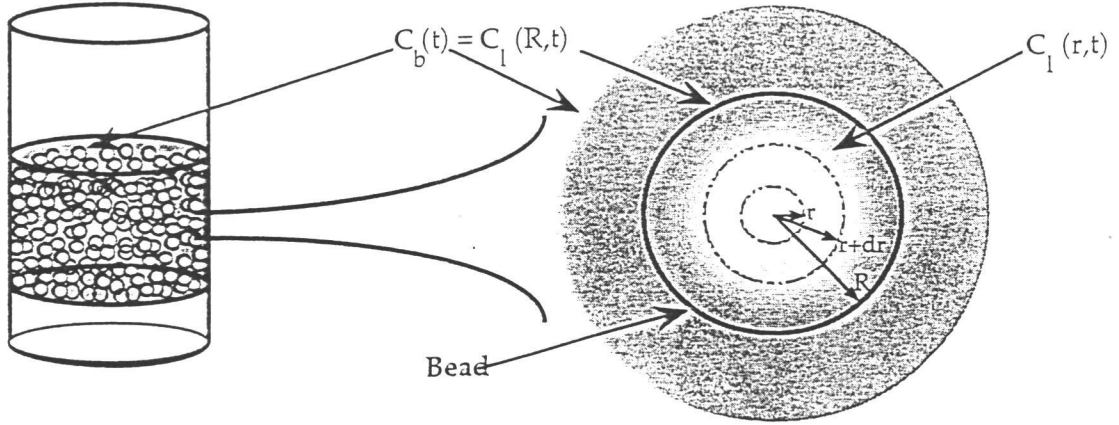


Figure 2.7: Mass balance on the dechlorination system for scenario 1.

A mass balance on alginate bead liquid is given as (Figure 2.7):

$$\frac{\partial C_l(r, t)}{\partial t} = D_e \left(\frac{\partial^2 C_l(r, t)}{\partial r^2} + \frac{2}{r} \frac{\partial C_l(r, t)}{\partial r} \right) \quad (2.40)$$

If mixing is sufficient to eliminate mass transfer resistance, then the boundary condition for Equation 2.40 at $r=R$ is:

$$C_l(R, t) = C_b(t) \quad (2.41)$$

To perform a mass balance on the bulk liquid, the change in bulk concentration, $C_b(t)$, is related to the amount of solute to diffuse into the alginate bead over a period of time as expressed by:

$$\frac{dC_b(t)}{dt} = -D_e \frac{\delta C_l(R, t)}{\delta r} \quad (2.42)$$

The initial conditions of the bulk and bead liquid as well as the boundary condition for the center of the bead, respectively are:

$$\text{Bead Liquid: } C_l(r, t = 0) = C_{l,0} \quad (2.43)$$

$$\text{Bulk Liquid: } C_b(t = 0) = C_{b,0} \quad (2.44)$$

$$\text{At the center of the bead for all time: } \left. \frac{\partial C_l(r, t)}{\partial r} \right|_{r=0} = 0 \quad (2.45)$$

2.2.2 Diffusion Through Beads Without Reaction and With External Mass Transfer Resistance

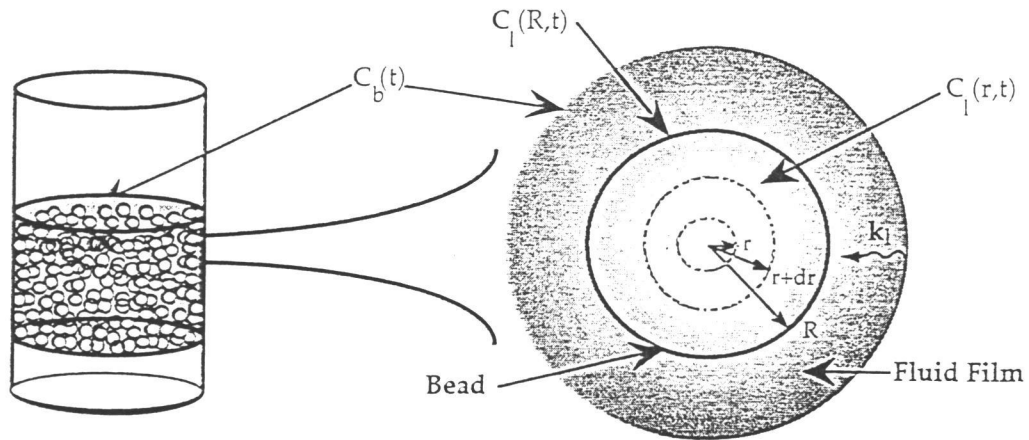


Figure 2.8: Mass balance on the dechlorination system for scenario 2.

A mass balance on the alginate bead liquid is given as (Figure 2.8):

$$\frac{\partial C_l(r,t)}{\partial t} = D_e \left(\frac{\partial^2 C_l(r,t)}{\partial r^2} + \frac{2}{r} \frac{\partial C_l(r,t)}{\partial r} \right) \quad (2.46)$$

However, if the mass transfer resistance cannot be neglected as a controlling factor, then the boundary condition at $r = R$ for the alginate bead is:

$$D_e \frac{\partial C_l(R, t)}{\partial r} = k_l \left[C_b(t) - \frac{C_l(R, t)}{K_b} \right] \quad (2.47)$$

A mass balance on the bulk concentration, $C_b(t)$, is related to the diffusion at the outer boundary as given by:

$$\varepsilon V \frac{dC_b(t)}{dt} = -V k_l a [C_b(t) - C_l(R, t)] \quad (2.48)$$

The initial conditions of the bulk and bead liquid as well as the boundary condition for the center of the bead, respectively are:

$$\text{Bead Liquid: } C_l(r, t = 0) = C_{l,0} \quad (2.49)$$

$$\text{Bulk Liquid: } C_b(t = 0) = C_{b,0} \quad (2.50)$$

$$\text{At the center of the bead for all time: } \left. \frac{\partial C_l(r, t)}{\partial r} \right|_{r=0} = 0 \quad (2.51)$$

2.2.3 Diffusion Through Beads With Reaction and Without External Mass Transfer Resistance

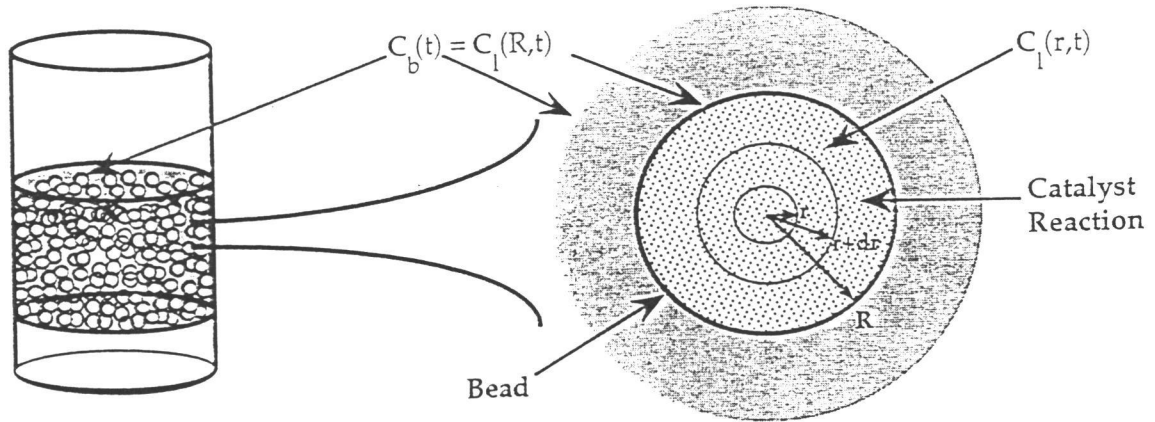


Figure 2.9: Mass balance on the dechlorination system for scenario 3.

To further incorporate the reaction and passivation mechanisms involved, the overall mass balance on the bead liquid is expressed as (Figure 2.9):

$$\frac{\partial C_l(r,t)}{\partial t} = D_e \left(\frac{\partial^2 C_l(r,t)}{\partial r^2} + \frac{2}{r} \frac{\partial C_l(r,t)}{\partial r} \right) - \frac{k^*}{V} C_l(r,t) a^n \quad (2.52)$$

with the outer boundary condition given by:

$$C_l(R, t) = C_b(t) \quad (2.53)$$

The last term in Equation 2.52 is representing the disappearance of compound A as discussed in the previous section. A mass balance on the bulk liquid (Equation 2.54) shows the change of bulk liquid concentration dependent on the diffusion of *p*-chlorophenol across the outer boundary of the alginate bead.

$$\frac{dC_b(t)}{dt} = -D_e \frac{\delta C_l(R, t)}{\delta r} \quad (2.54)$$

The initial conditions of the bulk and bead liquid as well as the boundary condition for the center of the bead, respectively are:

$$\text{Bead Liquid: } C_l(r, t = 0) = C_{l,0} \quad (2.55)$$

$$\text{Bulk Liquid: } C_b(t = 0) = C_{b,0} \quad (2.56)$$

$$\text{At the center of the bead for all time: } \left. \frac{\partial C_l(r, t)}{\partial r} \right|_{r=0} = 0 \quad (2.57)$$

2.3 Modeling *p*-Chlorophenol Desorption From Contaminated Soil

To model desorption and subsequent reaction of *p*-chlorophenol, it is important to quantify the soil surface. Important parameters of the soil include the fraction of organic matter, f_{om} , the fraction of organic carbon, f_{oc} , and the chemical's tendency to sorb to the soil which is usually expressed as its solid-water distribution ratio, K_d (Equation 2.58). The K_d value can also be described as a compound's relative concentration on the soil, C_s , and its concentration in the bulk liquid, C_b .

$$K_d = K_{om} * f_{om} = \frac{C_s}{C_b} \quad (2.58)$$

K_{om} is the organic matter-water distribution ratio calculated from various literature correlations with the octanol-water partition coefficient, K_{ow} , and f_{om} is assumed to be approximately $1.8-2 * f_{oc}$ (Schwarzenbach, 1993). This equilibrium relationship is used when developing the model describing transport from the soil to the surrounding bulk liquid.

2.4 Modeling of *p*-Chlorophenol Dechlorination of Contaminated Soil Using Entrapped Pd/Fe Catalyst in Alginate Beads

Another important aspect of dechlorination of *p*-chlorophenol from contaminated soil involves the mechanism of transport to the bulk liquid. To determine a reasonable model,

the soil particles were examined under scanning electron microscopy (SEM) to determine their surface properties. From the analysis of the SEM pictures it was concluded that the soil particles have an extremely low porosity which limits a compounds ability to diffuse into the interior of the soil (Figures 2.10a-d) (Kimura, 1998). The soil particles were also determined to have a bulk density of $2.38 \pm 0.06 \text{ [kg/m}^3\text{]}$. Due to the low porosity, the pore diffusion of the contaminant is considered negligible for modeling purposes and only mass transfer from the surface of the soil particles is considered. Figure 2.11 illustrates the overall mechanism for dechlorination of *p*-chlorophenol from contaminated soil and the following each step is modeled as follows.

The balance on the soil particles is given as:

$$\frac{dC_s(t)}{dt} = -k_{l,s}a' \left[\frac{C_s(t)}{K_{d,s}} - C_b(t) \right] \quad (2.59)$$

with an initial condition of:

$$C_s(t) = C_{s,0}(t) \quad (2.60)$$

The resulting balance equation for the bulk liquid phase is:

$$\epsilon V \frac{dC_b(t)}{dt} = -Vk_l a [C_b(t) - C_l(R, t)] + k_{l,s}a' \left[\frac{C_s(t)}{K_{d,s}} - C_b(t) \right] \quad (2.61)$$

with an initial condition for the bulk liquid given by:

$$C_b(t=0) = C_{b,0} \quad (2.62)$$

The mass balance on the alginate bead liquid is given as:

$$\frac{\partial C_l(r,t)}{\partial t} = D_e \left(\frac{\partial^2 C_l(r,t)}{\partial r^2} + \frac{2}{r} \frac{\partial C_l(r,t)}{\partial r} \right) - \frac{k^*}{V} C_l(r,t) a^n \quad (2.63)$$

with the initial condition given by:

$$C_l(r,t=0) = C_{l,0} \quad (2.64)$$

and boundary conditions given as:

$$D_e \frac{\partial C_l(R,t)}{\partial r} \Big|_{r=R} = k_l \left[C_b(t) - \frac{C_l(R,t)}{K_b} \right] \quad (2.65)$$

$$\text{and } \frac{\partial C_l(r,t)}{\partial r} \Big|_{r=0} = 0 \quad (2.66)$$

Implementation of this overall model to experimental data is presented in Chapter 5.

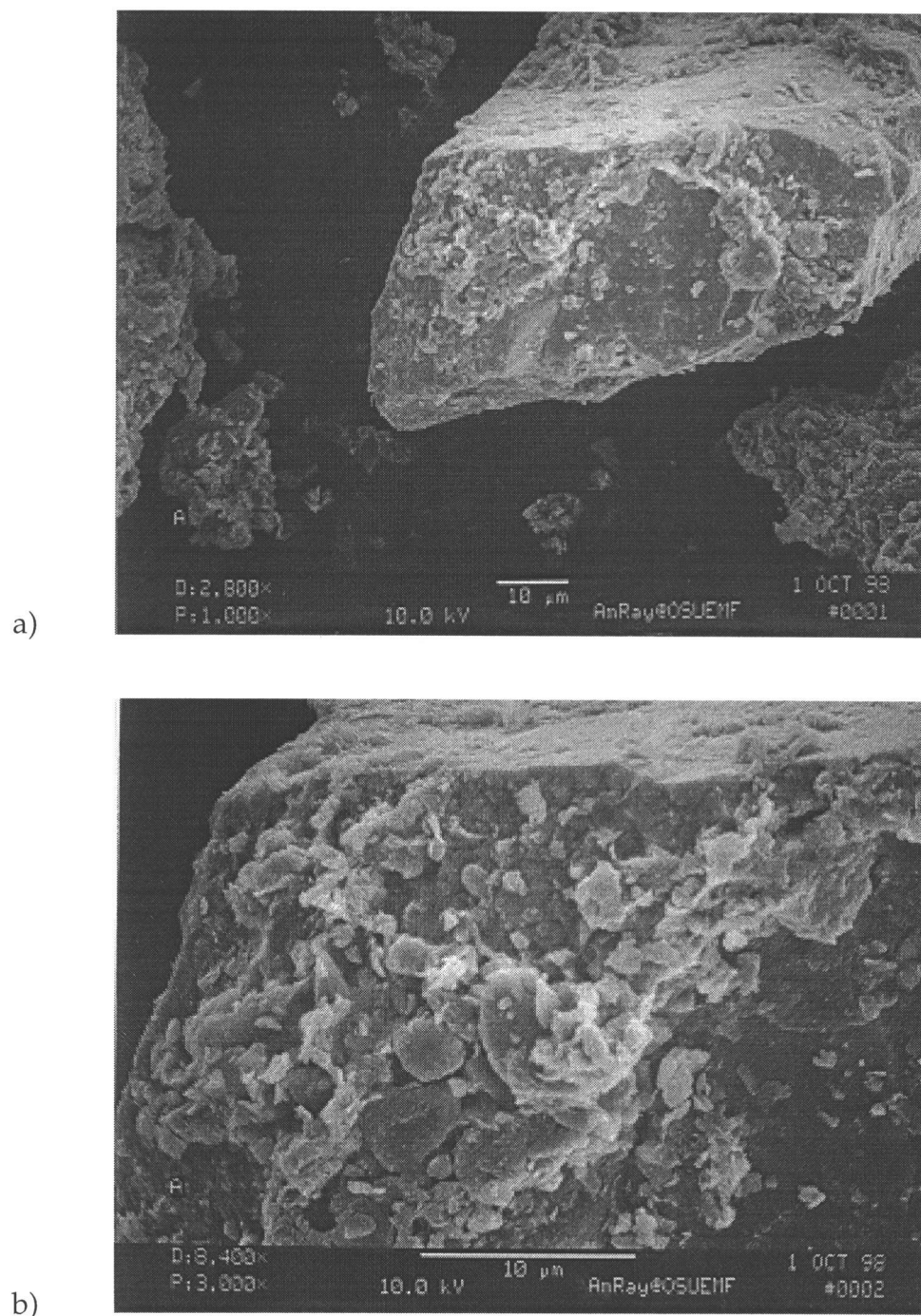


Figure 2.10: SEM pictures of Willamette Valley type soil (54-104 [μm])
 a) 1000x soil particle, b) 3000x rough surface, c) 3000x smooth surface,
 d) 30,000x showing negligible porosity.

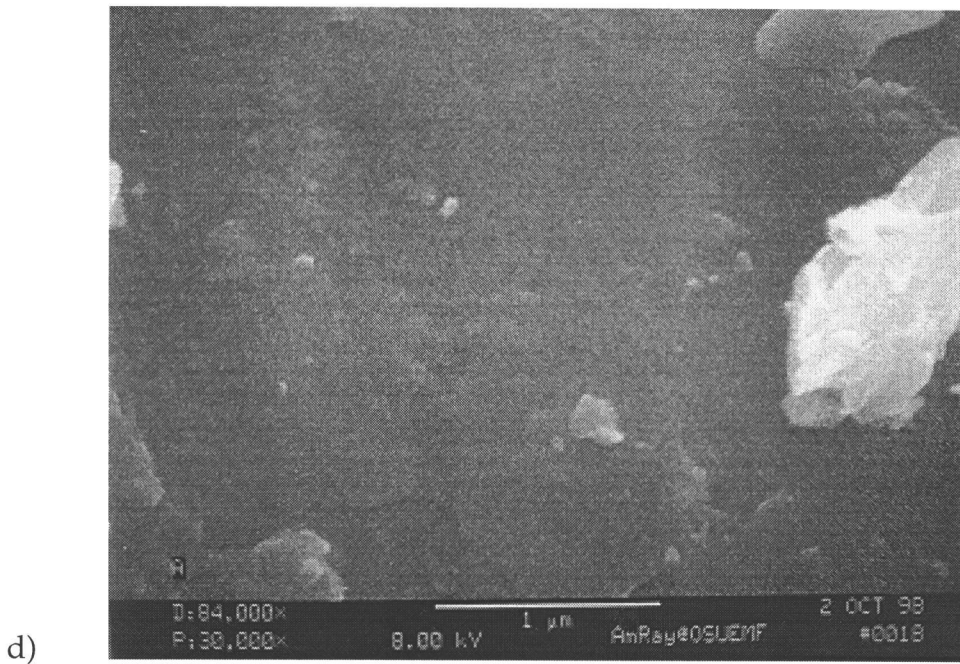
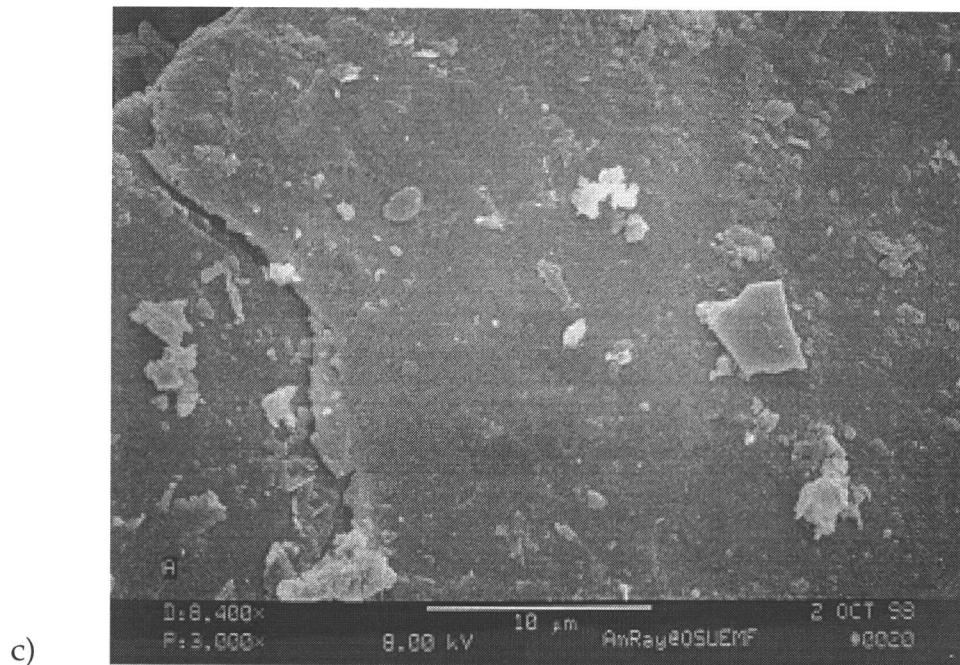


Figure 2.10 (con't): SEM pictures of Willamette Valley type soil (54-104 [μm])
 a) 1000x soil particle, b) 3000x rough surface, c) 3000x smooth surface,
 d) 30,000x showing negligible porosity.

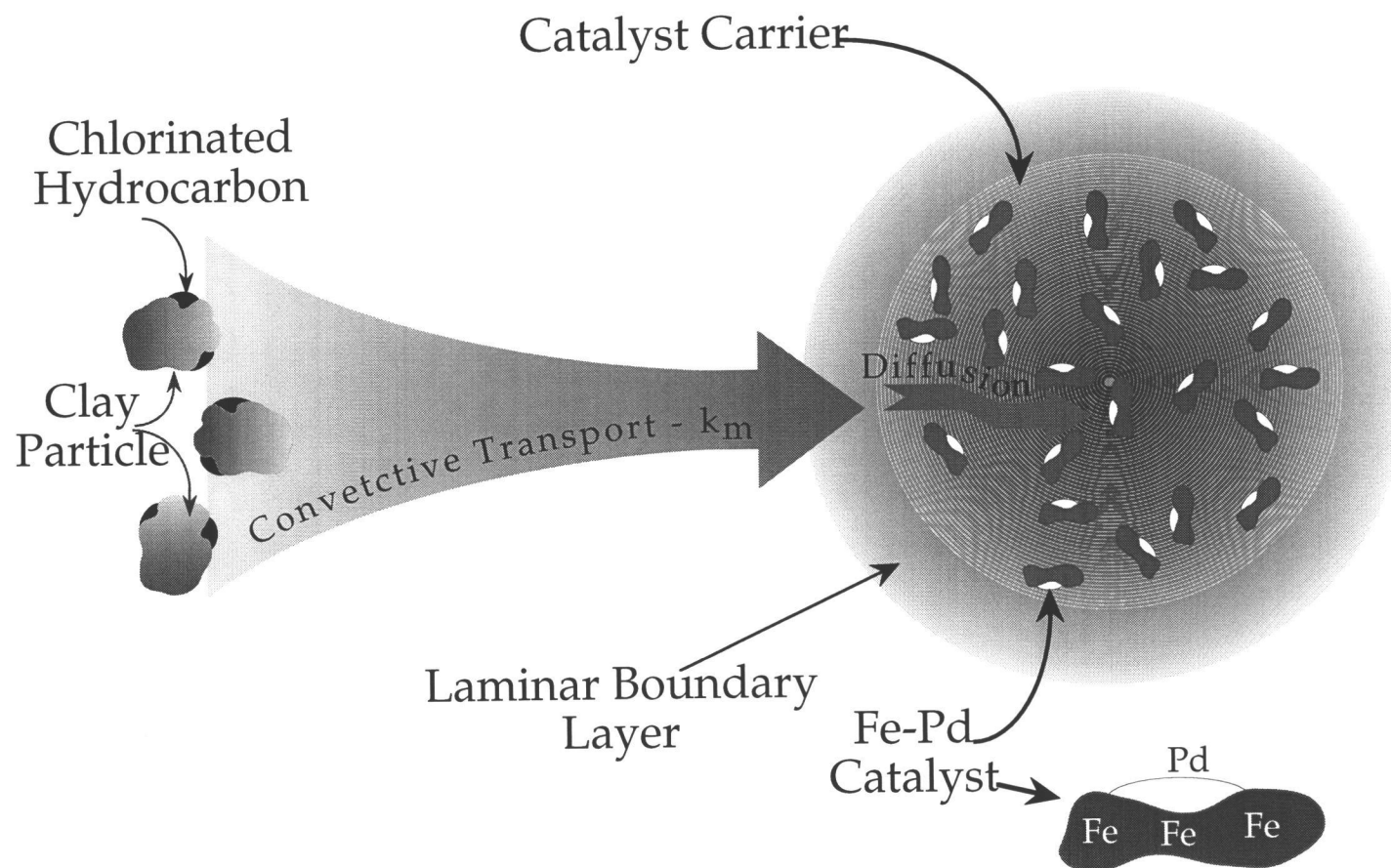


Figure 2.11: Overall mechanism for dechlorination of *p*-chlorophenol from soil particles.

2.5 MSFB Technology

Fluid-particle mass transfer in fluidized beds is a very important, often the limiting, transport parameter for operations such as adsorption, ion exchange, drying, and evaporation. It is well known that in a conventional fluidized bed, particles are subject to three macroscopic forces: the gravitational force, F_g , the drag force, F_d , and the buoyancy force, F_b . As soon as the drag force, which is determined by measuring the pressure drop across the bed, ΔP , balances the other two forces the particles are fluidized. In a gas-solid fluidized bed, velocities that surpass the minimum fluidization velocity produce rapidly rising bubbles. As a result, backmixing of solids may occur which can lower the efficiency of a chemical process or unit operation in the fluidized bed reactor. In liquid-solid fluidized beds, which are of greater interest for this study, the bed readily expands to compensate the increased liquid velocity. Thus the number of particles per unit volume of bed decreases, i.e. the voidage, ϵ , increases. This situation, in particular, is where the MSFB plays an important part in allowing for enhanced mass transfer conditions over the traditional fluidized bed.

In an MSFB, an additional force is created by applying the magnetic field to the magnetically susceptible fluidized particles. The magnetic field magnetizes the particles containing ferromagnetic material which results in two types of forces acting on the fluidization particle; the interparticle forces and the magnetic force from the gradient magnetic field. A uniform field does not create a net force within the MSFB, although interparticle forces are created which are of a cohesive nature. The induced particle-

particle forces tend to bring the particles together, which results in a decrease of the bed porosity, ε . However the introduction of a non-uniform field generates an additional force within the bed with the magnetic force acting proportionally to the magnetic field gradient (Rosensweig, 1979 b). These forces act colinearly with the magnetic field and can be visualized as an additional force acting on the fluidized particle which must be overcome by the fluid drag force. Hence, the fluid velocity through the bed must increase to compensate for these new macroscopic forces. Consequently, in an MSFB we are able to maintain lower bed voidage while increasing the superficial fluid velocity, u_o . Figure 2.12 schematically illustrates the influence of the magnetic field on the operation of the liquid-solid fluidized bed.

The reduction of the bed voidage, ε , due to the magnetic forces means that the relative velocity between the fluid and the particles, the interstitial velocity $u_{int} = u_o / \varepsilon$, can substantially increase; hence, the mass transfer coefficient between fluidizing particles and the fluid must also increase. Routinely observed enhancement of the mass transfer coefficient in an MSFB is 40% to 75% over that in a conventional fluidized bed at certain superficial velocities and magnetic field strengths (Figure 2.13). Kwauk *et. al* (1992) presented the following equation for the prediction of bed voidage as a function of magnetic field intensity and other system characteristics.

$$\frac{\varepsilon - \varepsilon_m}{\varepsilon_p - \varepsilon_m} = \exp \left[\left(\frac{H}{H_0} \right)^s \right] \quad (2.67)$$

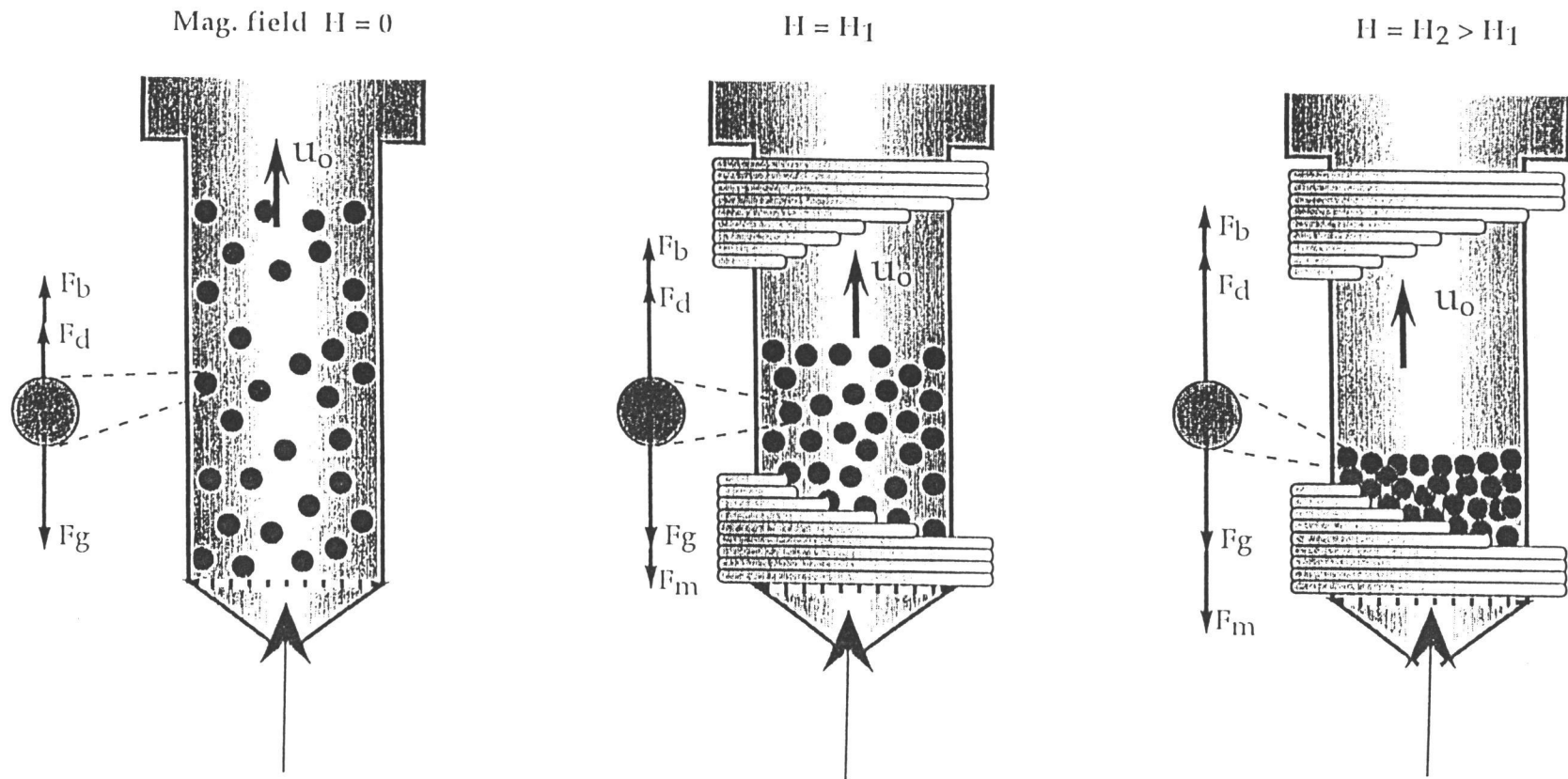


Figure 2.12: Effect of the magnetic field on fluidized particles within the MSFB.

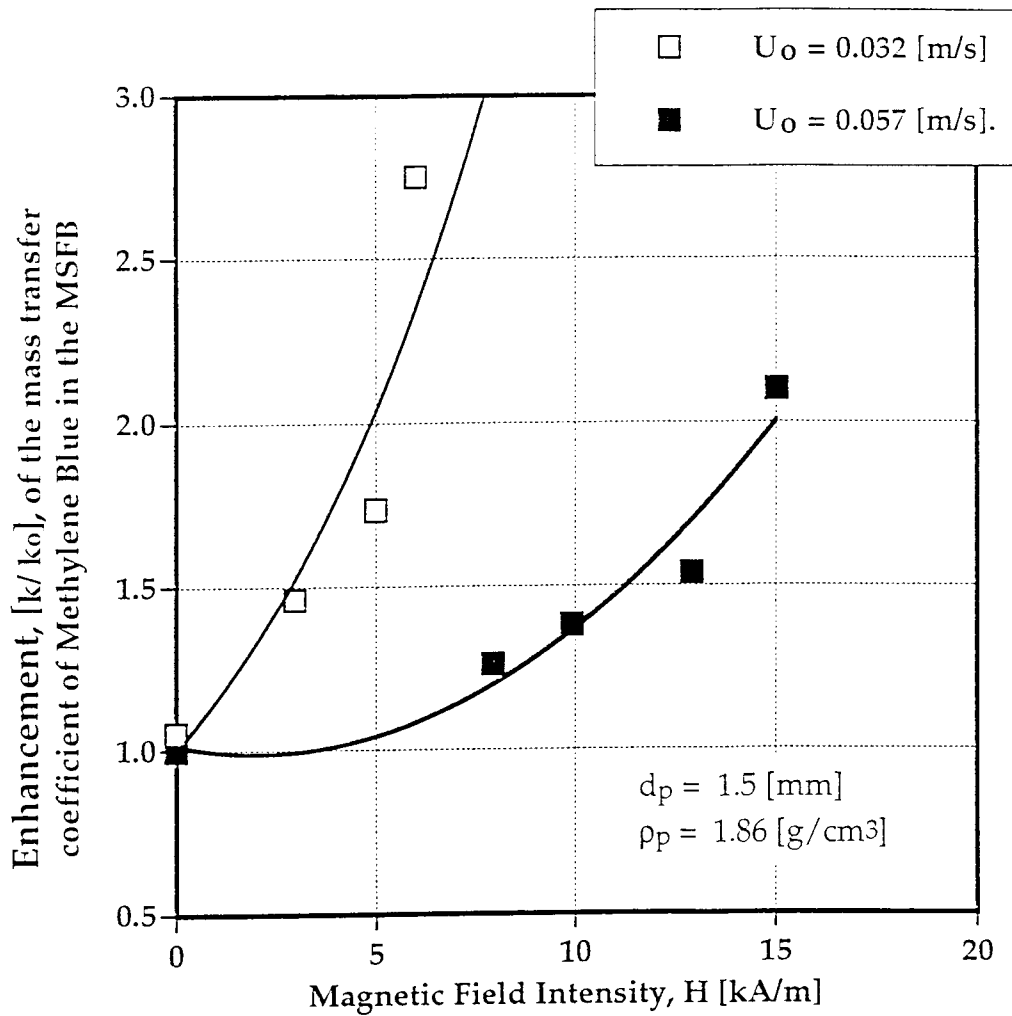


Figure 2.13: Enhancement of the mass transfer coefficient, k_t , in the MSFB (Al-Mulhim, 1995).

The average bed voidage in a stabilized regime is represented by ϵ_m and the bed voidage in the random motion regime is represented as ϵ_p . H_0 is the characteristic magnetic field strength.

Honorez (1995) presented the following correlation to determine the average bed voidage for given particles, velocity, and magnetic field intensity with the inclusion of the magnetic susceptibility of the ferromagnetic material as a key parameter.

$$\frac{H_{ms}}{1-\epsilon} \ln \left(\frac{\epsilon - \epsilon_{ms}}{\epsilon_{ff} - \epsilon_{ms}} \right) = -\chi H = -M \quad (2.68)$$

where ϵ_{ff} is the porosity of an ordinary fluidized bed ($H=0$). The bed porosity and magnetic field intensity at the transition between the partially stabilized and stabilized fluidization regimes are represented by ϵ_{ms} and H_{ms} . This characteristic transition is attained at the point of minimum bed porosity where an increase in the magnetic field intensity has no further effect; i.e. the ferromagnetic particles are “frozen”. Rosensweig (1981) and Honorez (1994) provide a detailed description of this and other fluidization regimes. Figure 2.14 shows experimental data for the decrease in bed voidage as the magnetic field intensity is increased (Honorez, 1995).

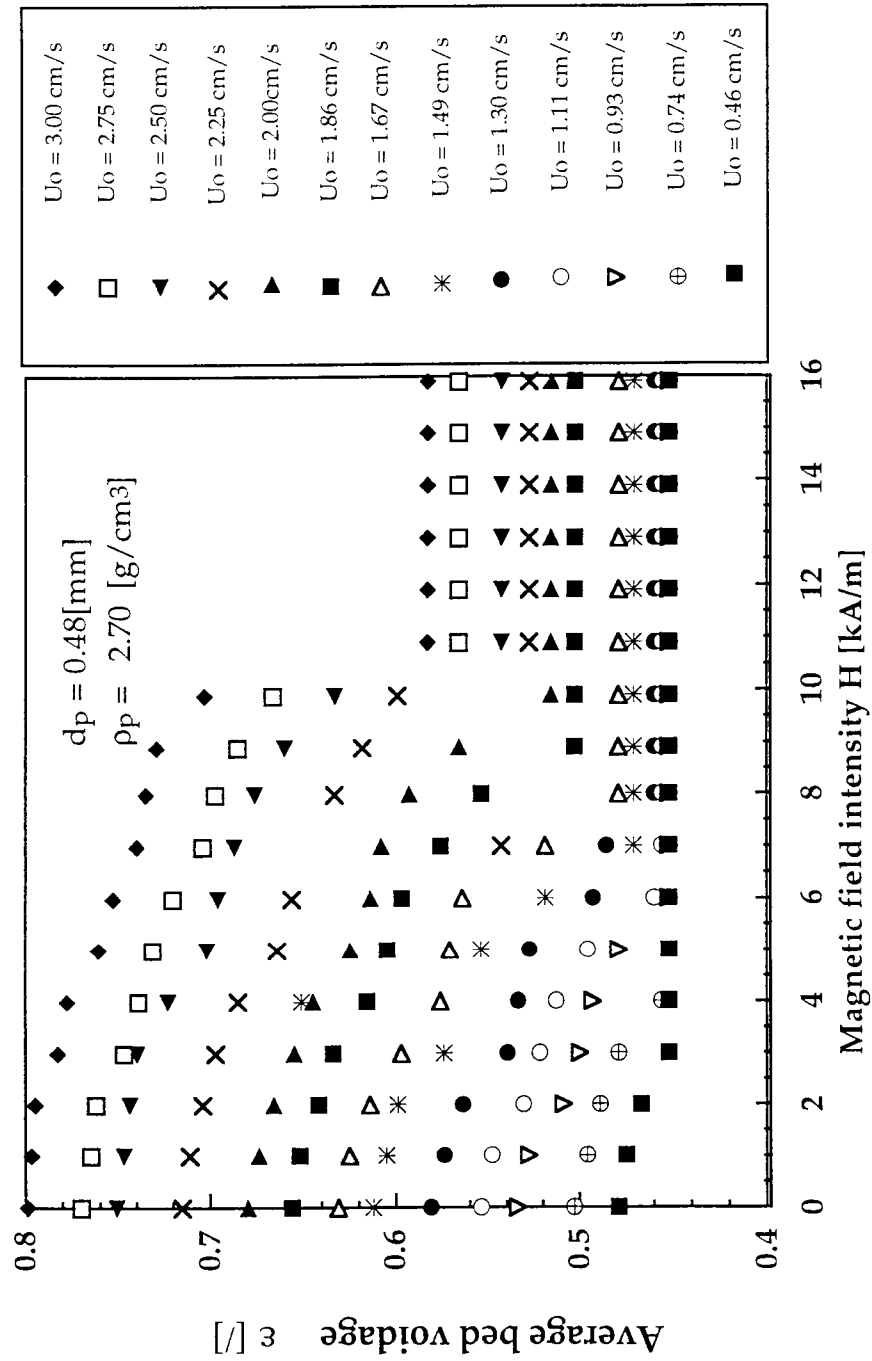


Figure 2.14: Effect of magnetic field strength on bed voidage.

Al-Mulhim (1995) presented the following correlation which excellently predicts the enhanced mass transfer coefficient in an MSFB within the range of experimental conditions in the presence of a homogeneous magnetic field.

$$Sh = \frac{0.054}{[\varepsilon_o - mx_{wt}H]^2} \frac{r^{0.67} u_o d_b}{m^{0.67} D_{AB} 0.33} \quad (2.69)$$

also,
$$Sh = \frac{k_l d_b}{D_{AB}} \quad (2.70)$$

$$k_l = \frac{0.054 u_o}{[\varepsilon - mx_{wt}H]^2} Sc^{0.67} \quad (2.71)$$

However, while these correlations attempt to provide a way to calculate the bed voidage, ε , or mass transfer coefficient, k_l , under a given set of conditions, they are limited to systems utilizing a homogeneous magnetic field. As a result of having a non-homogeneous magnetic field, we experimentally determined the bed voidage from the following definition:

$$\varepsilon = \frac{\text{Volume of bed} - \text{Volume between the particles}}{\text{Volume of bed}} \quad (2.72)$$

The correlations used to determine the liquid-particle mass transfer coefficient as reported by Coderc *et. al* (1972), Fan *et. al* (1960) and Cussler (1984), respectively, are.

$$Sh = \frac{0.054}{\varepsilon^2} Re Sc^{0.33} \quad (2.73)$$

$$Sh = 2 + 1.51(1 - \varepsilon) Re^{0.5} Sc^{0.33} \quad (2.74)$$

$$k_l = 2.0 + 0.6 Re^{0.5} Sc^{0.33} \quad (2.75)$$

The Sherwood number, Sh , is defined as in Equation 2.70.

$$\text{with } Re = \frac{\rho_l u_l d_b}{\mu_l} \quad (2.76)$$

$$\text{and } Sc = \frac{\mu_l}{\rho_l D_{AB}} \quad (2.77)$$

These correlations are implemented in Chapter 5 for comparison with the liquid-particle mass transfer coefficient obtained from optimization of the applied model developed in Section 2.2.

CHAPTER 3

EQUIPMENT, MATERIALS AND METHODS

3.1 Equipment

3.1.1 *Chemical Kinetic Apparatus*

To determine the chemical kinetics of dechlorination of *p*-chlorophenol on the Pd/Fe catalyst, a batch reactor is constructed in which freely suspended catalyst is continuously and vigorously stirred. A simple 400 [ml] reactor, an HCl metering pump, a pH controller with a pH probe and an N₂ supply line coupled with a variable speed mixer comprise the reactor system which provided sufficient control over process conditions. Figure 3.1 illustrates the apparatus. The acid supply for pH control is located on a balance to provide data for acid addition over the course of the reaction.

3.1.2 *Alginate Bead Generator*

The alginate bead generator, as shown in Figure 3.2, consists of a pressurized vessel, extrusion needle, air supply to the needle tip, and a catch beaker containing calcium chloride. The preparation of 1.5 [w/w %] alginate solution is described elsewhere (Appendix D). The solution is added to the pressurized vessel whereby it flows downward to the tip of the needle. The air supplied here allows for control of the particle size through control of the shear force. The bead drops into the catch beaker containing 1.5 [M] CaCl₂. Pd/Fe catalyst entrapment is described in further detail in section 3.4.2.

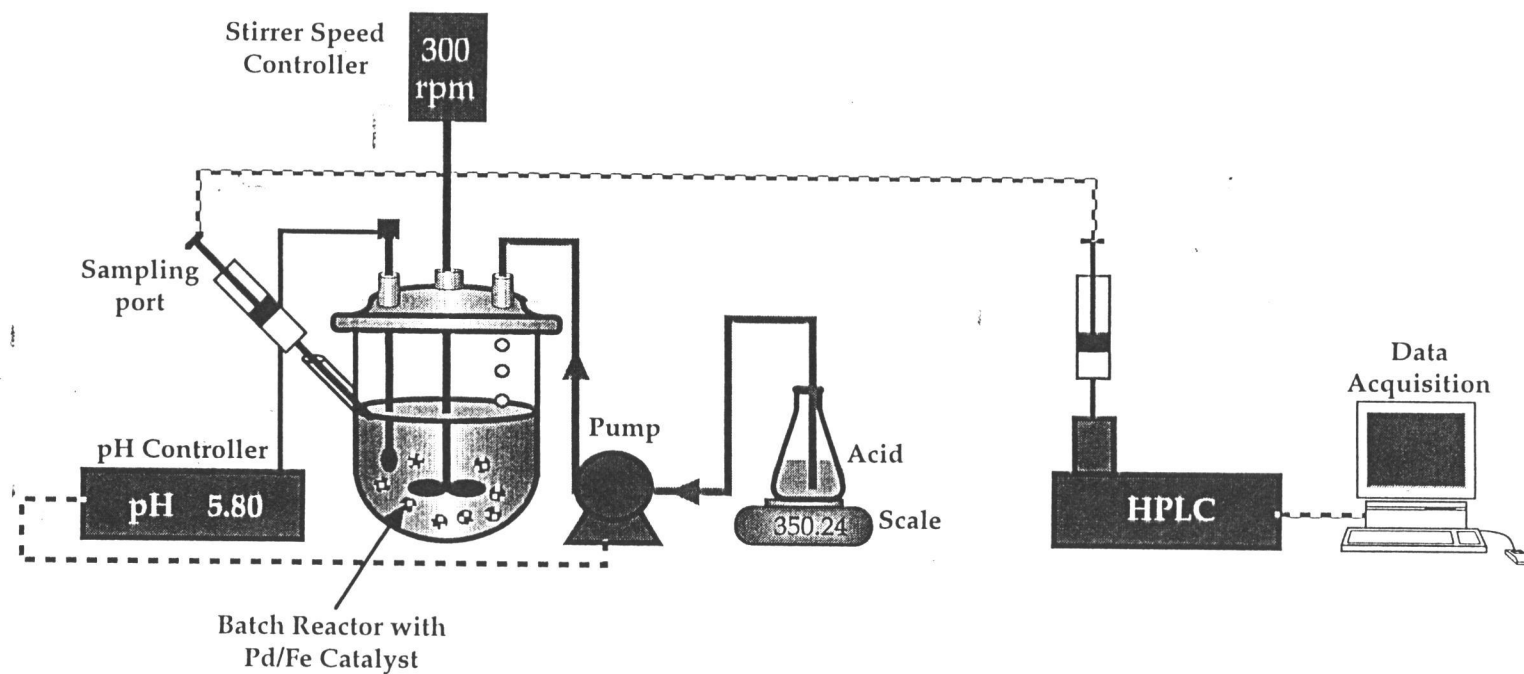


Figure 3.1: Chemical kinetic apparatus.

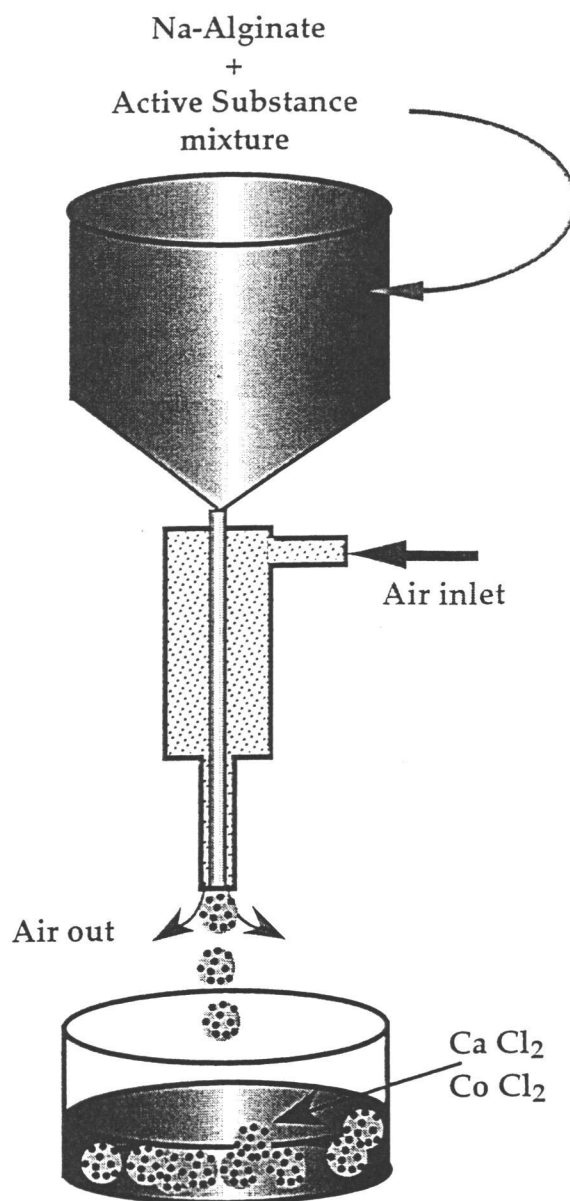


Figure 3.2: Alginate bead generator.

3.1.3 MSFB Apparatus

Figure 3.3 shows a schematic description of the MSFB apparatus used in this investigation. The reactor column measures 45 [cm] in height with a 3.8 [cm] inner diameter (i.d.) and 5.1 [cm] outer diameter (o.d.). The magnetic field is generated by wrapping copper wire ($d_{\text{wire}} = 1$ [mm]) around an acrylic tube measuring 40 [cm] in height with an i.d of 5.5 [cm] and o.d. of 6.0 [cm]. The coil consists of three layers of copper wire concentrically wrapped to varying heights which provides flexibility in generating a gradient magnetic field with a range of 6 to 12 [mT] (5,000-10,000 [A/m]) (Appendix G). A Masterflex peristaltic pump with tygon tubing recycles the liquid throughout the bed. Sampling is done on a small port located on the recycle line. An overflow box with lid allows insertion of a pH probe to monitor pH and allow acid addition during the experiment. All liquid is deoxygenated prior to use and an N₂ inlet prevents air from reaching the fluid thus maintaining deoxygenated conditions.

3.2 Materials

3.2.1 *p*-Chlorophenol and Phenol Properties

The physical properties of the model contaminant, *p*-chlorophenol, and the resulting product from the dechlorination reaction, phenol, are listed below. These properties include the solubility in water, volatility, density, molecular weight, boiling point and melting point (Table 3.1) (Perry and Green, 1984).

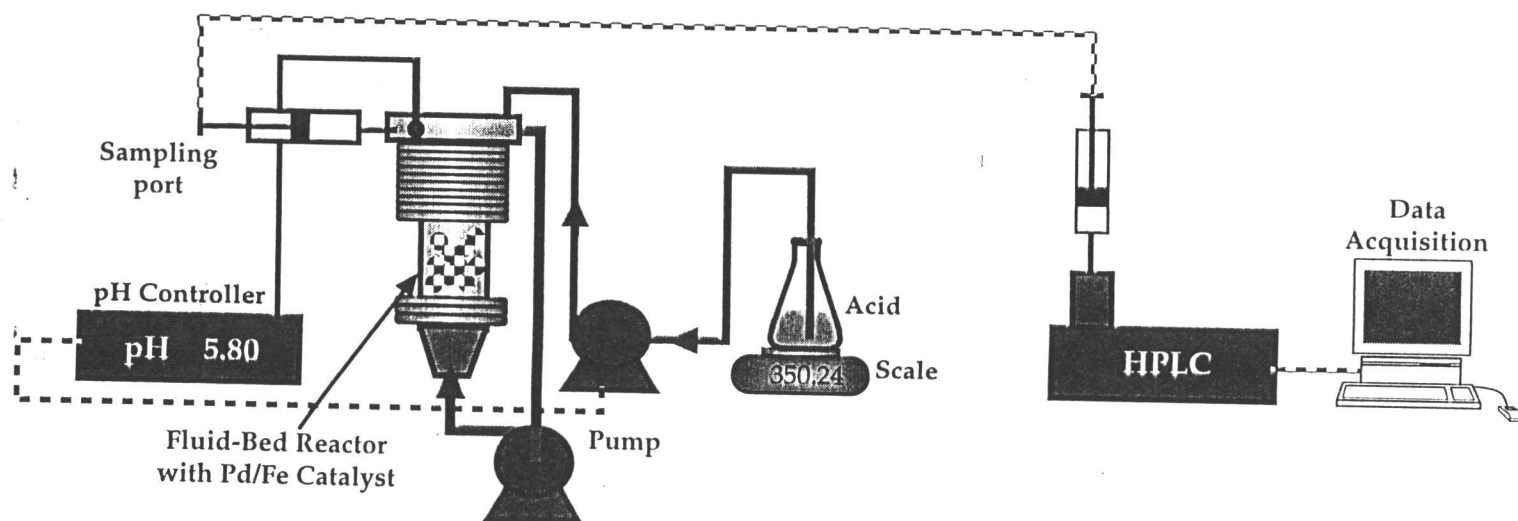


Figure 3.3: MSFB lab apparatus.

Table 3.1: Chemical Properties of *p*-Chlorophenol and Phenol

	<i>p</i> -Chlorophenol	Phenol
Chemical Formula	4-ClC ₆ H ₄ OH	C ₆ H ₅ OH
Molecular Weight (g/mol)	128.56	94.11
Boiling Point (°C) at 1 atm	-----	181.7
Melting Point (°C) at 1 atm	121-2	43
Specific Gravity	-----	1.0576
Vapor Pressure (atm) at 20°C	-----	2.6x10 ⁻⁴
Solubility in Water	1000 ppm	1500 ppm
pKa (20-25°C)	9.18	9.82

p-Chlorophenol was obtained from Acros Organics (purity: 99+%) and phenol (purity: 98.5%) was obtained from Baker Chemical Company. Both solid forms were maintained in a dessicator and stock solutions were maintained in volumetric flasks under fume hood.

3.2.2 Pd/Fe Catalyst

The iron used for this catalyst is a 5-8 [μm] iron powder obtained from Aldrich Chemical Company. The palladium was obtained from Aldrich Chemical Company in the form of a salt, hexachloropalladate (K₂PdCl₆), which was dissolved in water prior to palladization. The iron powder is pretreated with 6 [M] HCl for 15 [min] and rinsed with two 25 [ml] aliquots of deionized water. The iron is added to the hexachloropalladate solution and is mixed vigorously for 4 minutes. The palladized iron is then rinsed with 50 [ml] of deionized water. SEM were taken which show acid treated iron prior to palladization as well as with nano-size palladium islets. (Figure 3.4a,b). Further investigation into the preparation of the Pd/Fe catalyst is discussed in section 3.3.1.

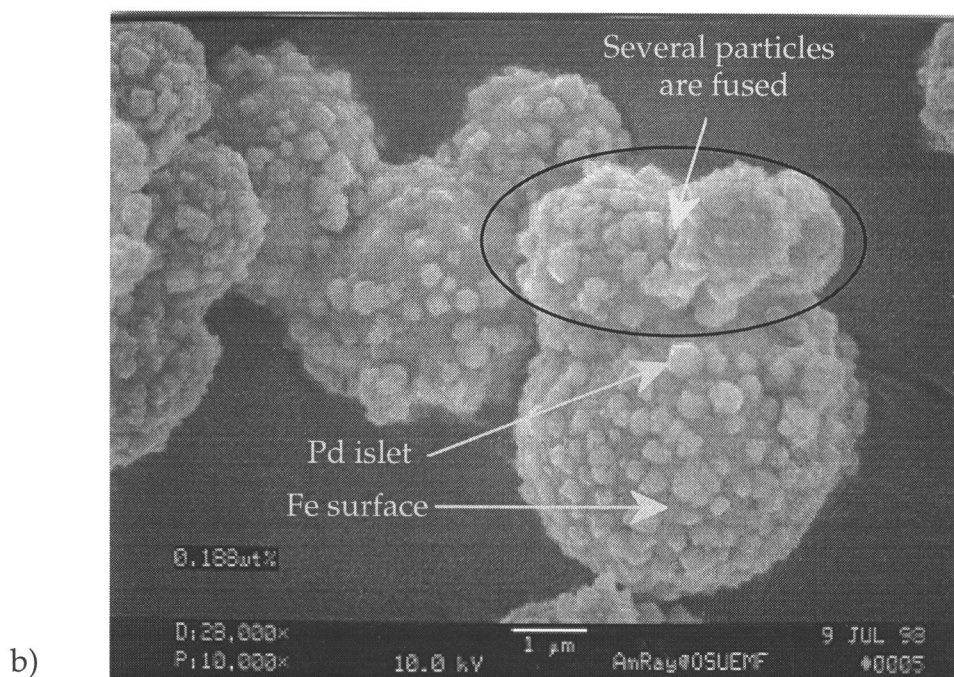
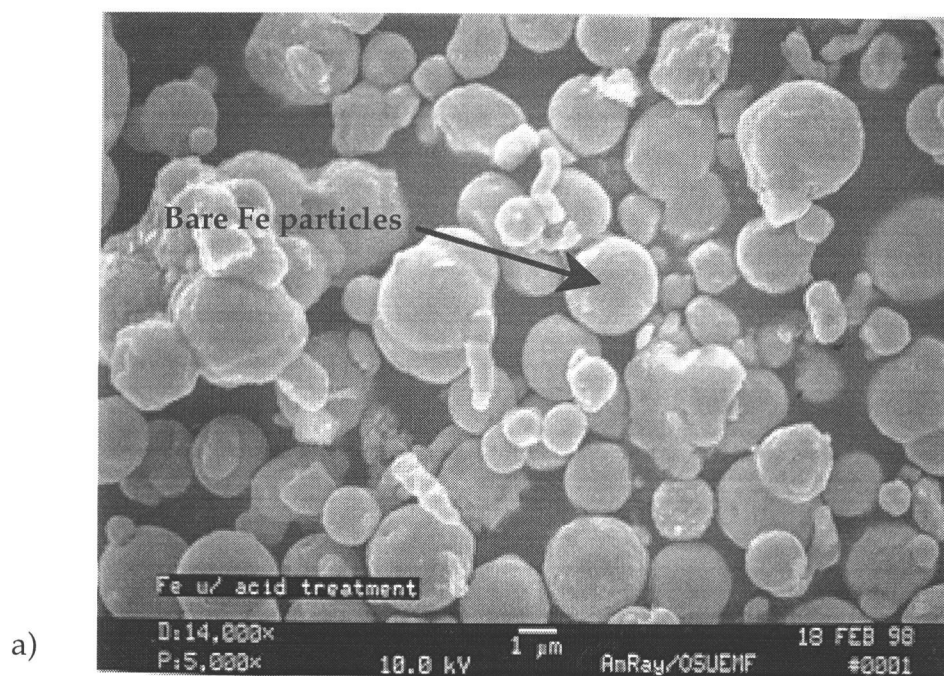


Figure 3.4: Scanning electron microscopy pictures: a) Acid pretreated Fe particles, b) Palladized Fe particles.

3.2.3 Alginate

Sodium alginate was donated by Kelco company under the trademark name, Keltone HV (Keltone Product, 1996). Keltone HV is derived from a giant brown kelp, *Macrocystis pyrifera*, and consists of alternating D-mannuronic and L-guluronic acid units. When dissolved in distilled water, a solution is prepared whose flow characteristics are affected by shear rate, polymer size, temperature, concentration in solution and the presence of miscible solvents. For all experimental work, a 1.5 [%] solution of algin and 98.5 [%] distilled water was prepared at room temperature before any active substance was added for entrapment (Appendix D).

3.2.4 Soil Properties/ Contaminant Interaction

The mass transfer between contaminated solids and aqueous solutions is an important phenomena in the overall treatment of contaminated media. The knowledge of the fate of organic contaminants within a soil system is of utmost importance for modeling purposes. Since there are many types of soils consisting of varying degrees of sand, silt, clay and organic matter, it is important to test for the fraction of organic matter responsible for sorption behavior since the organic content of the soil is the most important soil fraction determining sorption. Sorption depends on the interaction of a contaminant with particular characteristics of the soil surface and thus it is necessary to know the chemical characteristics. Both *p*-chlorophenol and phenol are examples of neutral organic compounds at common environmental conditions. The pKa values of *p*-chlorophenol and phenol at 20-25°C are approximately 9.18 and 9.82, respectively. At pH values below a

pH of 9.18 and 9.82, 99.3 and 99.8% of the *p*-chlorophenol and the phenol are in acid form (Schwarzenbach, 1993). Therefore, the organic compounds are assumed neutral for this reaction in which the pH is always below 7. This is important when determining the sorption behavior of the chlorinated organics onto the soil by using correlations for sorption of neutral organic compounds.

Two distinct soils were examined as described in the methods section and their respective particle sizes and fractions of organic carbon were determined (Appendix E). The two soils exhibit quite different properties. A high organic fraction, $f_{oc}=2.18 \pm 0.08$, of the Willamette Valley type soil indicates the higher capacity for sorption of *p*-chlorophenol and phenol. Due to the low organic content of the soil from the government site in Idaho, $f_{oc}=0.692 \pm 0.009$, it was not used for adsorption testing. The Willamette Valley type soil was used for all adsorption and decontamination experiments.

3.3 Methods for Dechlorination

3.3.1 Pd/Fe Catalyst Preparation

Exactly 4.0 [g] of iron powder (< 5-8 [μ m] , 99.9+%, from Aldrich, Milwaukee, WI) is washed with 25 [ml] of 6 [M] HCl for 15 minutes and rinsed with distilled water to remove surface oxide layers prior to palladization. An aqueous solution of hexachloropalladate (K_2PdCl_6 , 99% from Aldrich, Milwaukee, WI) is prepared to give a 0.02-0.75 [w/w %] palladium coverage. Electrochemical deposition produces a palladized iron surface according to the following reaction (3.1).



The reaction is considered complete when the dark orange solution turns to a pale yellow within 5 minutes as described by Grittini *et. al* (1995). The palladized iron is then rinsed twice with 25 [ml] aliquots of deionized water and used for reaction without drying.

The preparation procedure for the Pd/Fe catalyst is an important element for understanding the kinetics of dechlorination. Several factors in the preparation of the Pd/Fe catalyst which must be considered are a) the acid pretreatment of the iron, including strength of HCl and application time, b) the palladium concentration in solution during palladization, and c) the palladium to iron weight ratio or surface coverage by palladium.

a) Acid Pretreatment of the Iron Particles

An important function of the Pd/Fe catalyst is the reaction involving the dissolution of iron from the catalyst surface into the aqueous solution as expressed by equation 3.2.



4.0 [g] of iron was reacted at varied pH and the consumption of H^+ was recorded in Figure 3.5. The graph shows H^+ consumption over the course of the dechlorination reaction which can be plotted as a function of weight of Pd/Fe available for the surface dissolution reaction (Equation 3.2) (Figure 3.6). A balance on the moles of H^+ utilized for the dechlorination reaction accounts for only 1% of the H^+ added while the dissolution of Fe^0 by water accounts for nearly 99%.

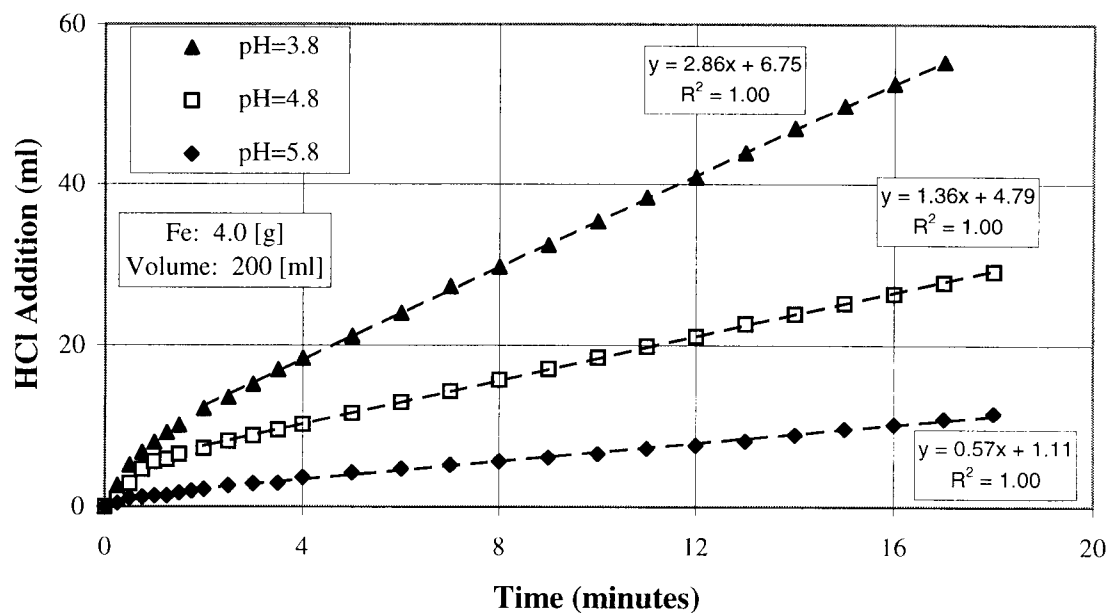


Figure 3.5: Addition of H^+ ions to maintain pH as a result of iron dissolution.

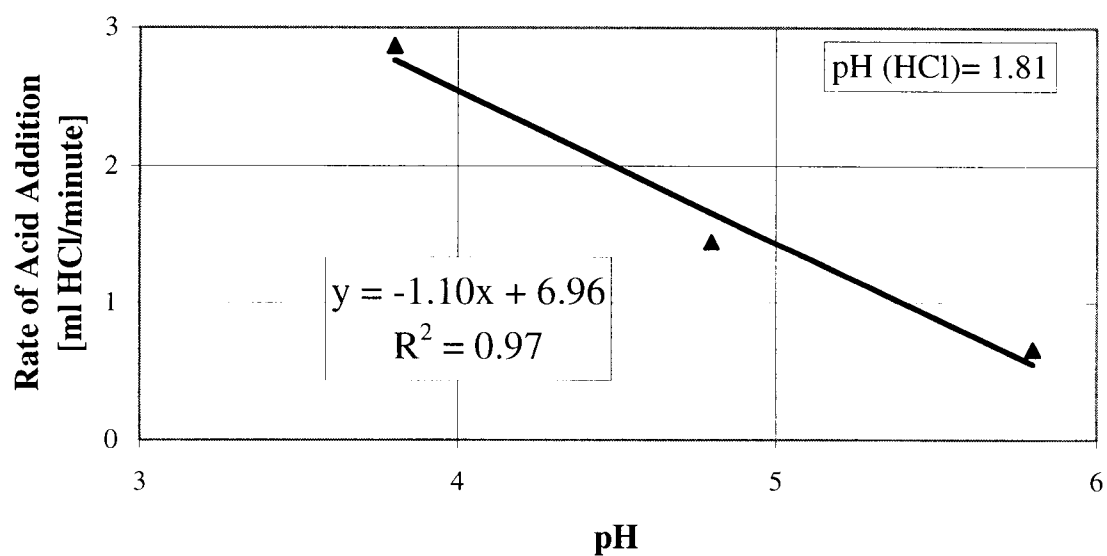


Figure 3.6: H^+ consumption on the Pd/Fe surface as a function of Pd/Fe catalyst available for reaction.

There is an indication in the literature that pretreatment of Fe with acid is an important step. However, the level of importance has not been fully established with investigators using a range of acid strengths and pretreatment times (Grittini *et. al*, 1995). To test the effect of the acid pretreatment of iron to remove surface oxide layers prior to palladization, the acid strength for 15 minutes was varied for the three separate runs and no statistical difference was observed using an F-test (Figure 3.7).

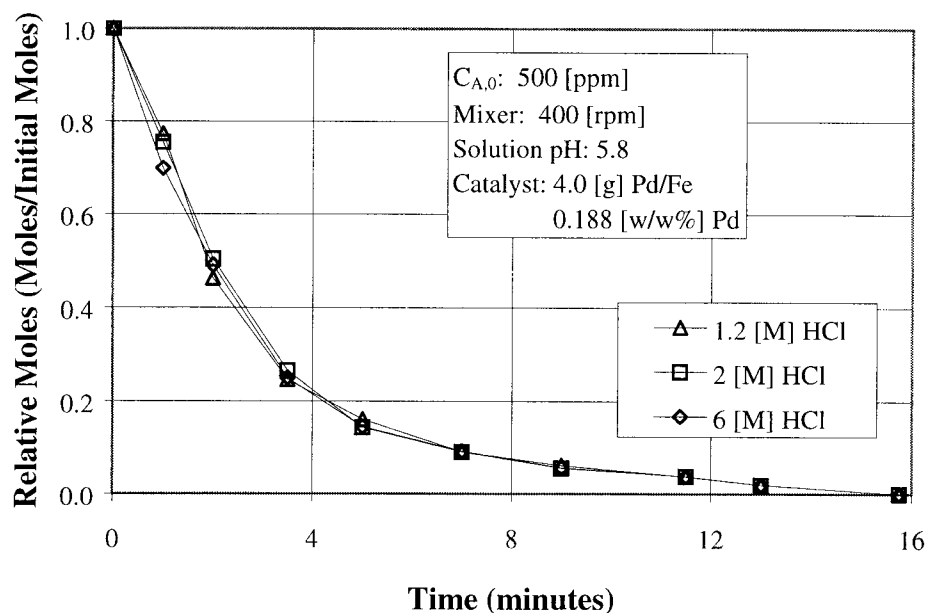


Figure 3.7: Effect of acid strength during Fe pretreatment on *p*-chlorophenol dechlorination.

b.) Pd Concentration During the Pd/Fe Palladization Reaction

A surprising observation was made with respect to the concentration of palladium during the palladium deposition reaction. Three catalyst samples were made with identical weights of iron and palladium. The iron was pretreated with 6 [M] HCl for 15 minutes as described above. 0.030 [g] of the palladium salt, K_2PdCl_6 , was dissolved in

800 [ml], 400 [ml] and 100 [ml] distilled water, respectively. The catalysts were reacted separately with a 450 [ppm] *p*-chlorophenol solution at pH=5.8. As shown in Figure 3.8, a slightly faster rate was observed in the 400 [ml] over the 800 [ml]. The palladium salt, which had been initially dissolved in 100 [ml] of distilled water, demonstrated a much faster initial rate. All three reactions completed the dechlorination at approximately the same time. Statistical F-tests indicate that the 800 [ml] and 400 [ml] runs are statistically similar while the 400 [ml] and 100 [ml] runs are statistically different. The 800 [ml] and 100 [ml] runs are also statistically different.

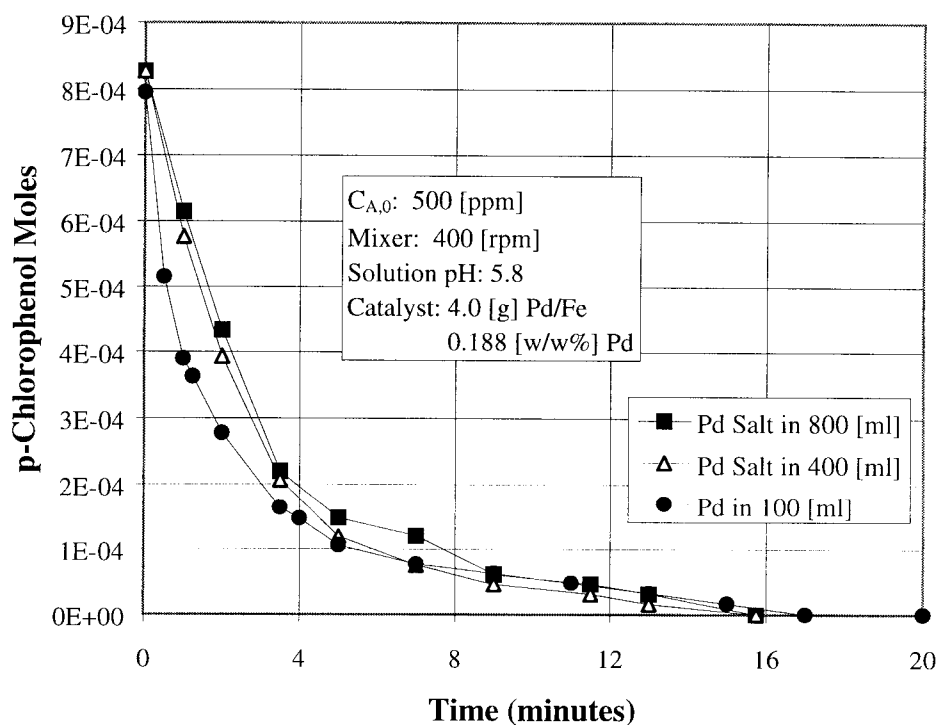


Figure 3.8: Effect of palladium concentration during catalyst preparation on reaction rate

Scanning electron microscopy (SEM) pictures were taken to determine the cause of this behavior. Figures 3.9a-b are SEM pictures of the Pd/Fe catalyst surface from the 400 [ml] and 100 [ml] palladization solutions. Since Pd/Fe interfacial area is important for rate of dechlorination, some possible explanations for the behavior in Figure 3.8 include the deposited size and crystalline shape of the palladium islets upon the iron surface. The SEM pictures indicate that different crystallization conditions are present with the average Pd islet size being much larger for the 400 [ml] than the 100 [ml] case, respectively. As a result, the preparation of the Pd/Fe catalyst included was prepared under uniform conditions of iron pretreatment and concentration of palladium in the palladization solution for all rate data reported.

c.) Palladium to Iron Weight Ratio/ Surface Coverage by Palladium

As the Pd/Fe interfacial area is important for the reaction, catalyst samples are prepared which have 0.045 [w/w %], 0.188 [w/w %], and 0.67 [w/w %] and 0.75[w/w %] (Figures 3.10a-d). As shown, the amount of palladium islets increases from the smallest weight percentage with bare iron showing as a dark gray between islets up to the largest weight percentage which demonstrates nearly complete coverage with secondary layer formation. As discussed by Graham and Jovanovic (1998a), extreme coverage of the iron surface results in negligible surface area and no reaction is observed. A careful method of surface preparation was followed in all experiments. For further kinetic study, 0.188 [w/w %] Pd/Fe is used to maintain consistency of the surface performance.

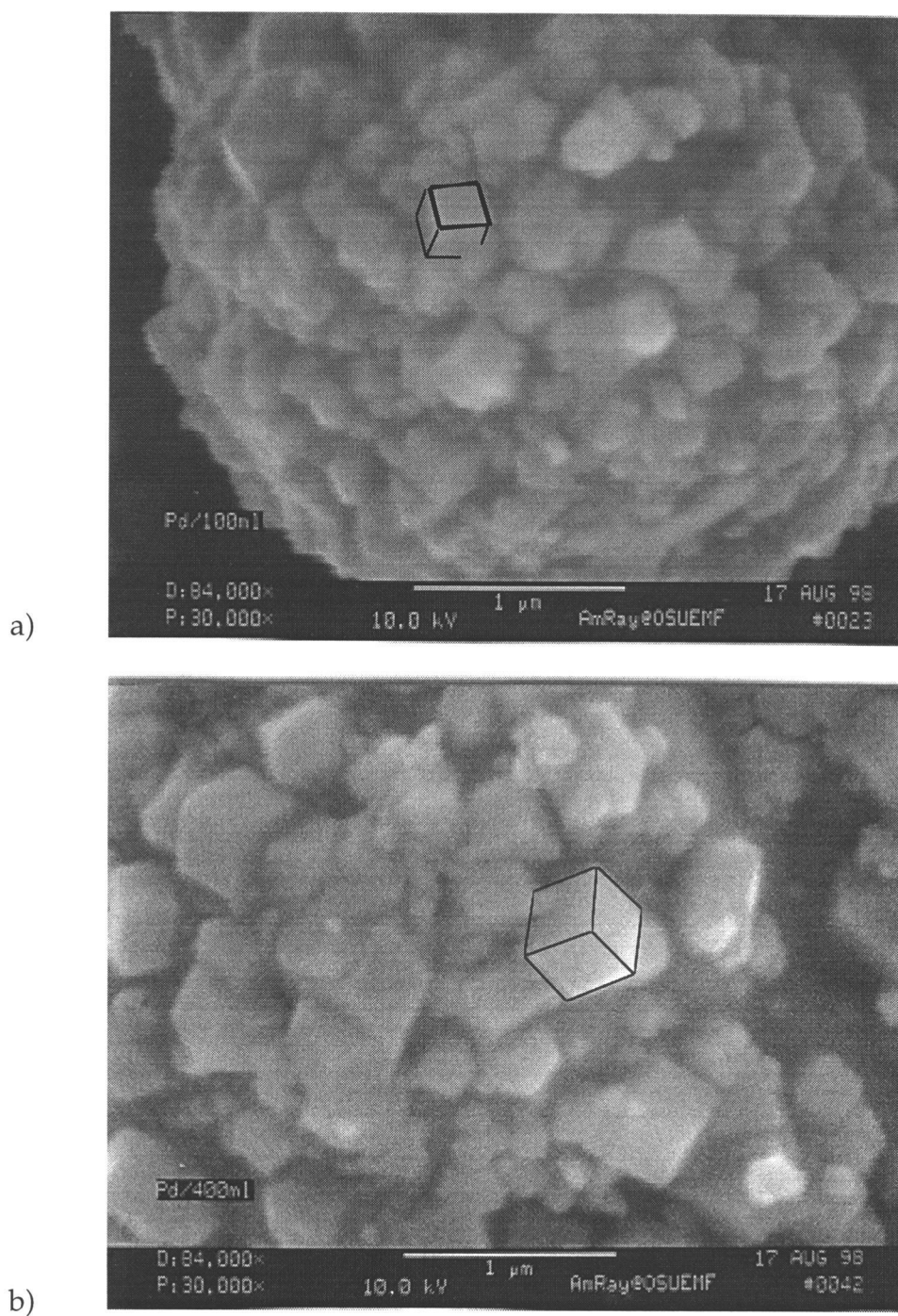


Figure 3.9: SEM pictures of Pd/Fe catalyst with a) high palladium solution concentration, b) low palladium solution concentration.

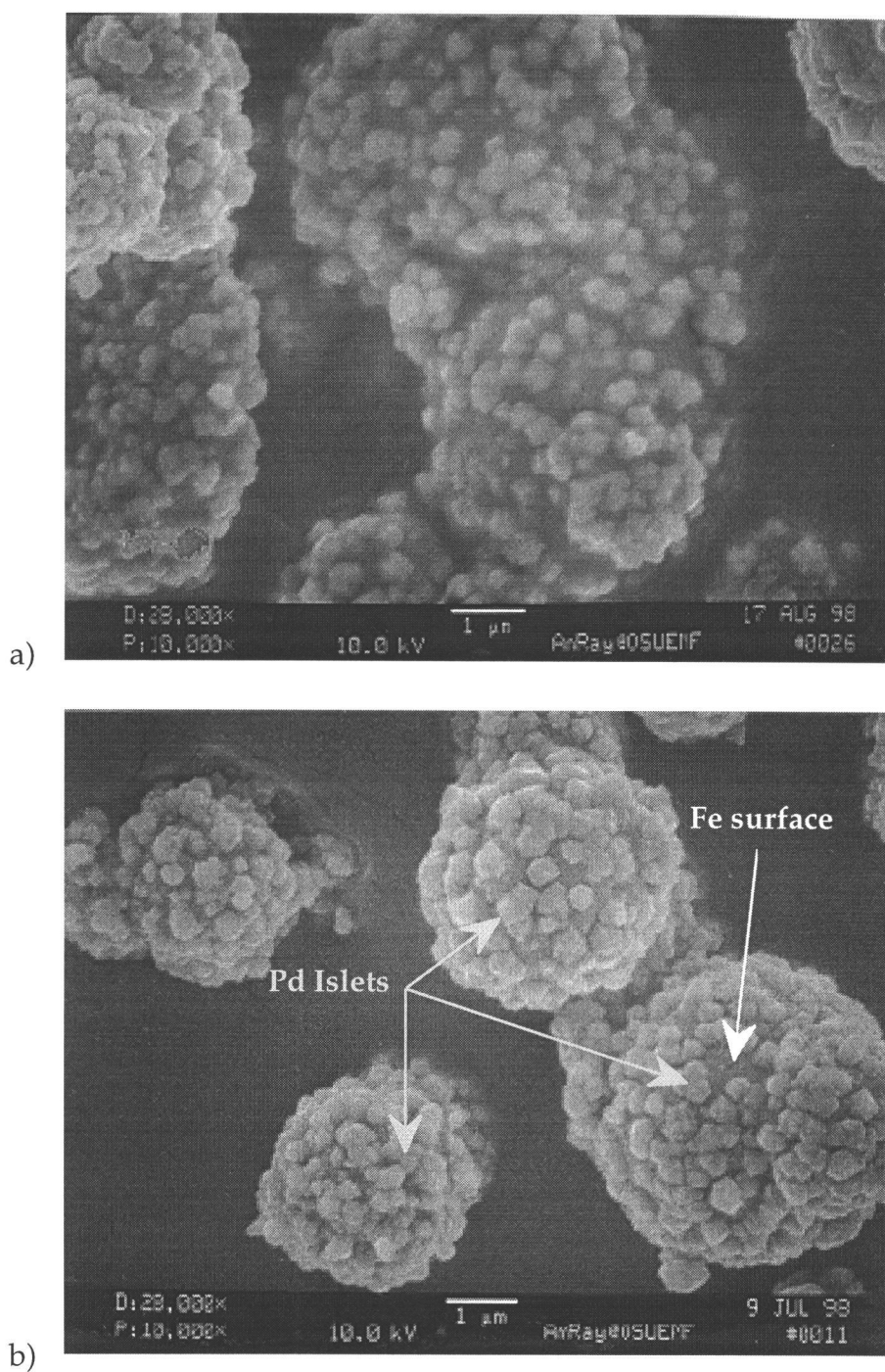


Figure 3.10: Varied surface coverage of iron by palladium (Pd/Fe [w/w%])
 a) 0.048 [w/w%], b) 0.188 [w/w%], c) 0.67 [w/w%], d) 0.75 [w/w%].

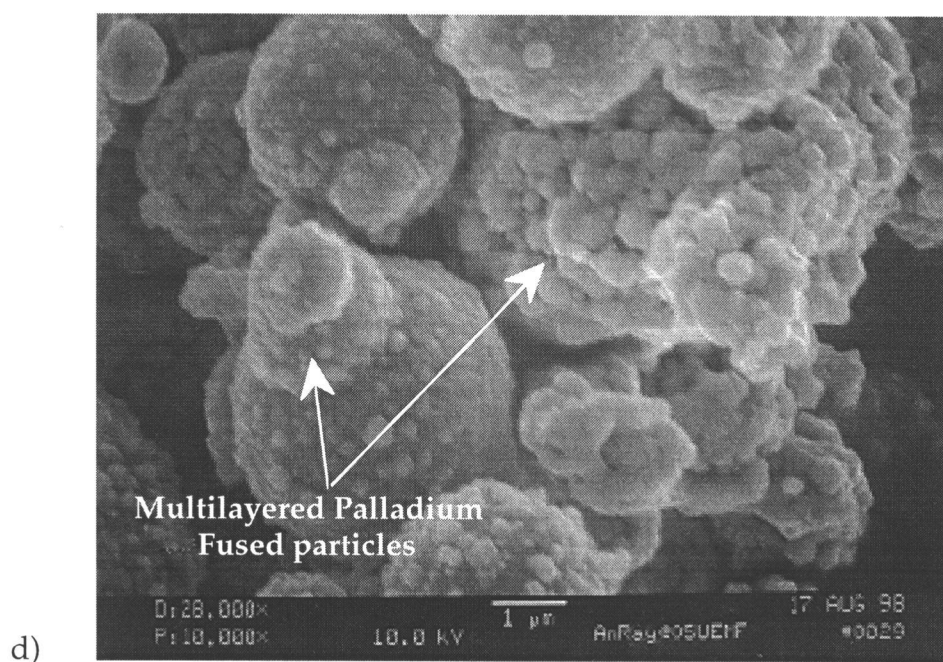
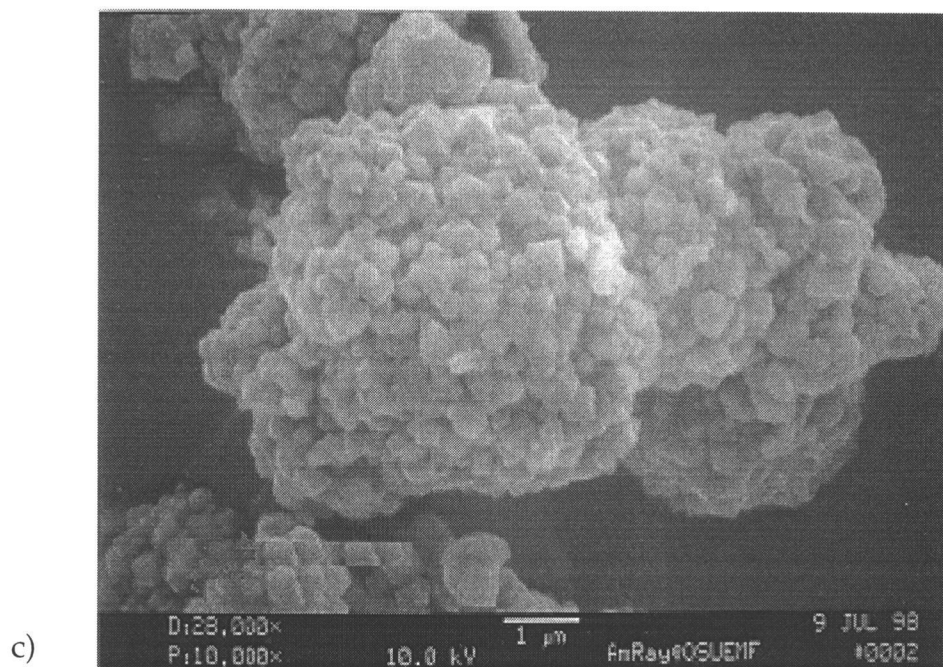


Figure 3.10 (con't): Varied surface coverage of iron by palladium (Pd/Fe [w/w%])
a) 0.048 [w/w%], b) 0.188 [w/w%], c) 0.67 [w/w%], d) 0.75 [w/w%].

3.3.2 Repeatability and Reusability of Pd/Fe Catalyst

Repeatability of Pd/Fe Catalyst

The three steps involved in the preparation of the Pd/Fe catalyst include:

1. Iron Acid Pretreatment
2. Palladization Solution Preparation
3. Palladization Reaction on Iron/ Pd/Fe Distilled Water Rinse

It was important to establish the repeatability of this procedure to ensure accurate results from all kinetic rate experiments. Figure 3.11 represents three individual dechlorination experiments, with all conditions being equal, which reflect the duplication of results from one run to the next. An F-test for statistical analysis demonstrates that the runs are not statistically different. From this data, a catalyst preparation procedure was developed and followed for all subsequent dechlorination reactions with 0.188 [w/w %] Pd/Fe.

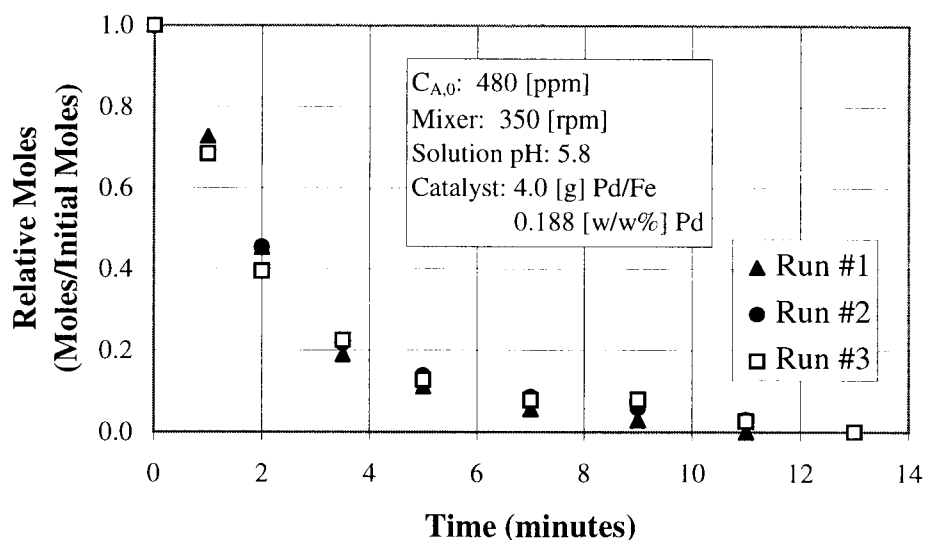


Figure 3.11: Repeatability of Pd/Fe catalyst preparation for *p*-chlorophenol dechlorination.

Reusability of Pd/Fe Catalyst for Subsequent Reactions

The reusability of the Pd/Fe catalyst was also explored during this investigation. The dissolution of iron from Fe^0 to Fe^{2+} as discussed in Chapter 2 introduces the loss of iron substrate and the eventual loss of the deposited palladium islets. As a result, the overall iron particle size and number of palladium islets (Pd/Fe interfacial area) is decreased for subsequent reactions. Two experiments are reported showing a 63 [%] decrease in overall dechlorination for a 62.5 [%] loss in Pd/Fe catalyst weight (Figure 3.12). SEM pictures were taken both before and after reactions were performed under acidic conditions which show a decrease in the average Pd/Fe particle size as well as “jagged” edges from acid dissolution of the spherical particles (Figures 3.13a-b).

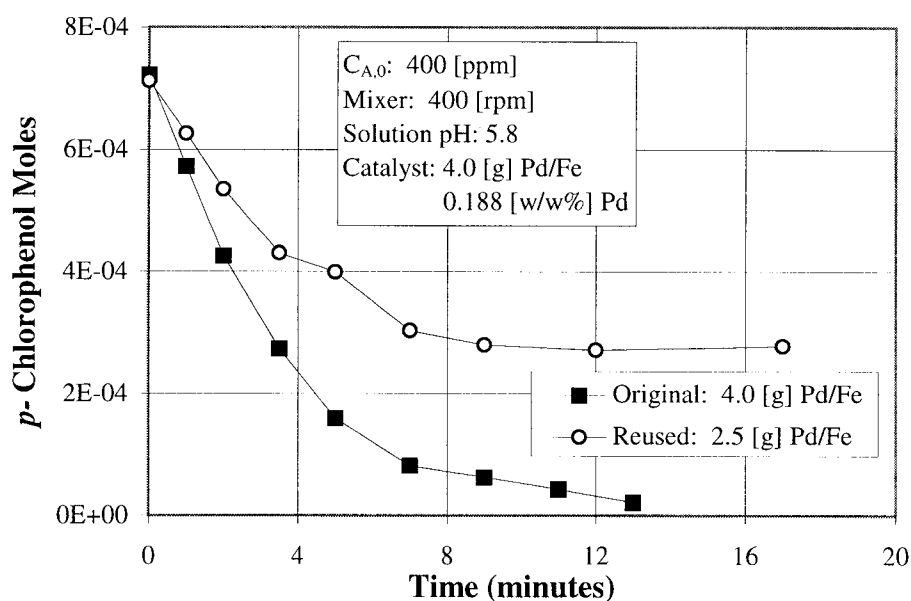


Figure 3.12 : Reusability of Pd/Fe catalyst with loss from iron dissolution reaction.

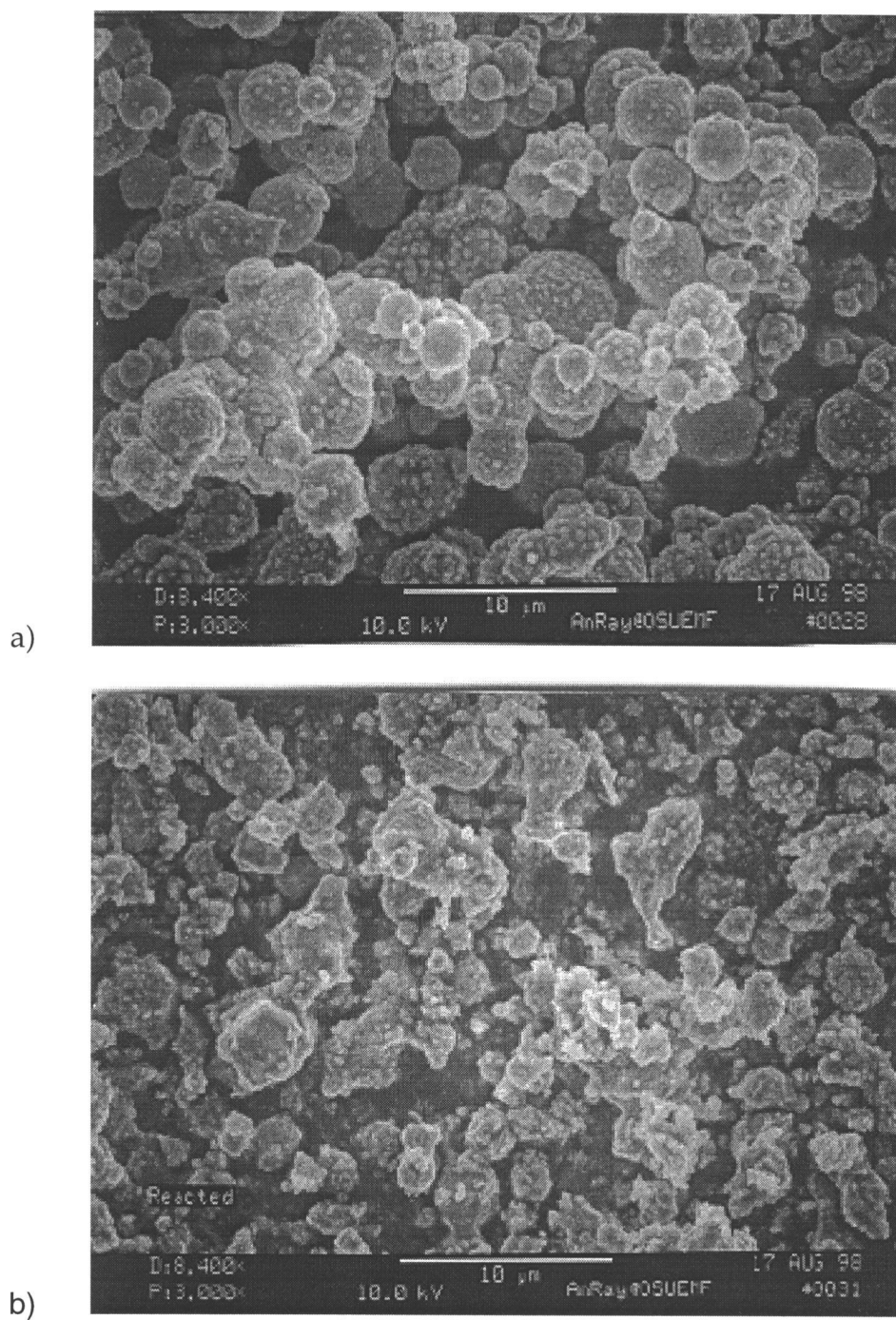


Figure 3.13: SEM pictures of the Pd/Fe catalyst showing extent of recoverability
a) Freshly prepared Pd/Fe, b) Reacted Pd/Fe.

3.3.3 Pd/Fe Entrapment / Particle Design Flexibility

For reactions involving the entrapment of the Pd/Fe catalyst, a solution of 1.5 [%] sodium alginate and 98.5 [%] deionized water is prepared. The alginate solution is mixed with the powdered 0.188 [w/w%] Pd/Fe to obtain a 5-15 [w/w %] solution. This solution is poured into a pressurized vessel and extruded into a calcium chloride solution. Air supplied to the tip of the nozzle and the amount of pressurization of the vessel allows for control of bead size ($d_p=1000-2000$ [μm]).

The alginate bead is released into CaCl_2 solution where the alginate exchanges two Na^+ ions for a Ca^{2+} which immediately creates the protective “skin” of the particle. To ensure reproducible gel beads, the particles are left in a 1.5 [M] CaCl_2 solution for exactly 30 minutes to maintain a consistent extent of polymerization.

The fluidization particles used in MSFB are composite ferromagnetic particles which are prepared from the mixture of sodium alginate and Pd/Fe powder. In the process of dechlorinating the *p*-chlorophenol from a liquid or slurry, the Pd/Fe catalyst is added into the alginate particles to form OSU-Sorb-2R types of particles. The individual bead characteristics are shown in Table 3.2.

Table 3.2: Particle Characteristics

		Sorb-OSU-1 (Alginate)	Sorb-OSU-2R (OSU-Sorb-1 + Pd/Fe)
Nominal Particle Diameter	d_p [mm]	1.0 - 3.0	2.0
Particle Density	ρ_p [g/ml]	1.10	1.173
Bed Voidage at u_{mf}	ϵ_{mf}	0.375	0.375
Minimum Fluidization Velocity	u_{mf} [cm/s]	0.02 - 1.4	1.04
Na-alginate wt. % in beads	w/w %	1.5	1.5
Ferro. magnetic material/ Pd/Fe	w/w %	0	12.0

3.3.4 Determination of *p*-Chlorophenol and Phenol Concentrations

To analyze the *p*-chlorophenol and/or phenol concentrations, high-performance liquid chromatography (HPLC) is used. The apparatus consists of a pump to deliver the mobile phase at 2.0 [ml/min], a 20 [μ L] sample loop, a LC-8 column from Supelco with reverse phase silica gel packing, and a Gilson uv detector set to a wavelength of 254 [nm]. The mobile phase consists of 60 [%] acetic acid-methanol solution (1 [%] CH_3COOH , 99 [%] $\text{CH}_3\text{CH}_2\text{OH}$) and 40 [%] acetic acid-distilled water solution (1 [%] CH_3COOH , 99 [%] H_2O). A series of known *p*-chlorophenol and phenol solutions of concentrations ranging from 0 [ppm] to 1000 [ppm] are prepared and injected into the sample loop. Two peaks, *p*-chlorophenol and phenol, are eluted from the silica gel column within the HPLC at different characteristic times with their individual peaks being well separated. The voltage output from the absorbance in the uv detector is delivered to Visual Designer, a software package used for data acquisition. Peak heights and peak areas were checked

and gave linear relationships for the aqueous compounds concentration. Therefore, standard curves for peak absorbance vs. concentration are determined for both *p*-chlorophenol and phenol and plotted in Figures C.1 and C.2, respectively in Appendix C.

3.3.5 Absorption of *p*-Chlorophenol to Alginate Beads

To determine the adsorption isotherm of alginate beads, several flasks are set up with varied amounts of alginate beads. Each flask receives 25 [ml] of a 3.91×10^{-3} [M] solution of *p*-chlorophenol solution. The flasks are placed in a shaker for 24 hours and the equilibrium concentrations are recorded. Mass balance equations give the amount sorbed into the alginate in relation to the amount remaining in the bulk solution. The flasks are sampled again after another 24 hours to ensure that the system has reached equilibrium. The absorption isotherm is shown in Figure 3.14 with the linear relationship expressed as

$$C_{bd} = K_b * C_b \quad (3.3)$$

with C_{bd} [moles/kg soil] representing the amount of *p*-chlorophenol sorbed on the gel beads, C_b [moles/L solution] representing the amount of *p*-chlorophenol in the bulk solution, and K_b as the slope of the line.

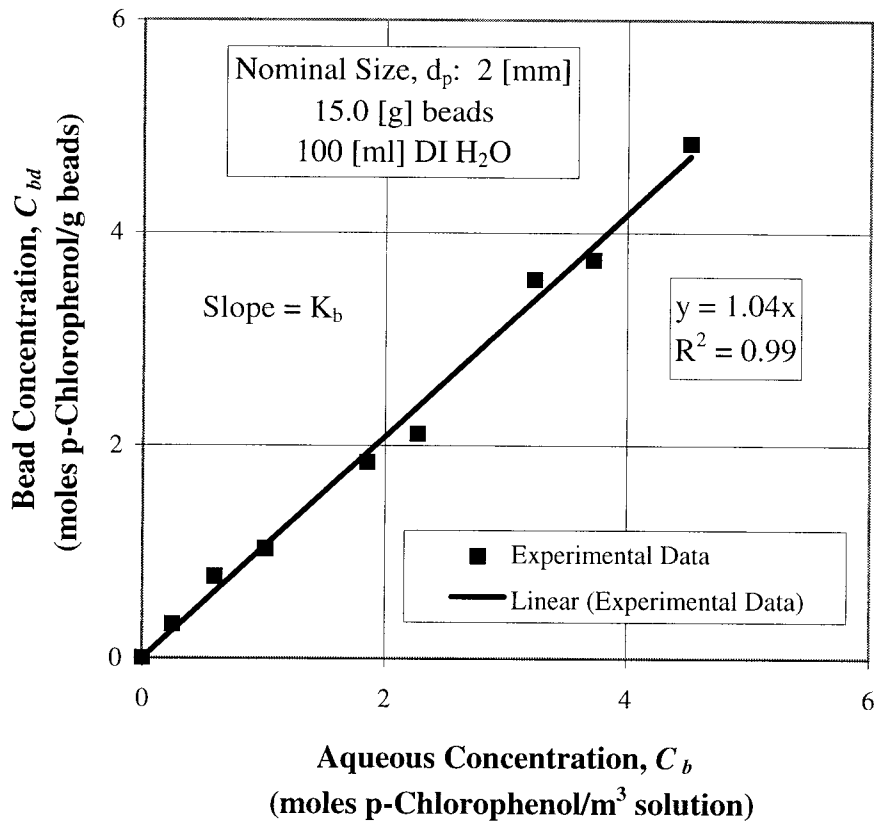


Figure 3.14: *p*-Chlorophenol absorption isotherm on alginate beads.

3.3.6 Soil Adsorption and Desorption of *p*-Chlorophenol

To quantify the abundance of adsorbed organic material on the soil particles at equilibrium, a sorption isotherm for *p*-chlorophenol on Willamette type soil is developed. A common experimental method of determining the solid-water partition coefficient, K_d , involves the application of the Freundlich isotherm, where n measures nonlinearity.

$$C_s = K_d * C_w^n \quad (3.4)$$

C_s represents the concentration of the organic compound on the soil and C_w represents the concentration of the organic compound in the aqueous solution (Schwarzenbach, 1993).

Another method for obtaining the K_d value is by developing the relationship between the octanol-water partition coefficient values, K_{ow} , and the distribution coefficient between water and the organic matter, K_{om} , which are available in literature as well as the fraction of organic matter characteristic of the soil being examined, f_{om} . An empirical relationship between the K_{om} and K_d values has been determined by investigators to be:

$$K_d = K_{om} * f_{om} \quad (3.5)$$

with f_{om} assumed to be approximately $1.8-2 * f_{oc}$ (Schwarzenbach, 1993).

The results from applying the two methods for determining the K_d value for *p*-chlorophenol on Willamette Valley soil are as follows:

Freundlich Approach:

The Freundlich sorption isotherms for *p*-chlorophenol on Willamette Valley soil at 20°C and pH = 6.0 ± 0.05 is shown in Figure 3.15.

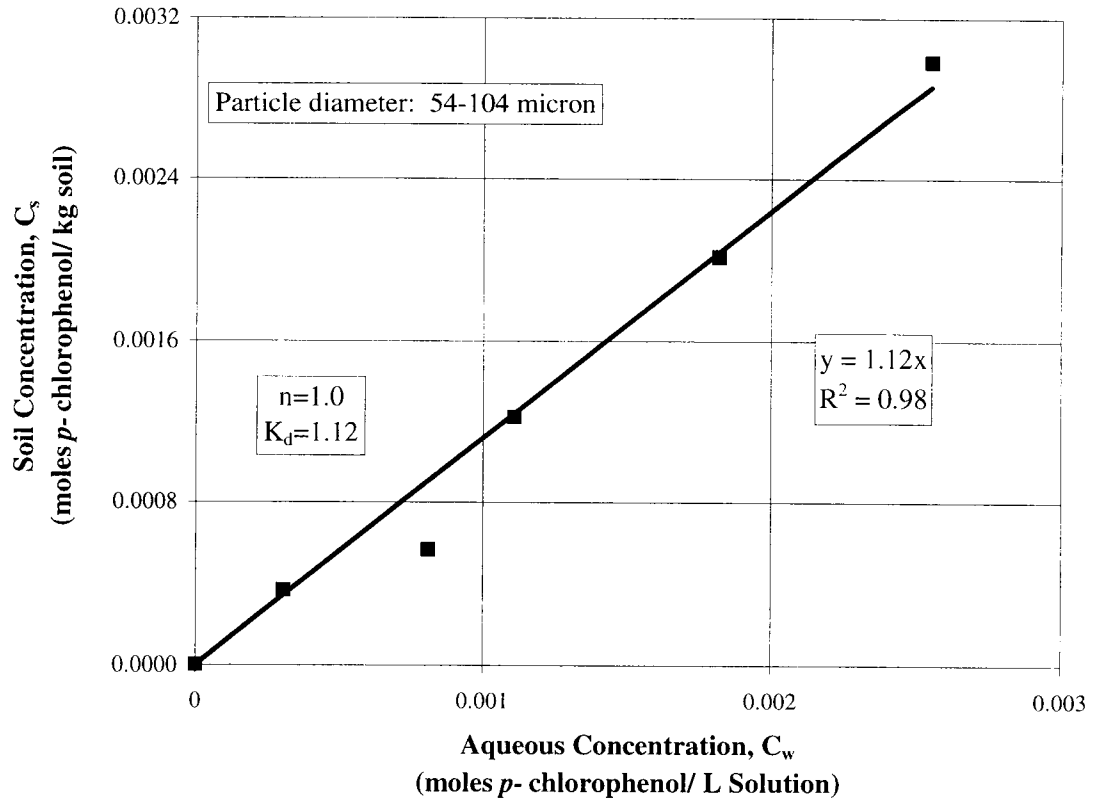


Figure 3.15: Adsorption isotherm for *p*-chlorophenol onto Willamette Valley type soil.

The application of a Freundlich isotherm model with $n=1$ fits the experimental data adequately ($R^2=0.98$). The experimentally determined value of the partition coefficient (slope in Figure 3.15) K_d value is:

p-chlorophenol:
$$K_d = 1.12 \frac{\text{moles/kg}_{\text{soil}}}{\text{moles/L}_{\text{solution}}}$$

This experimentally obtained value can be compared with values of the partition coefficient calculated from Equation (3.7) and utilizing the values of $K_{om}=31.43$ and

$f_{oc}=2.18 \pm 0.08$ at a system pH of 6.0 (Calculations are reported in Appendix F using correlations found in literature).

$$f_{om}=1.8-2.0 *f_{oc} \quad (3.6)$$

$$K_d = K_{om} * f_{om} \quad (3.7)$$

p-chlorophenol: $K_d = 1.37 \frac{\text{moles/kg}_{soil}}{\text{moles/L}_{solution}}$ with $f_{om}=2.0*f_{oc}$

The two methods of calculating the partition coefficient give comparable results with uncertainty arising only from the assumption for the f_{om} value and the determination of the K_{om} value for p-chlorophenol. If the f_{om} value was calculated at $1.8*f_{oc}$ instead of the approximated $2*f_{oc}$ then the value would be as follows:

p-chlorophenol: $K_d = 1.19 \frac{\text{moles/kg}_{soil}}{\text{moles/L}_{solution}}$

For modeling purposes, however, the experimentally determined K_d value for *p*-chlorophenol was used.

After investigating the soil/bulk liquid equilibrium, a *p*-chlorophenol desorption curve from the Willamette Valley type soil was determined. 10 [ml] of hexane containing 0.0086 [g] of *p*-chlorophenol was added to 20 [g] of soil (54-104 [μm]) and mixed for 5

minutes before allowing hexane to evaporate. Once dry, the contaminated soil was added to a beaker containing 200 [ml] of deionized water and mixed at 170 [rpm]. The aqueous concentration of *p*-chlorophenol was measured over time. Figure 3.16 shows that nearly 87% of the mass of *p*-chlorophenol on the soil is desorbed immediately while the remaining fraction has a slower desorption rate. Based upon the equilibrium study discussed above, the expected equilibrium line is also plotted.

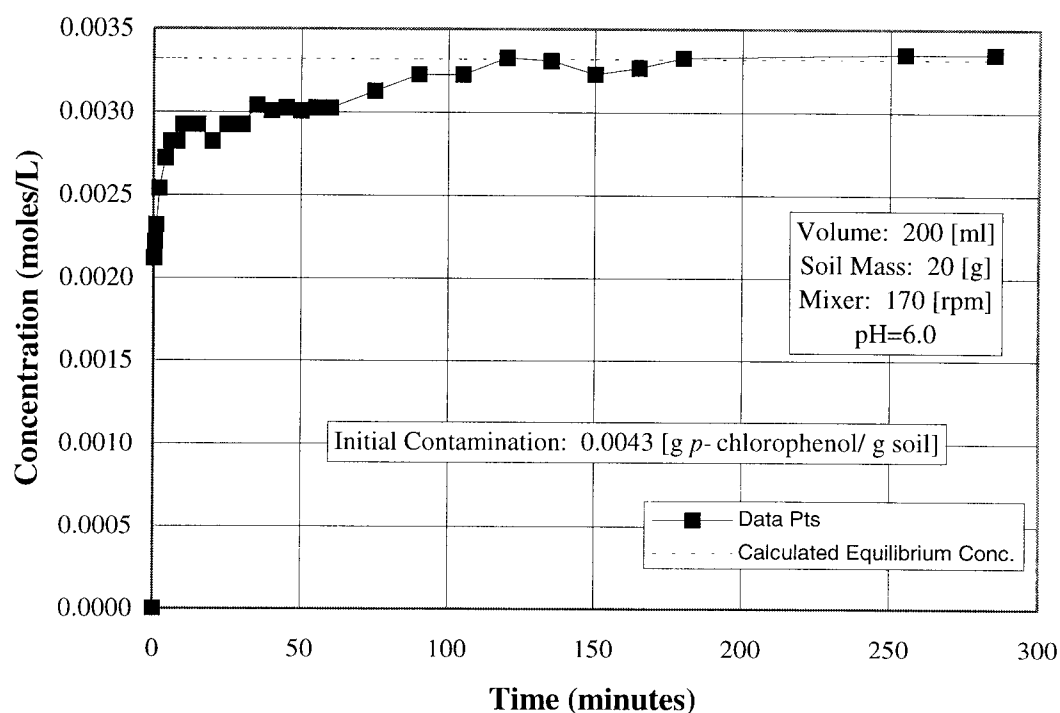


Figure 3.16: Desorption of *p*-chlorophenol from Willamette Valley type soil.

3.3.7 p-Chlorophenol Dechlorination Experimental Procedure for Freely Suspended Pd/Fe Catalyst

The Pd/Fe catalyst is prepared as described in the methods section. To avoid the effects of iron hydroxide formulation on the catalyst surface as reported by Graham and Jovanovic (1998), all experiments were performed in a deoxygenated environment with controlled pH from 3.5-6.

A *p*-chlorophenol solution of known volume and initial concentration is added to a known mass of Pd/Fe powder and mixed at a mixing rate sufficient to eliminate mass transfer resistance between the bulk fluid and the Pd/Fe particles. The palladium to iron weight ratio, or interfacial surface area, the amount of active catalyst to the amount of chlorine to be removed, and the pH at which these reactions are to occur are studied. Specifically, the interrelationship between the operating parameters and the two important resistances of iron hydroxide formation and hydrogen gas formation is investigated. Results of these experiments are presented in Chapter 4.

3.3.8 Diffusion Coefficient of p-Chlorophenol into Alginate

An important detail of this investigation is the determination of the value of the diffusion coefficient of *p*-chlorophenol through alginate beads, D_e , as a parameter which may have an important part in the overall process rate. Though there is some published data on the diffusion of different compounds through alginate gels beads, we specifically investigated the diffusion of *p*-chlorophenol through the beads used in this study

(Shishido *et. al*, 1995, Oyaas *et. al*, 1995a,b). The beads are made of 1.5% algin and 98.5% deionized water and are extruded to give desired particle diameters. Typically, the beads used were in the size range of 2.0 - 4.0 [mm]. Particle standard deviation is determined to be ± 0.04 [mm] from measurement of the diameters of beads from each batch of particles. The larger bead size is used to promote a longer diffusion time in order to follow the decrease in aqueous concentration of *p*-chlorophenol experimentally. A known mass of beads with a nominally determined radius are added to a solution of *p*-chlorophenol with high mixing intensity to eliminate mass transfer resistance between the bulk fluid and the beads. The solution concentration of *p*-chlorophenol is measured until steady state measurements are obtained and equilibrium between the beads and bulk solution is achieved. The size of the beads is checked before and after experiments with no change detected.

Alginate beads were prepared as outlined above. A known quantity of beads were added to a solution of *p*-chlorophenol and were mixed at 400 [rpm]. The concentration of *p*-chlorophenol was followed over time. Figure 3.17 shows the initial concentration of *p*-chlorophenol is decreasing until an equilibrium is reached. A series of experiments were performed using gel beads which had been in 1.5 [M] CaCl_2 for 5 [min], 30 [min], and 1 [hr] with immediate use of the beads. For the determination of the diffusion coefficient, the work of Oyaas *et. al* (1995b) is followed to fit the data to a non-steady state model in which the diffusion coefficient was determined. The diffusion coefficients calculated from this data are the same within experimental error for all three cases ($D_e =$

$8.0\text{E-}10 \text{ [m/s}^2\text{]})$. A published value of phenol as a similar compound in similarly prepared beads of the same alginate percentage was given as $8.5 \times 10^{-10} \text{ m}^2/\text{s}$ which was approximately 85% of its aqueous diffusivity (Shishido *et. al*, 1995). The effective diffusion coefficient, D_e , in 1.5 [w/w%] gel is reported to be approximately 10-15% smaller than its aqueous diffusivity, D_{AB} (Oyaas *et. al*, 1995). The aqueous diffusion coefficient, D_{AB} , for p-chlorophenol in water was calculated from three separate correlations as described in Appendix H. This coefficient is compared to the D_e value produced during optimization in the model describing diffusion through alginate beads and subsequent reaction on the entrapped Pd/Fe catalyst as discussed in Chapter 5.

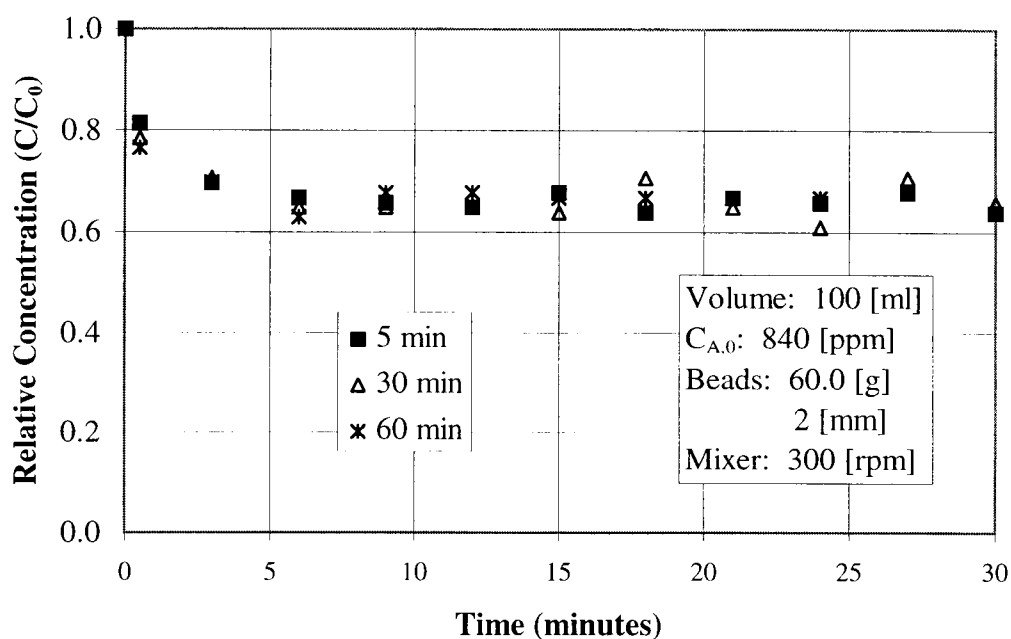


Figure 3.17: Diffusion of *p*-chlorophenol through alginate beads with varied polymerization times (Nominal bead size: 2 [mm]).

3.3.9 *p*-Chlorophenol Dechlorination Experimental Procedure for Alginate Entrapped Pd/Fe Catalyst

As mentioned in Chapter 1 (Section 1.2), the MSFB has two distinct advantages. First, it can treat liquid media laden with solid particulates (sludge type media). Second, it enhances the mass transfer coefficient between the fluidized particles and the fluidization media. Both of these advantages take place when the sludge type solution is treated for dechlorination of chlorinated hydrocarbons.

A 12 [w/w%] Pd/Fe catalyst-alginate solution was prepared and alginate beads produced as described in Appendix D (Nominal size: 2 [mm]). The Pd/Fe entrapped alginate beads were added to a deoxygenated *p*-chlorophenol solution within the MSFB. Immediately, the pump and magnetic field strength were set to achieve the desired operating conditions. Samples were periodically taken and run through the HPLC analytical column to obtain the *p*-chlorophenol and phenol bulk concentrations during the reaction. Second, direct soil decontamination is followed through the addition of *p*-chlorophenol contaminated Willamette Valley particulates (54-104 [μm]) to the MSFB in a 2 [w/w%] slurry. The MSFB advantage for this system is the ability to retain the active beads within the reactor while the slurry is recirculated. The aqueous concentration of *p*-chlorophenol is measured as dechlorination takes place within the alginate beads. In separate experiments, the solid concentration in the sludge was varied up to 30 [w/w%] (Graham *et. al*, 1998).

CHAPTER 4

EXPERIMENTAL RESULTS

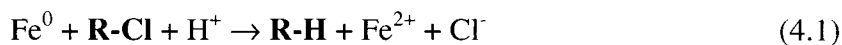
4.1 Aqueous Solution Dechlorination of *p*-Chlorophenol on Powdered Catalyst

4.1.1 Overall Mass Balance in the Dechlorination Reaction System

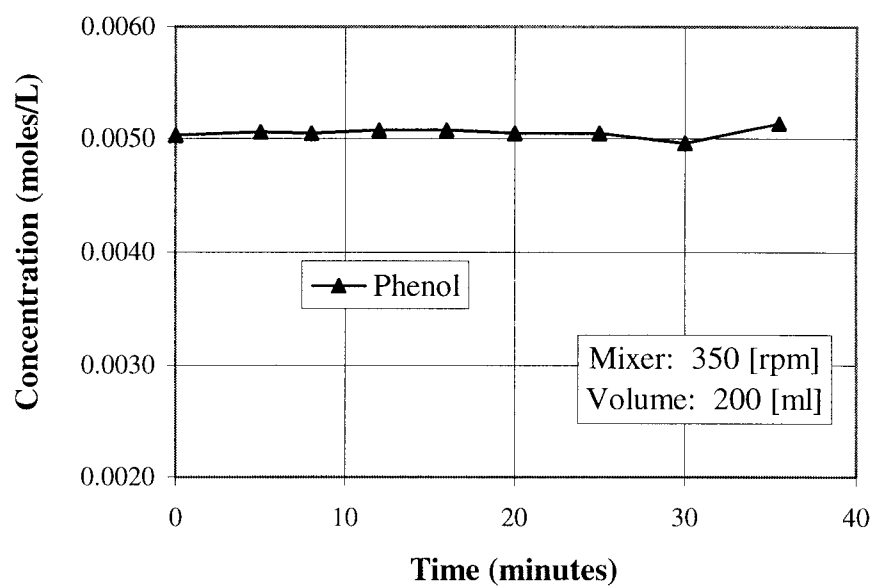
To ensure that the decrease in the concentration of *p*-chlorophenol within the reactor system is only due to conversion to phenol, two tests were performed.

First the volatility of both *p*-chlorophenol and phenol were tested by rapidly mixing a known concentration of each and following their respective concentrations in the solution with time. Figures 4.1a-b show that no apparent loss was observed for either compound.

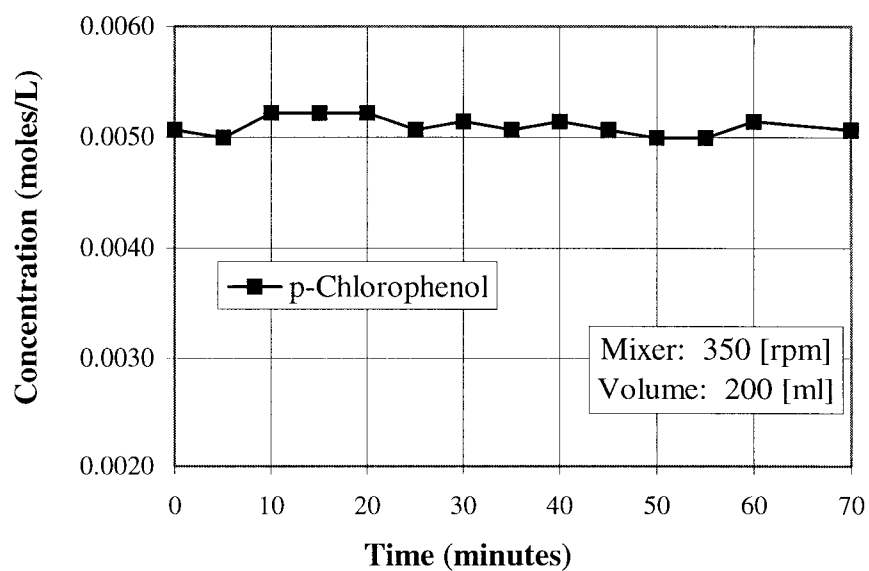
Second, the overall mass balance of the system was calculated according to the overall reaction equation.



The moles of *p*-chlorophenol (R-Cl) and phenol (R-H), as well as the total moles, were graphed as a function of time in Figure 4.2. The decrease in *p*-chlorophenol concentration was balanced by the moles of phenol formation thus resulting in the total moles remaining constant.



a)



b)

Figure 4.1: a) Volatilization check on phenol, b) Volatilization check on *p*-chlorophenol.

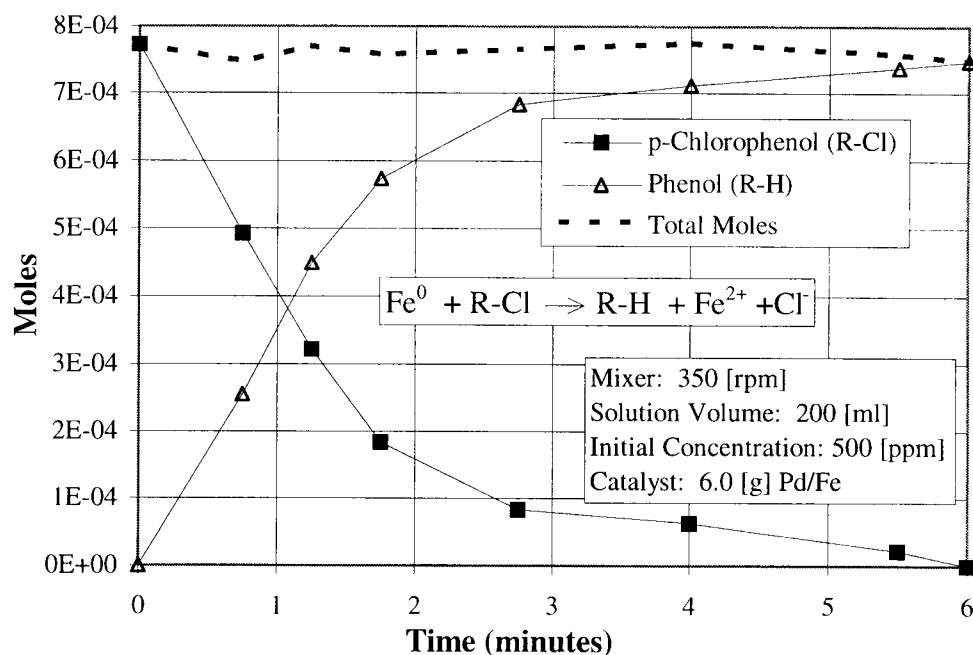
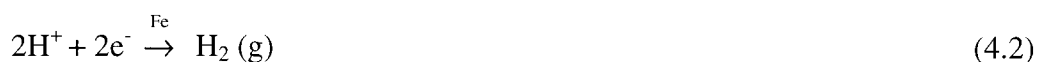


Figure 4.2: Overall mass balance on the dechlorination reaction.

4.1.2 Formation of $\text{Fe}(\text{OH})_2$ and $\text{Fe}(\text{OH})_3$

Freely Suspended Pd/Fe Catalyst for Dechlorination with O_2 present

Initial studies of dechlorination of *p*-chlorophenol by Pd/Fe catalyst were performed at a pH between 6 and 8 without pH control. A 4.0 [g] sample of a 0.188 [w/w%] Pd/Fe catalyst was added to 200 [ml] of a 500 [ppm] *p*-chlorophenol solution which was initially adjusted to pH=4.5. The solution was vigorously mixed and was allowed contact with O_2 in the air. The pH of the solution was monitored (but not controlled) during the reaction. Figure 4.3 plots the pH as a function of reaction time. Initially, the bare Pd/Fe surface removes H^+ according to:



and



and the pH rapidly rises above pH=8.0. The *p*-chlorophenol concentration rapidly decreased during the initial rise in pH but remained constant once the pH rose above 8.5. Even with a decrease in pH, no further dechlorination was observed. This pH range resulted in the formation of hydroxide layers on the surface of the Pd/Fe catalyst which was visibly observed as an orange layer. From this experiment, one can conclude that the rust layer inhibited the reaction thereby decreasing catalyst activity.

As referenced by Graham and Jovanovic (1998a), a change in the reaction rate was readily observed which coincided with a visual observation of the growth of an orange layer, or rust, on the originally gray surface. A SEM picture shows the change in the surface appearance between a freshly prepared catalyst (Figure 4.4a) and a Pd/Fe catalyst with hydroxide formation (Figure 4.4b). Investigation into the dissolution reaction of Fe^0 indicated that $\text{Fe}(\text{OH})_2$ forms above a pH of 6 (Kragten, 1978). However, Fe^{2+} can undergo further reaction to Fe^{3+} in the presence of oxygen. $\text{Fe}(\text{OH})_3$ can form on the catalyst above a pH of 3 thus further inhibiting catalyst performance even at low pH's (Kragten, 1978). Therefore, it is extremely important to avoid conditions that favor the formation of either $\text{Fe}(\text{OH})_2$ or $\text{Fe}(\text{OH})_3$. Further experiments were performed below pH=6 and under deoxygenated conditions to avoid this mechanism for deactivation while still allowing a pH range within which the reaction could be followed.

Dechlorination of *p*-Chlorophenol with Uncontrolled pH And Oxygenated Conditions

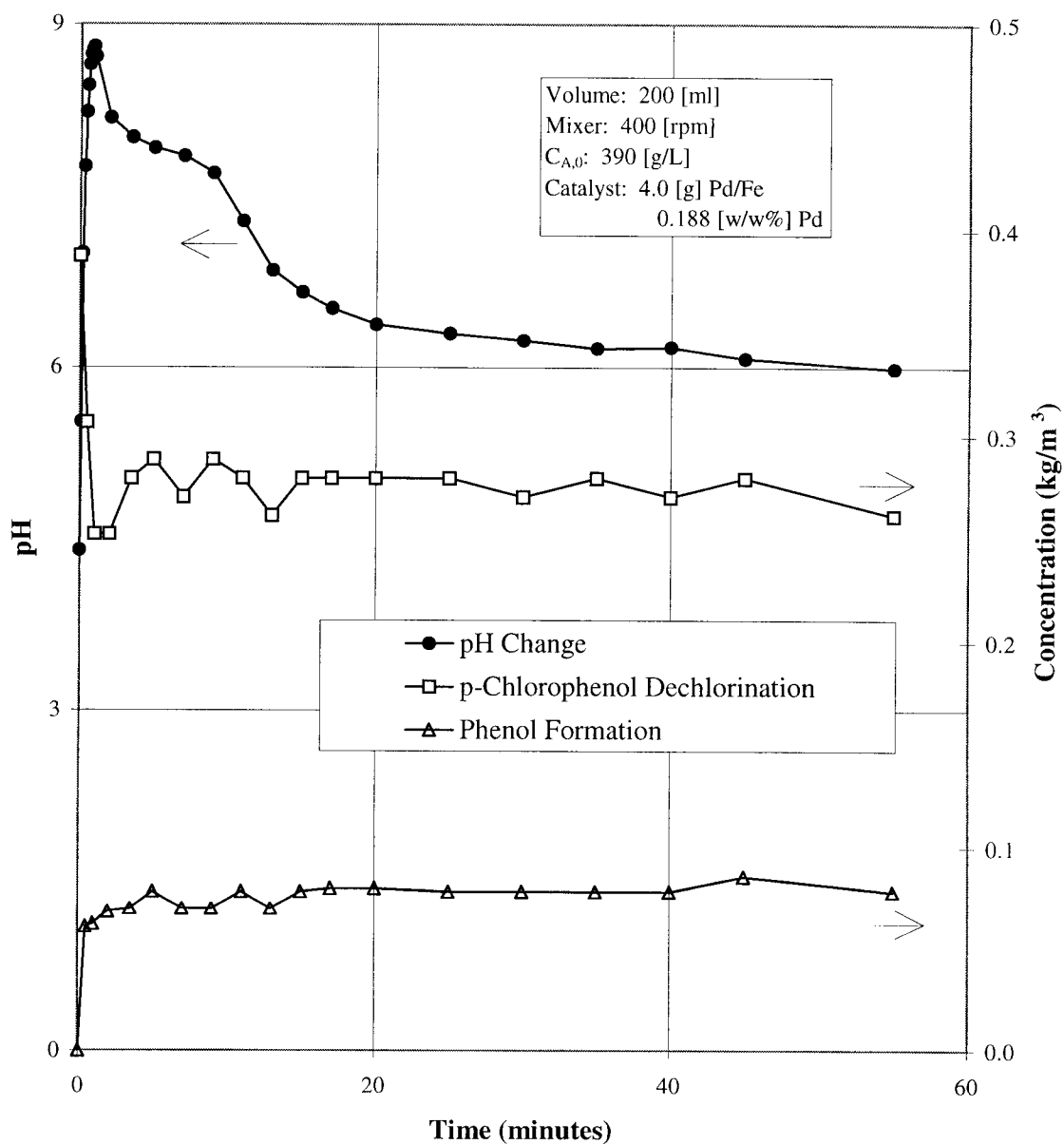


Figure 4.3: pH change during dechlorination reaction under oxygenated conditions.

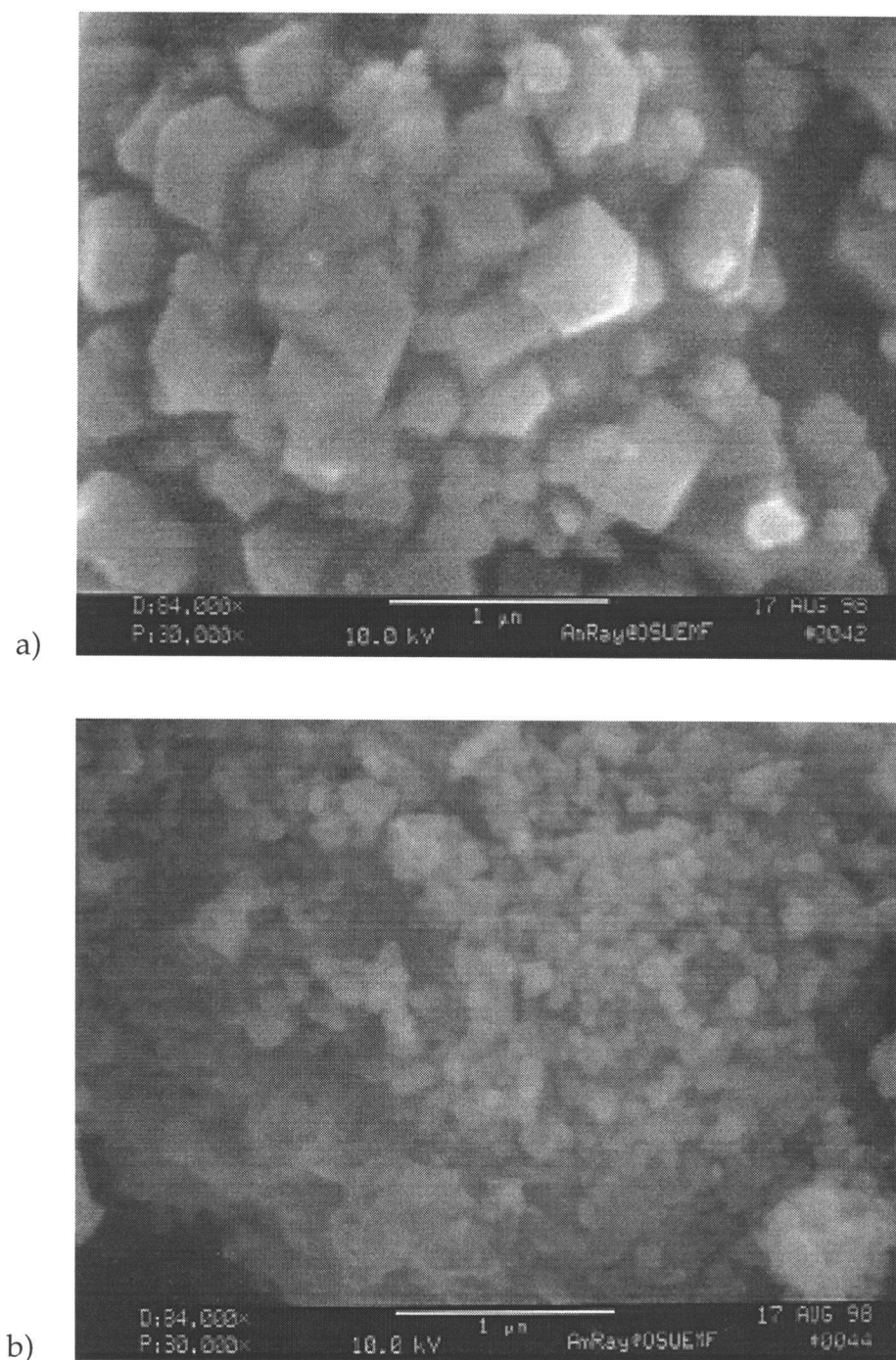


Figure 4.4: Development of a hydroxide layer on the Pd/Fe catalyst a) Freshly prepared Pd/Fe, b) Pd/Fe surface with hydroxide layer.

4.1.3 Acidic Conditions With Varied Mixer Speed

To facilitate data analysis for the chemical reaction rate constant without the interference of mass transfer resistance between the bulk liquid and catalyst surface, a series of experiments were run over a range of mixing speeds (100-350 [rpm]) until the dechlorination curve was no longer dependent upon the impeller speed. Figure 4.5 demonstrates that between 100 and 150 [rpm], significant increase in the rate was observed. However, as mixer speed increased from 250-350 [rpm], little change was observed. This is related to a change in the fluid mechanics of the system which is important for scale up of a process. The calculated Reynolds number indicates a change to turbulent conditions at the highest mixer speeds ($Re > 20,000$). An F-test was performed to check for statistical difference and both are considered to have the same dechlorination overall rate within experimental accuracy.

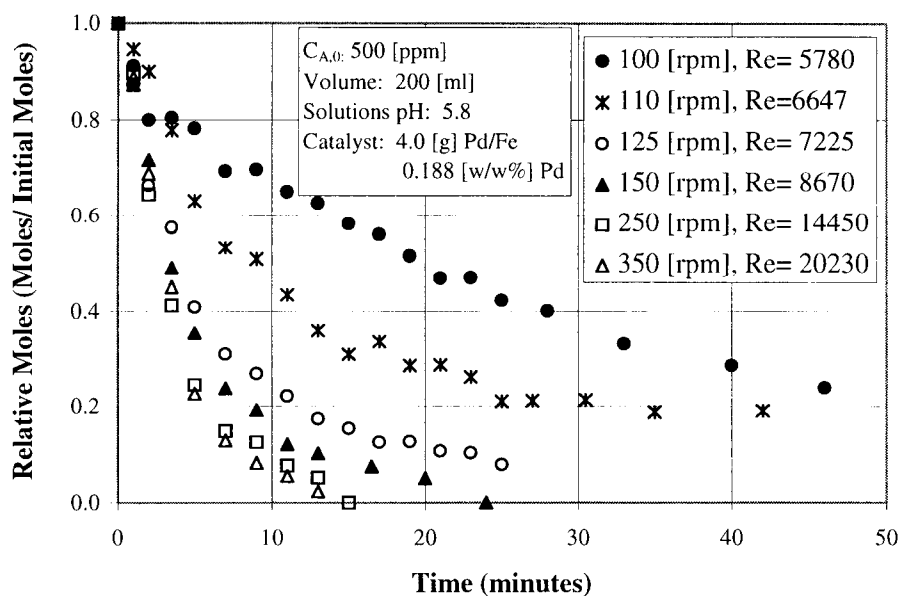


Figure 4.5: Dechlorination of p-chlorophenol under varied mixing conditions.

4.1.4 Dechlorination of *p*-Chlorophenol at Various pH

Investigation into pH effect on reaction and deactivation resulted in interesting observations (Figure 4.6). The higher pH of 5.8 had a slower initial dechlorination rate but dechlorinated over a longer period of time before leveling off due to deactivation. The other extreme, pH of 3.8, had the steepest initial dechlorination rate with a high incidence of catalyst passivation at a much earlier time. The average pH of 4.8 had intermediary performance. These observations can be explained by the reaction equations describing the catalyst rate kinetics. The lowest pH of 3.8 increases the reaction rate by increasing the amount of reactive intermediate hydrogen, H^* , that is formed in Equation 4.4. This reactive intermediate is responsible for the dechlorination step represented in Equation 4.5 thus resulting in a greater initial rate of dechlorination than at a pH of 5.8.



However, the increase in the concentration of hydrogen ion, H^+ , at the lower pH of 3.8 also provides for an increase in the amount of hydrogen ion available for conversion to $H_2(g)$ as given in Equation 4.6.



Therefore, one can conclude that the reaction pH (hydrogen ion, H^+ concentration) is a function of the two competing reactions; conversion to H^* for dechlorination and conversion to $H_2(g)$.

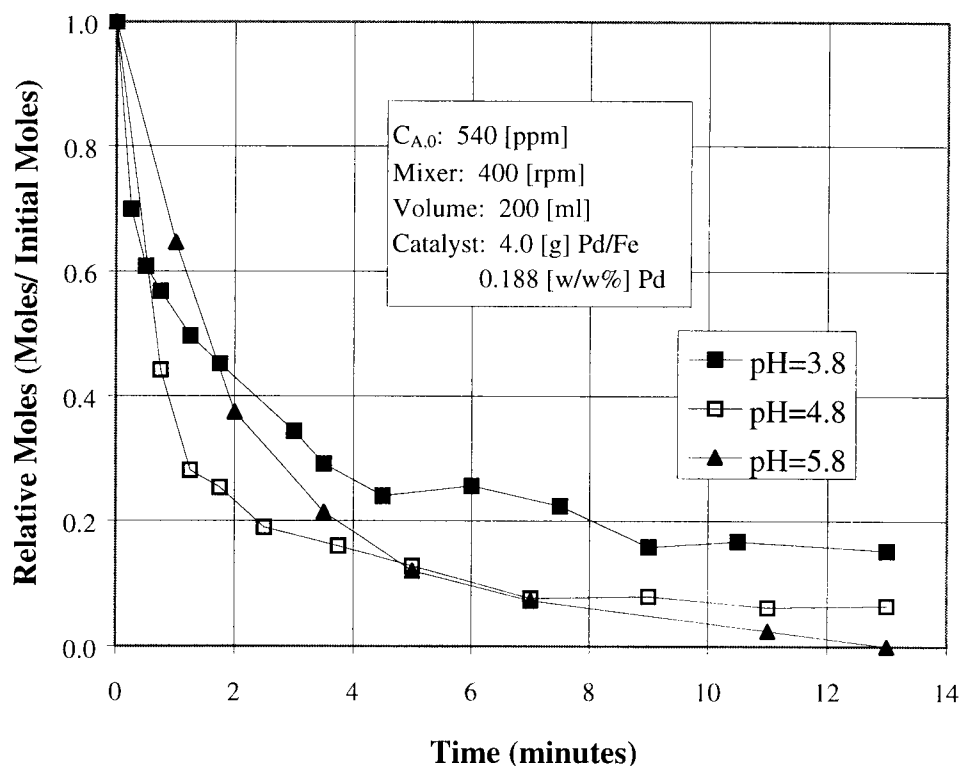


Figure 4.6: Effect of pH on dechlorination of *p*-chlorophenol.

4.1.5 Dechlorination With Varied Amounts of Pd/Fe Catalyst

Further, the effect of the amount of Pd/Fe catalyst to the amount of chlorine to be removed is shown in Figure 4.7. Three experimental runs were performed in which a 450 [ppm] solution of *p*-chlorophenol was reacted with 2.0 [g], 4.0 [g], or 6.0 [g] of 0.188 [w/w%] Pd/Fe catalyst, respectively. The aqueous *p*-chlorophenol concentration was measured as the dechlorination reaction proceeded. Figure 4.7 shows that when the Pd(Fe)/Cl ratio is increased, the dechlorination rate is also increased as a larger surface is

available for the dechlorination reaction. The larger amount of Pd/Fe catalyst relative to the amount of chlorine to be removed allows for complete reaction before passivation of the surface. This situation will be modeled in Chapter 5 in order to determine the reaction rate constant, k [$\text{m}^3/\text{g}_{\text{cat}}\text{min}$], and deactivation constant, k_d [$1/\text{s}$], as a function of Pd/Fe available for reaction as expressed by:

$$-\frac{d(vC_A)}{dt} = k^* C_A a \quad (4.7)$$

with $k = \frac{k^*}{W}$ (4.8)

and $a = \exp(-k_d t)$ (4.9)

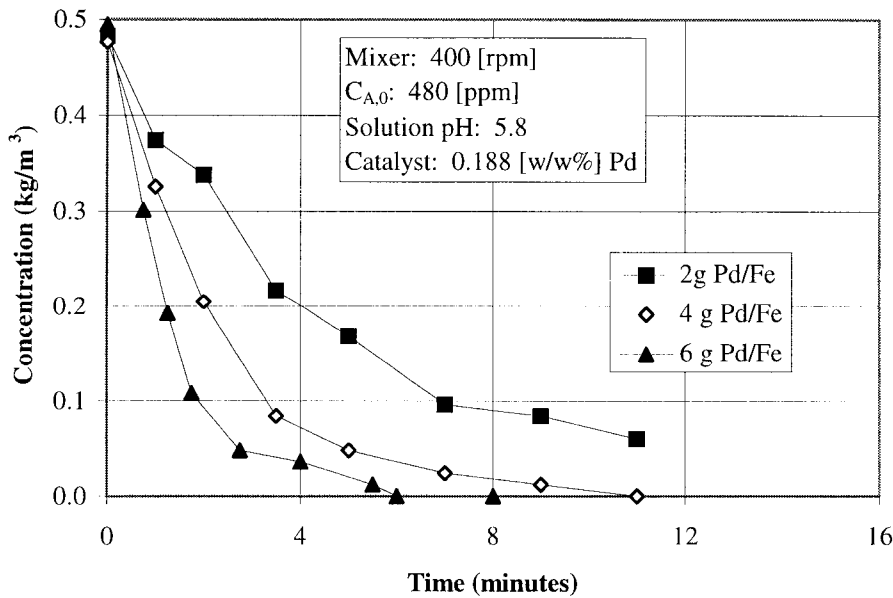


Figure 4.7: Effect of Pd/Fe to chlorine ratio on overall rate of dechlorination.

4.2 Aqueous Solution Dechlorination of *p*-Chlorophenol on Alginate Entrapped Catalyst

Alginate Entrapped Pd/Fe Catalyst for Dechlorination under O₂ Free Conditions

Advantages for Pd/Fe catalyst entrapment within alginate beads include the following:

- The alginate beads allow control over the 5-8 [μm] powder in particle laden systems.
- There is little possibility to achieve the mixing intensity in a real reactor vessel similar to what we can achieve in a beaker.

The dechlorination process with the Pd/Fe catalyst entrapped within the alginate beads has different characteristics from the dechlorination reaction with non-entrapped Pd/Fe catalyst due to the addition of diffusion resistance within the beads. A 8 [w/w%] Pd/Fe catalyst-alginate solution was prepared and alginate beads produced as described in Appendix D (Nominal size: 2 [mm]). 20 [g] of the Pd/Fe bead were added to a 200 [ml] of a 450 [ppm] solution of *p*-chlorophenol and vigorously mixed at 200 [rpm] in the stirred tank batch reactor (Chapter 3, Section 3.3.1). The aqueous *p*-chlorophenol and phenol concentrations were measured as the reaction proceeded (Figure 4.8)

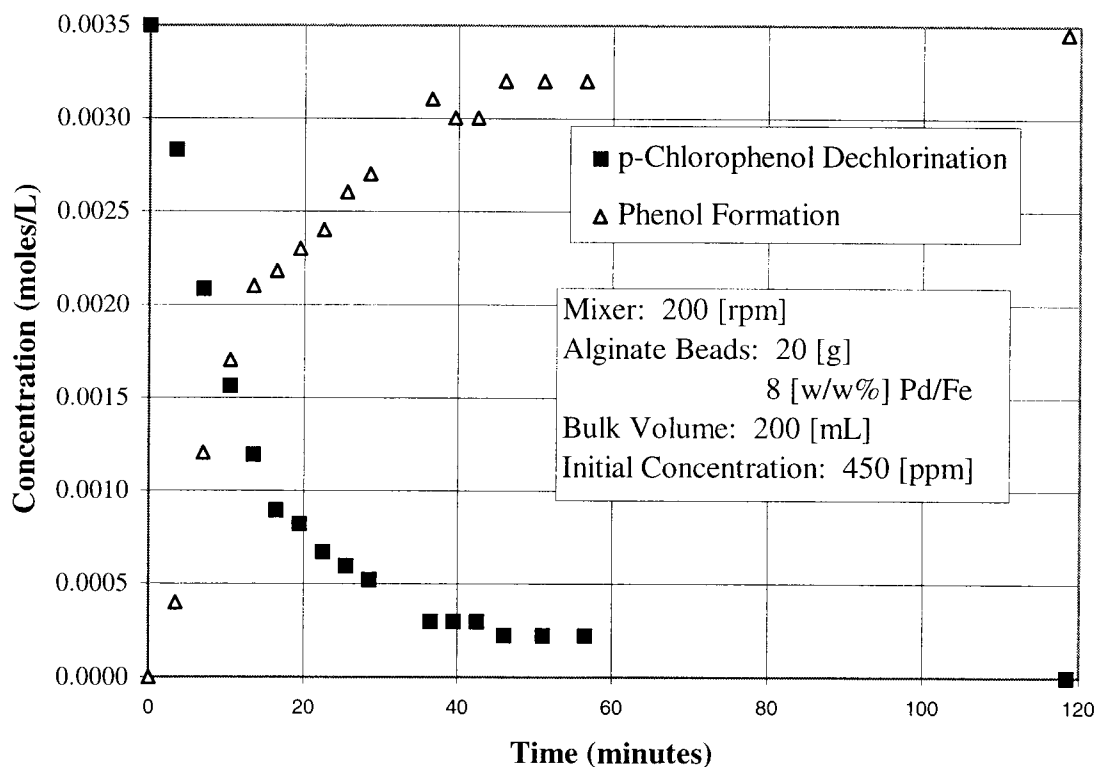


Figure 4.8: Dechlorination of *p*-chlorophenol with alginate entrapped Pd/Fe catalyst

To illustrate the enhancement effect on the mass transfer coefficient within the MSFB, two experiments were performed. The first was run without an applied field (Figure 4.9). The second was run with a gradient field (Figure 4.10). To compare the rates of dechlorination with a constant bed voidage with varied interstitial velocity, the decrease in *p*-chlorophenol with time for both situations is illustrated in Figure 4.11.

Dechlorination in a MSFB Without an Applied Field

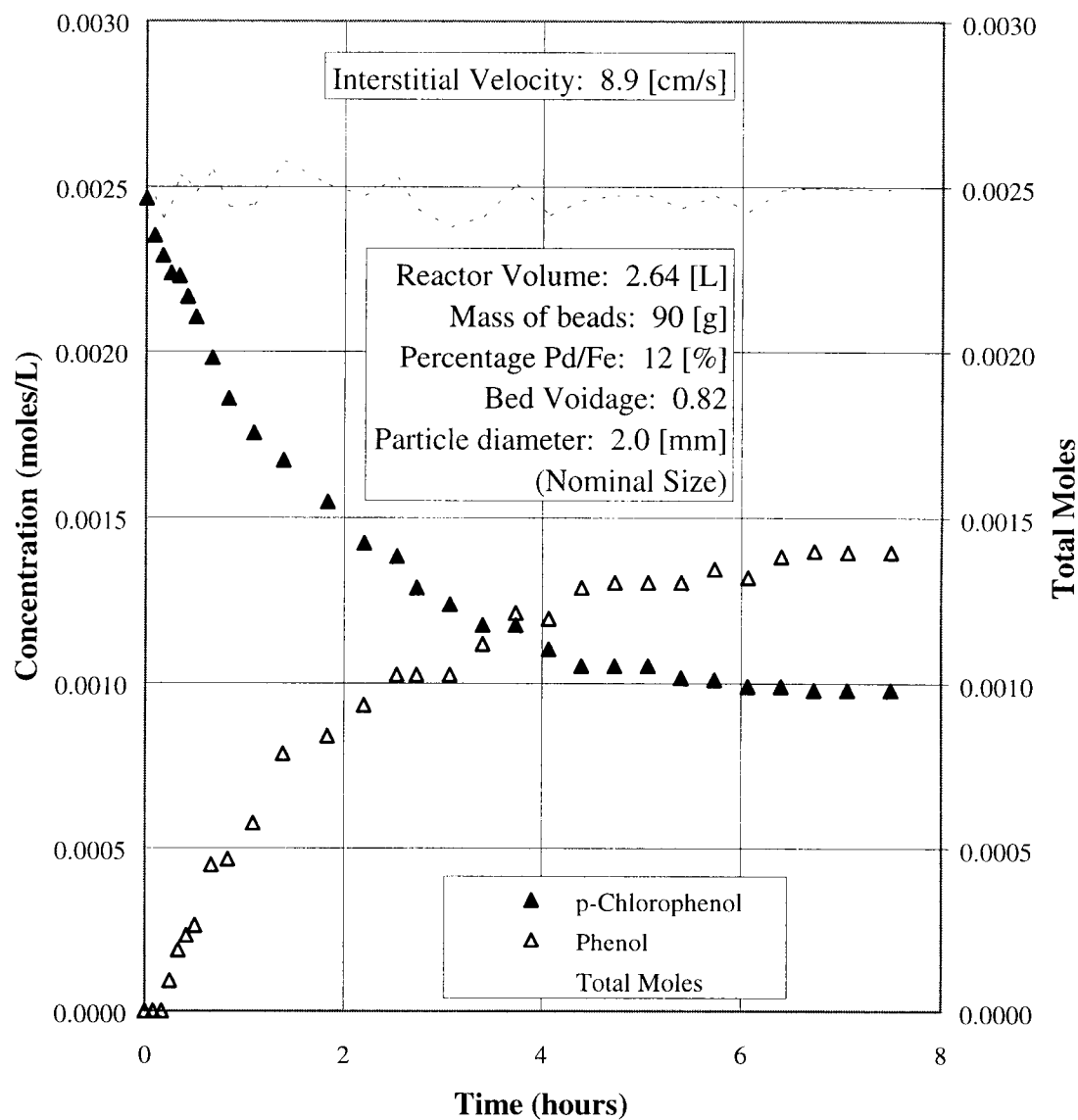


Figure 4.9: Entrapped Pd/Fe *p*-chlorophenol dechlorination without an applied field.

Dechlorination in a MSFB With an Applied Field

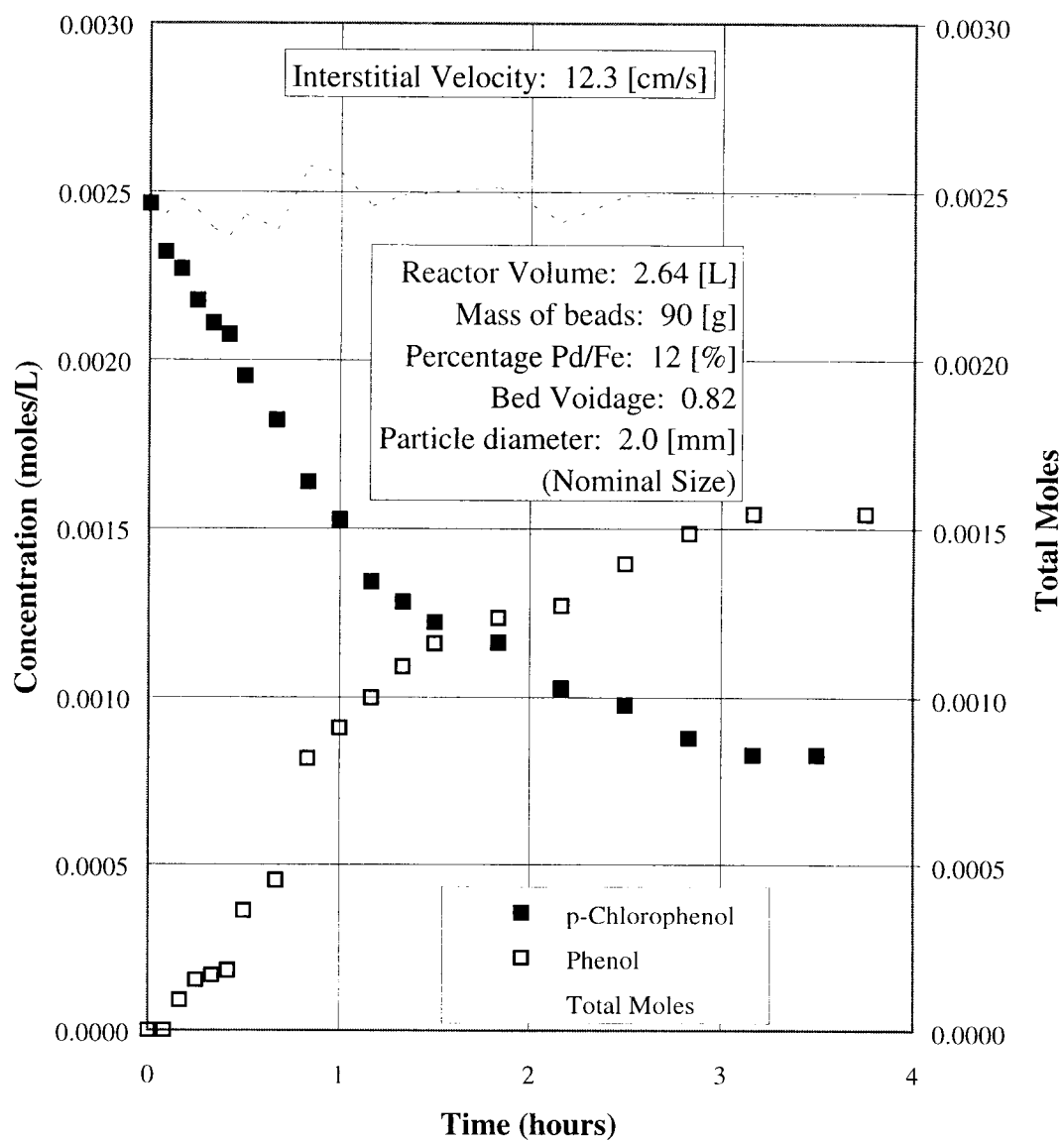


Figure 4.10: Entrapped Pd/Fe *p*-chlorophenol dechlorination with an applied field.

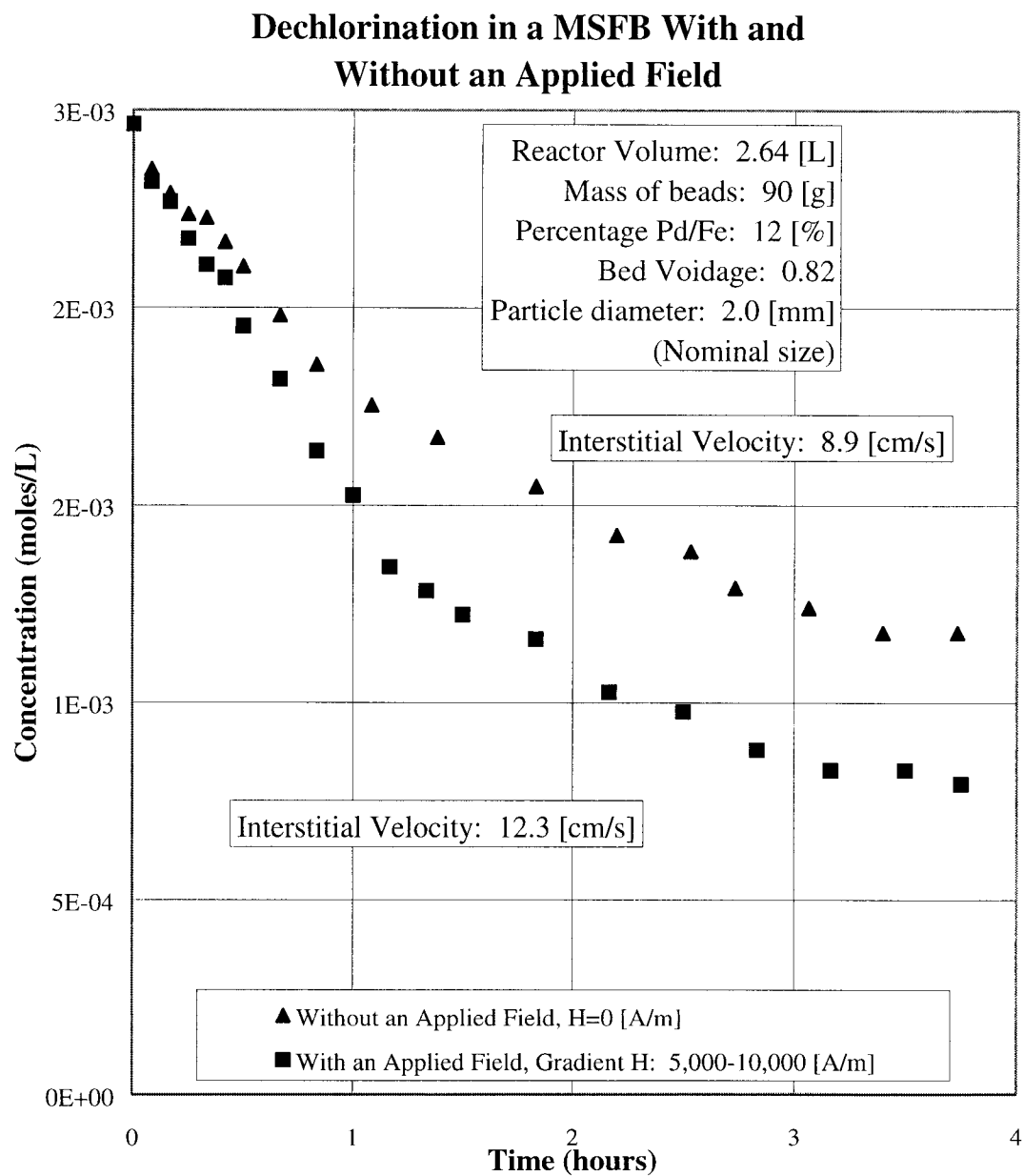


Figure 4.11: Comparison of dechlorination rates with the MSFB enhancement.

4.3 Soil/Liquid Solution Dechlorination of *p*-Chlorophenol on Alginate Entrapped Catalyst

200 [g] of Pd/Fe entrapped alginate beads was added to 2.64 [L] of deionized water under deoxygenated conditions. The pump was adjusted to a superficial velocity of 5.0 [cm/s] with a gradient field (5,000 [A/m]-10,000 [A/m]) to attain a bed height of 40 [cm]. The system was adjusted to pH=5.4 and 50 [g] of Willamette Valley type soil (54-104[μm]) was added immediately to the vessel. Samples were periodically taken and rapidly centrifuged to obtain the *p*-chlorophenol and phenol bulk concentrations during the reaction. The slurry was recycled through the bed while the alginate beads were maintained by the field within the fluidized bed.

Figure 4.12 represents the dechlorination of *p*-chlorophenol from the contaminated soil/slurry system within the MSFB. The *p*-chlorophenol concentration dropped with time as the phenol concentration rose, thus decontaminating the soil. These kinetics are modeled in Chapter 5 using the soil model developed in Chapter 2, Section 2.3.2.

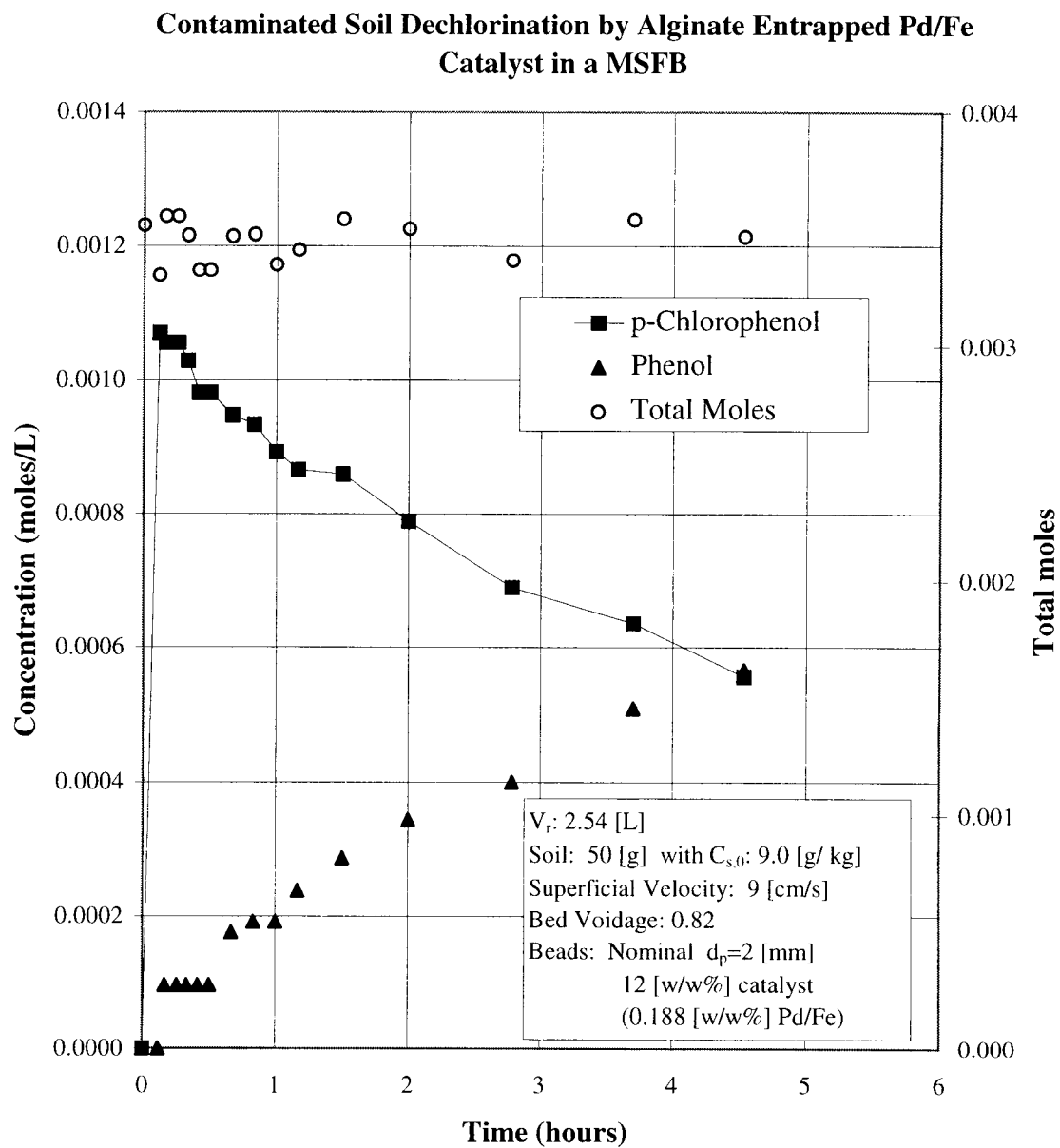


Figure 4.12: Dechlorination of contaminated soil in the MSFB.

CHAPTER 5

DATA INTERPRETATION AND MODELING

5.1 Results of *p*-Chlorophenol Dechlorination on Powdered Catalyst

To determine the kinetic rate constant for *p*-chlorophenol dechlorination, k^* [m³/s], and the deactivation rate constant for the Pd/Fe catalyst, k_d [1/s], the rate expressions from Equations 2.15-16 in Chapter 2 were integrated with first order deactivation kinetics ($n=1$). Note that a changing volume due to acid addition for maintaining a constant pH must also be properly incorporated.

$$-\frac{d(VC_A)}{dt} = (Wk)C_A = k^* C_A^a \quad (2.15)$$

$$-\frac{da}{dt} = k_d a^n \quad (2.16)$$

A Fortran program utilizing IMSL subroutines was written to solve the differential equation and produce model output of the bulk concentration. An optimization routine (UMCGF: Appendix J) was also implemented to search for the reaction rate constant, k^* , and the deactivation constant, k_d , until the objective function, F , as expressed by Equation 5.1 reached a minimum.

$$F = \sum \left(C(t)_{model} - C(t)_{expt} \right)^2 \quad (5.1)$$

The model output as compared to the experimental data was then graphed for a variety of experimental situations. For the compiled data shown on Figure 4.6 in Chapter 4,

Figures 5.1-5.3 demonstrate the modeling results with pH as a parameter (ranging from 3.8 to 5.8).

The normalized reaction rate constant, k , and the deactivation constant, k_d , were then plotted as a function of pH or $[H^+]$ [moles/m³] as shown in Figure 5.4a,b. The results of linear correlations are given by Equations 5.2 and 5.3. As illustrated, decreasing pH results in an increase in reaction rate constant while the rate of deactivation is dependent upon the concentration of hydrogen ions, $[H^+]$ [moles/m³], in solution. The activity of the catalyst, as defined in Equation 2.16 above, decreases over reaction time. This decrease is much faster at high $[H^+]$ concentrations (Figure 5.5).

$$k = -0.025 [pH] + 0.161 \quad [m^3/s \cdot kg_{catalyst}] \quad pH \text{ range } 3 \text{ to } 5.8 \quad R^2 = 0.94 \quad (5.2)$$

$$k_d = 0.091 [H^+] \quad [1/s] \quad pH \text{ range } 3 \text{ to } 5.8 \quad R^2 = 0.99 \quad (5.3)$$

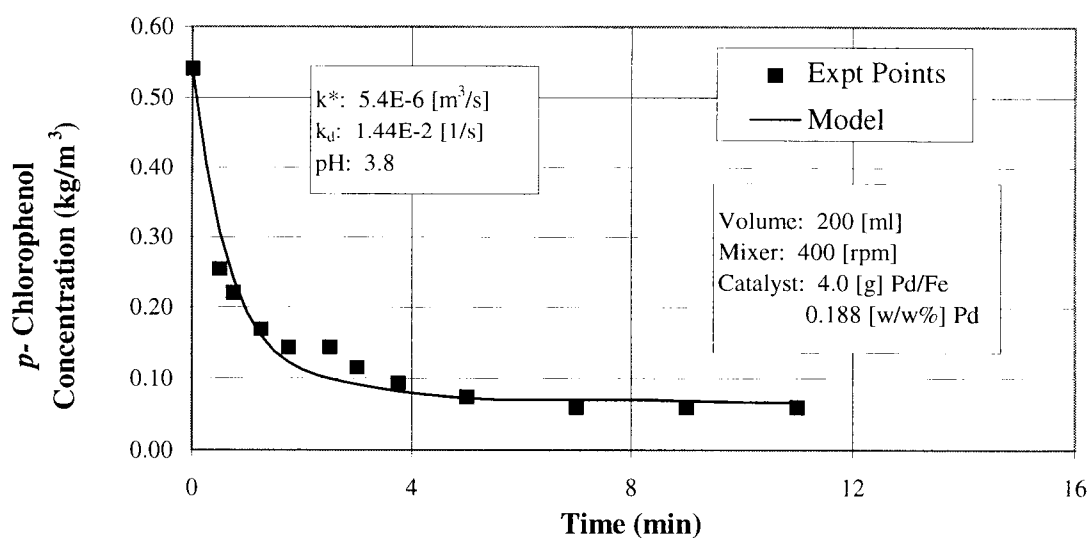


Figure 5.1: Dechlorination of *p*-chlorophenol at pH=3.8 with an optimized model.

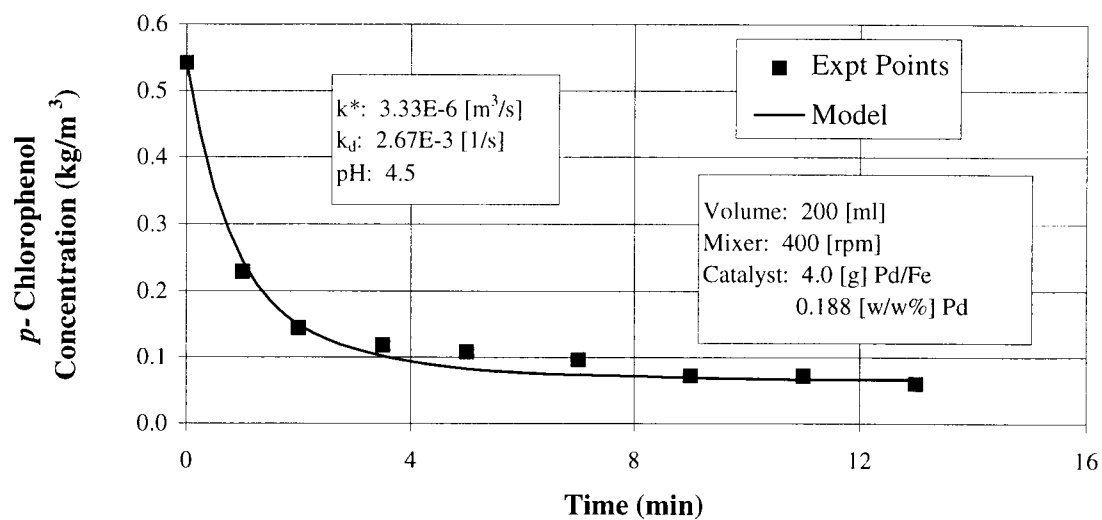


Figure 5.2: Dechlorination of *p*-chlorophenol at pH=4.5 with an optimized model.

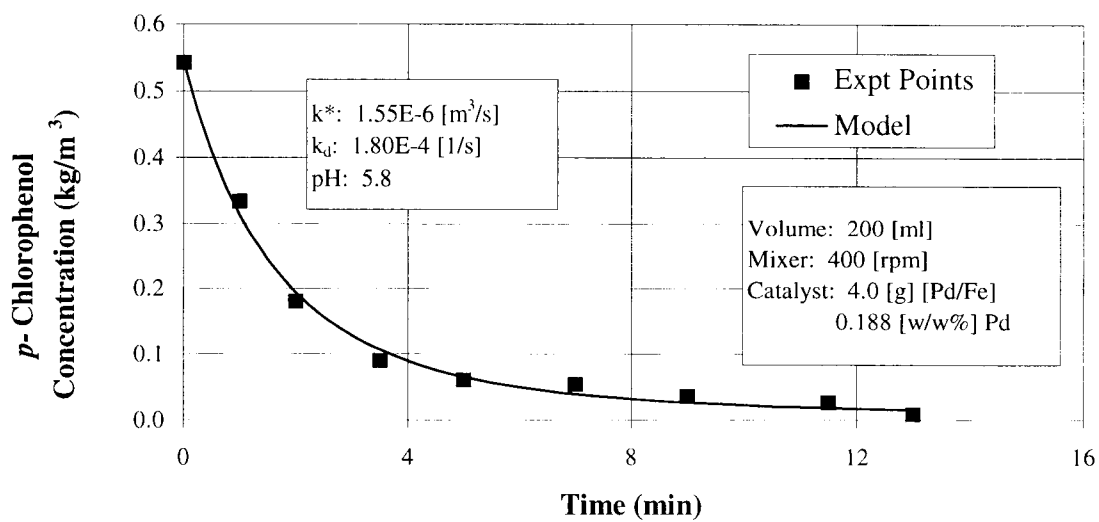
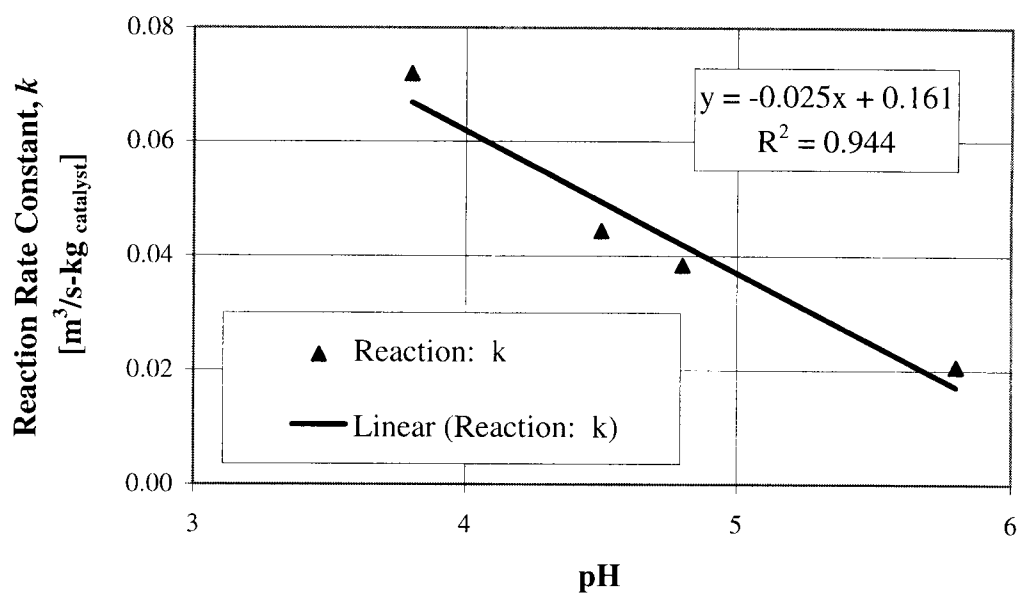
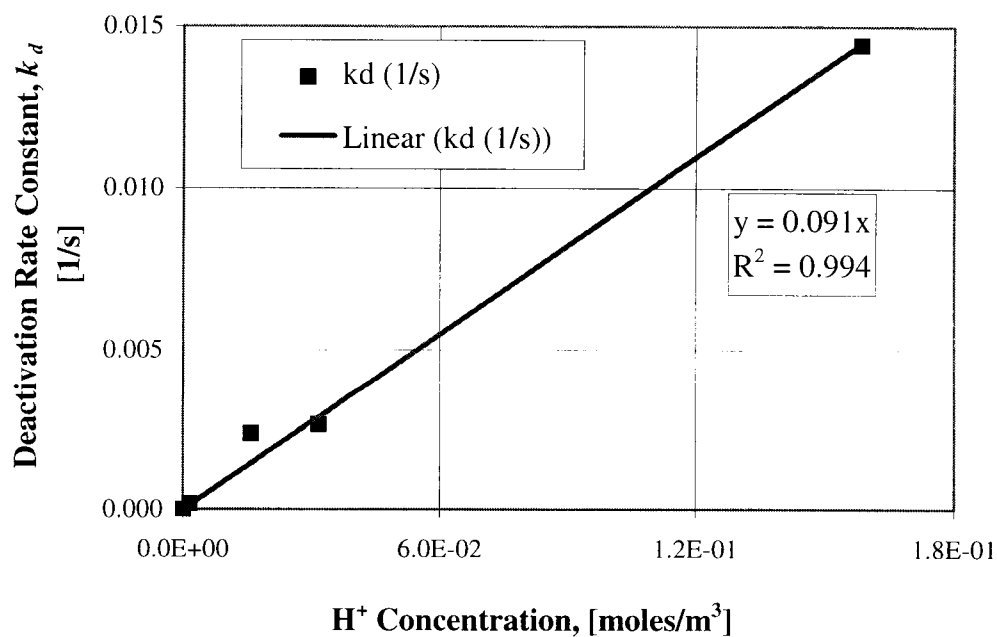


Figure 5.3: Dechlorination of *p*-chlorophenol at pH=5.8 with an optimized model.



a)



b)

Figure 5.4: a) Effect of pH on the normalized reaction rate constant, k [$\text{m}^3/\text{s}\cdot\text{kg}_{\text{catalyst}}$].
b) Effect of $[\text{H}^+]$ on the deactivation rate constant, k_d [1/s].

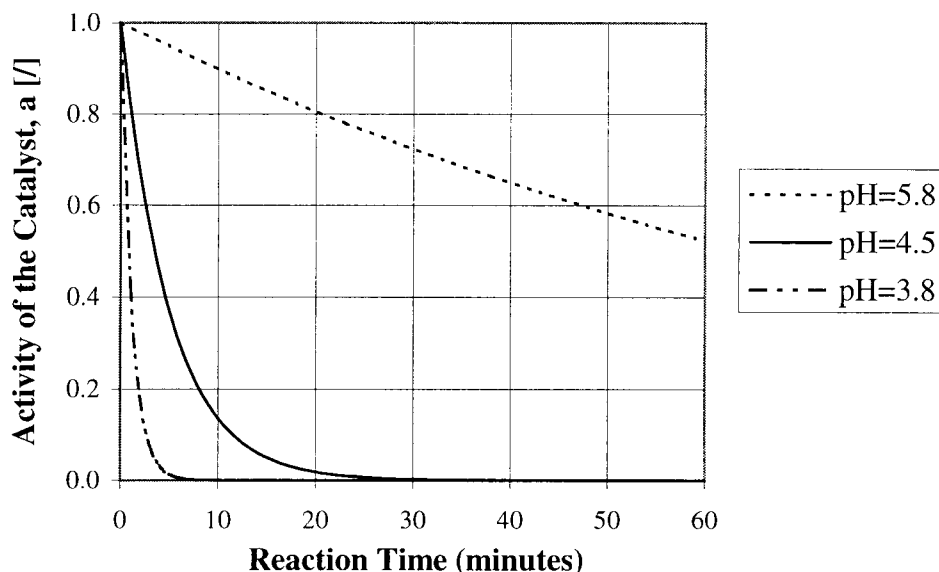


Figure 5.5: Loss of catalyst activity with time over the pH range.

To determine the reaction rate constant, k^* [m^3/s], and the deactivation rate constant, k_d [$1/\text{s}$], over a range of catalyst weights at a $\text{pH} = 5.8 \pm 0.087$, the model was applied to experimental data for 2.0 [g], 4.0 [g] and 6.0 [g] of Pd/Fe (Figure 4.6, Chapter 4). Figure 5.6 illustrates the resulting reaction rate constant (k^*) values as a function of weight of catalyst (Pd), W , with the resulting correlation given by:

$$k^* = 0.0126 [W] \quad [\text{m}^3/\text{s}] \quad R^2 = 0.99 \quad (\text{Pd/Fe: 2-6 [g]; 0.188 [w/w\%] Pd}) \quad (5.4)$$

The normalized reaction rate constant is given as $k = 0.20 \pm 0.2 \text{ [m}^3/\text{s} \cdot \text{kg}_{\text{catalyst}}]$ at a $\text{pH} = 5.8 \pm 0.087$. The deactivation rate constant remains independent of the amount of

catalyst at a constant pH and is given as $k_d = 1.8 \times 10^{-4} \pm 2.1 \times 10^{-6}$ [1/s] (pH= 5.8 ± 0.087) (Figure 5.7).

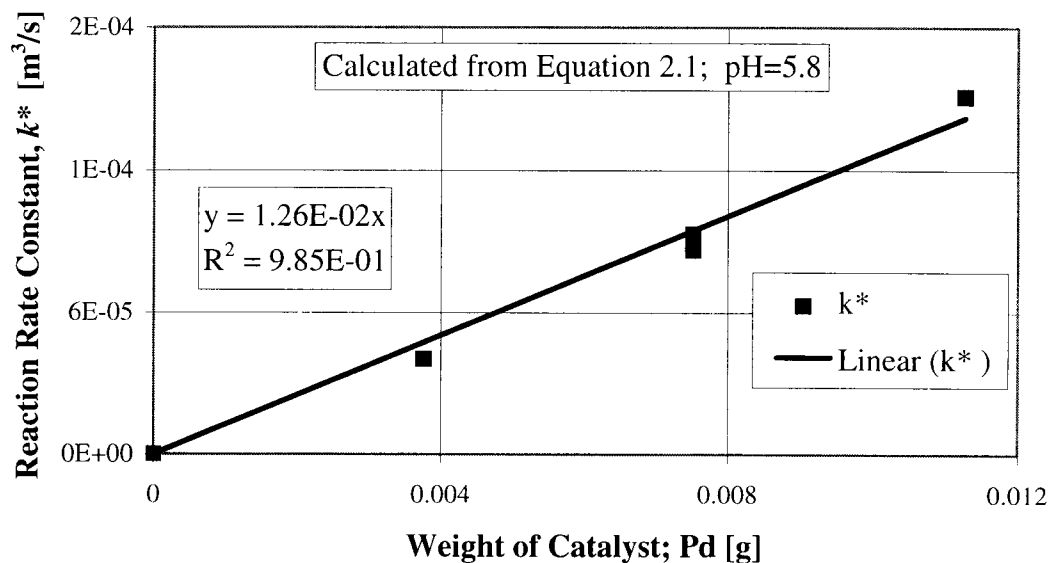


Figure 5.6: Reaction rate constant, k^* , as a function of catalyst weight at pH= 5.8 ± 0.087 .

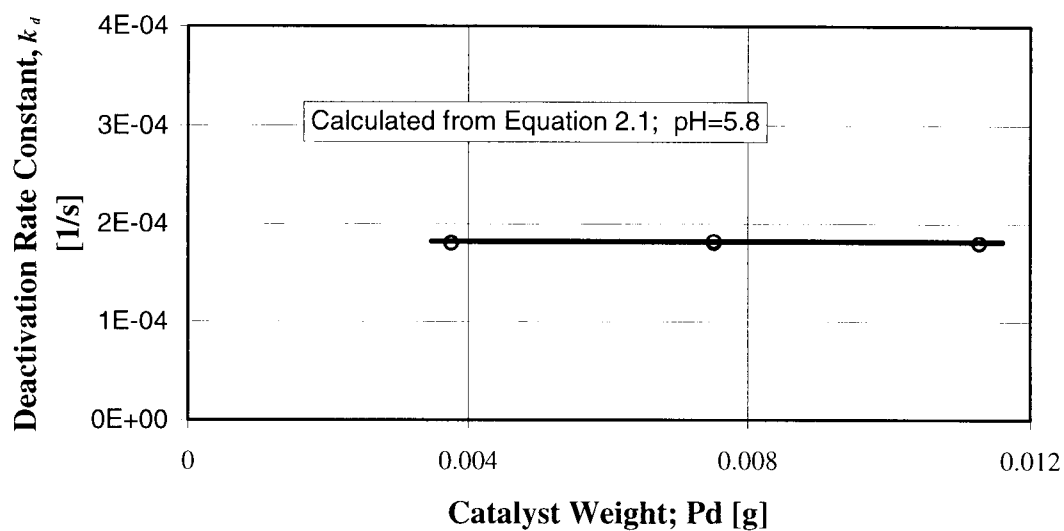


Figure 5.7: Determination of the deactivation rate constant, k_d , as a function of catalyst weight.

5.2 Determination of the Diffusion Coefficient, D_e , in Alginate Beads

To determine the effective diffusion coefficient for *p*-chlorophenol into 1.5% alginate beads, the expression and its accompanying boundary and initial conditions from Equations 2.40-2.45 were solved using Euler's finite divided difference method. A similar approach was developed by Wheeler and Middleman (1970).

The diffusion coefficient was determined at the minimum value of the least squares objective function. The output describing the bulk liquid concentration change with time was plotted against the experimental data (Figure 5.8). The diffusion coefficient was determined to be $8.0 \times 10^{-10} \text{ m}^2/\text{s}$ for *p*-chlorophenol in 1.5% alginate gel beads with a nominal diameter of 2.0 [mm].

A published value of phenol as a similar compound in similarly prepared beads of the same alginate percentage was given as $8.5 \times 10^{-10} \text{ m}^2/\text{s}$ which was approximately 85% of its aqueous diffusivity (Shishido *et. al*, 1995). The effective diffusion coefficient, D_e , in 1.5 [w/w%] gel is reported to be approximately 10-15% smaller than its aqueous diffusivity, D_{AB} (Oyaas *et. al*, 1995). The aqueous diffusion coefficient, D_{AB} , for *p*-chlorophenol in water was calculated from three separate correlations as described in Appendix H. A 10-15 % reduction in these correlated D_{AB} values gives D_e to be $7.0 \times 10^{-10} \text{ [m}^2/\text{s]}$, $9.3 \times 10^{-10} \text{ [m}^2/\text{s]}$, and $1.1 \times 10^{-9} \text{ [m}^2/\text{s]}$.

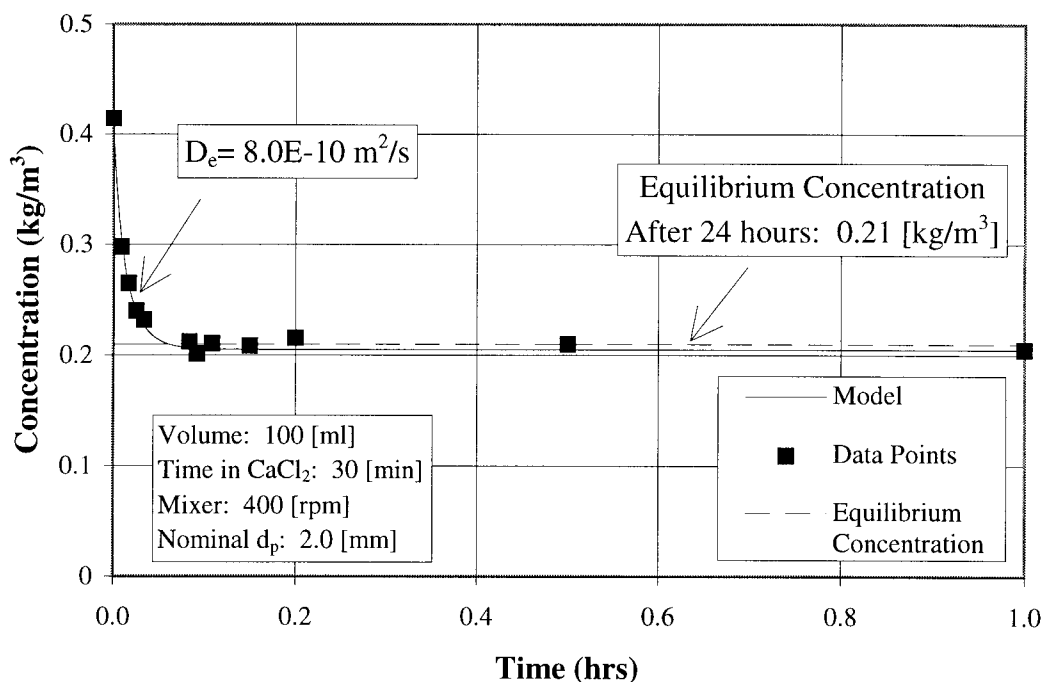


Figure 5.8: Determination of the effective diffusion coefficient, D_e , for *p*-chlorophenol into alginate beads (Nominal diameter: $d_p=2.0$ [mm]).

5.3 Results of *p*-Chlorophenol Dechlorination on Alginate Entrapped Pd/Fe Catalyst

The model developed in Equations 2.34-2.39 (Chapter 2, Section 2.2.4), which represents the change of aqueous *p*-chlorophenol concentration with time due to mass transfer from the bulk liquid to the bead surface, diffusion into the alginate beads and subsequent reaction and deactivation on the Pd/Fe entrapped catalyst powder, was applied to the experimental data. The model was solved utilizing a numerical finite divided difference method.

Figure 5.9 represents the results of the modeling efforts as they are applied to two MSFB experiments described in Chapter 4. In both experiments, a constant bed voidage is maintained at varied interstitial velocity. A four parameter optimization method gave the following values for k_d , k , D_e , and k_l (Tables 5.1 and 5.2). For comparison, the values of these parameters obtained from separate, controlled experiments or from existing correlations are also shown in Tables 5.1 and 5.2.

Section 5.1 provides the foundation for determining k and k_d . Section 5.2 describes the procedure by which the diffusion coefficient, D_e was determined. Chapter 2, Section 2.4 introduces the correlations from literature for calculation of the mass transfer coefficient, k_l . Another important aspect of this system is the loss of activity of the catalyst within the alginate beads due to the deactivation mechanisms.

Also plotted on Figure 5.9 is the corresponding loss of catalyst activity which is increasing with time. This demonstrates that at the higher initial dechlorination rate, most of the catalyst is still active. However, as the activity of the catalyst declines, the dechlorination rate slows and begins to level off.

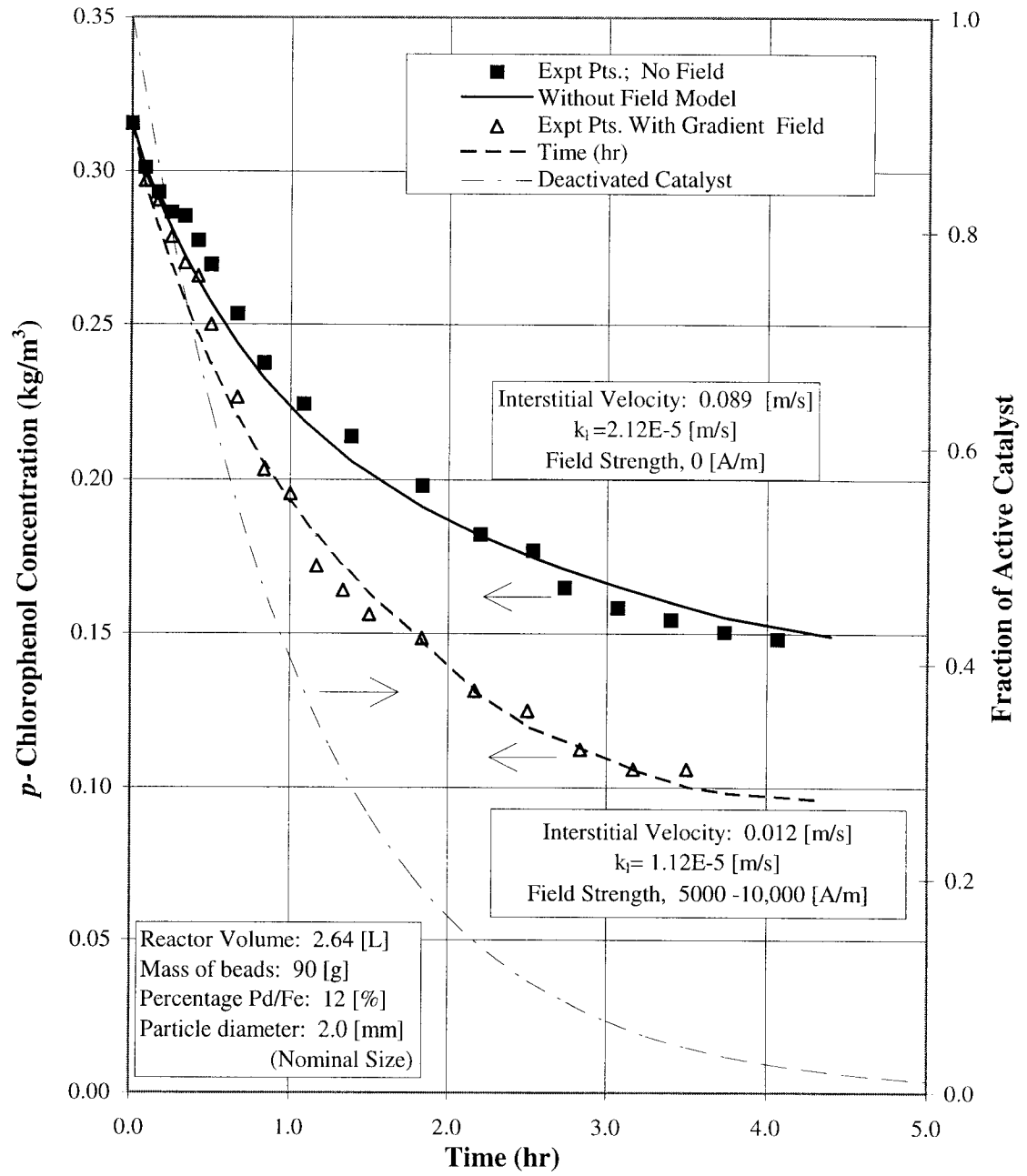


Figure 5.9: Applied dechlorination model for dechlorination within Pd/Fe entrapped alginate beads with catalyst passivation.

Table 5.1: Comparison of Values Without an Applied Field

Parameter	Units	Optimized Values	Independently Determined Values
k_d	1/s	3.6×10^{-4}	3.62×10^{-4}
k_l	m/s	1.12×10^{-5}	1.75×10^{-5} (Fan <i>et. al</i> , 1960) 6.49×10^{-5} (Coderc <i>et. al</i> , 1972) 3.73×10^{-5} (Cussler, 1984)
k	$\text{m}^3/\text{s} \cdot \text{kg}_{\text{catalyst}}$	0.0260	0.0262
D_e	m^2/s	8.2×10^{-10}	8.0×10^{-10} Experiment 7.0×10^{-10} Correlation (Appendix H) 9.3×10^{-10} Correlation (Appendix H) 1.1×10^{-9} Correlation (Appendix H)

Table 5.2: Comparison of Values for an Applied Field

Parameter	Units	Optimized Values	Independently Determined Values
k_d	1/s	3.6×10^{-4}	3.62×10^{-4}
k_l	m/s	2.12×10^{-5}	2.03×10^{-5} (Fan <i>et. al</i> , 1960) 8.98×10^{-5} (Coderc <i>et. al</i> , 1972) 4.37×10^{-5} (Cussler, 1984)
k	$\text{m}^3/\text{s} \cdot \text{kg}_{\text{catalyst}}$	0.0263	0.0262
D_e	m^2/s	8.1×10^{-10}	8.0×10^{-10} Experiment 7.0×10^{-10} Correlation(Appendix H) 9.3×10^{-10} Correlation(Appendix H) 1.1×10^{-9} Correlation(Appendix H)

There is very good agreement between the parameter values obtained from the “integrated” approach where all four coefficients were changed to achieve a minimized objective function and the independently determined values from controlled experiments or existing correlations.

5.4 Results of p-Chlorophenol Dechlorination on Alginate Entrapped Catalyst in Soil/Liquid System

As reported in Chapter 4, section 4.6, (Figure 4.12) contaminated soil was dechlorinated as a slurry within the MSFB utilizing alginate bead entrapped Pd/Fe catalyst. The model developed in Chapter 2 (Section 2.3.2) Equations 2.59-2.66 which represent the change of aqueous *p*-chlorophenol concentration with time due to mass transfer from the soil surface to the bulk liquid, mass transfer from the bulk liquid to the bead surface, diffusion into the alginate beads and subsequent reaction and deactivation on the Pd/Fe entrapped powder, was applied to the experimental data. The model was solved utilizing a numerical finite divided difference method. Figure 5.10 represents the applied model with independently determined values for parameters given in Table 5.3.

Table 5.3: Soil Dechlorination with Applied Model Parameters

Parameter	Units	Model Parameters	Independently Determined Values
k_d	1/s	2.3×10^{-4}	2.3×10^{-4}
k_l	m/s	1.3×10^{-5}	1.33×10^{-5} (Fan <i>et. al</i> , 1960) 8.98×10^{-5} (Coderc <i>et. al</i> , 1972) 4.37×10^{-5} (Cussler, 1984)
k	$\text{m}^3/\text{s} \cdot \text{kg}_{\text{catalyst}}$	0.021	0.021
D_e	m^2/s	8.2×10^{-10}	8.0×10^{-10} Experiment 7.0×10^{-10} Correlation (Appendix H) 9.3×10^{-10} Correlation (Appendix H) 1.1×10^{-9} Correlation (Appendix H)
K_d	(mol/kg soil)/ (mol/ L H ₂ O)	1.12	1.12

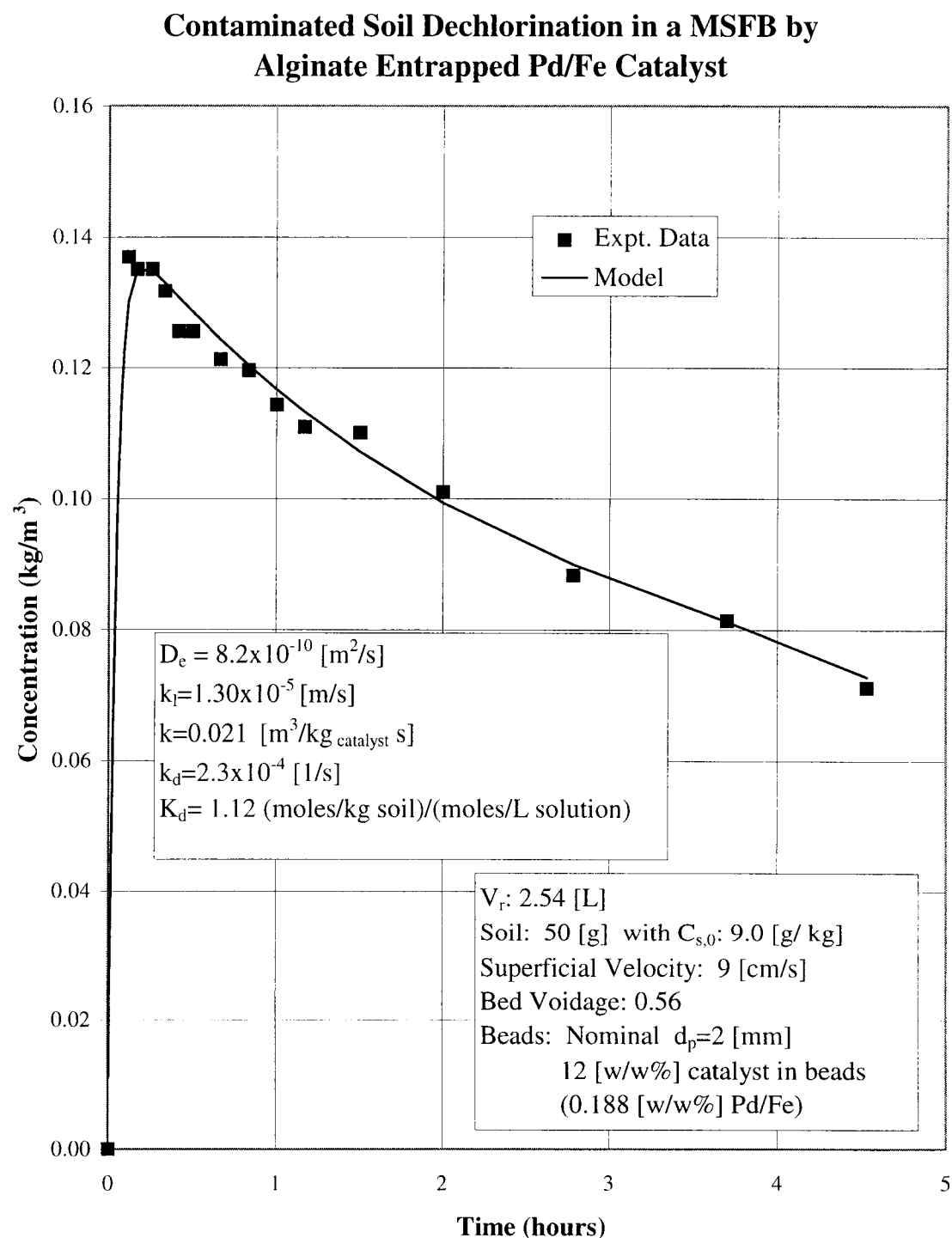


Figure 5.10: Applied soil *p*-chlorophenol dechlorination model by alginate entrapped Pd/Fe catalyst.

CHAPTER 6

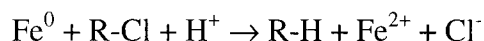
CONCLUSIONS AND RECOMMENDATIONS

6.1 Conclusion

In this work we a) explored the chemical kinetics of the dechlorination of *p*-chlorophenol, a chlorinated aromatic hydrocarbon, on the Pd/Fe catalyst including the characterization of factors governing catalyst preparation, reusability, and deactivation effects and b) investigated the mass transfer phenomena related to the technological application of the Pd/Fe catalyst for potential remediation of contaminated liquids and sludges within the Magnetically Stabilized Fluidized Bed (MSFB).

The heterogeneous chemical reactions for the dechlorination of chlorinated aromatic hydrocarbons (*p*-chlorophenol) have many important characteristics affecting the reaction kinetics. These include system pH, Pd/Fe interfacial area, Pd (Fe)/chlorine removal, and dissolved O₂. It is important to note that the resistances introduced by iron hydroxide precipitation and hydrogen gas formation can be controlled through pH adjustment.

The dechlorination process consists of a series of steps with the following overall reaction:



The pseudo-first order rate with respect to the chlorinated hydrocarbon (*p*-chlorophenol) concentration is found to be the most appropriate kinetic model.

$$-\frac{d(VC_A)}{dt} = (kW)C_A^a = k^* C_A^a \quad (2.15)$$

$$-\frac{da}{dt} = k_d a^n \quad (2.16)$$

To account for the passivation effects on the Pd/Fe surface, an activity term, a , is integrated into the reaction kinetics as shown above. This term accounts for the decrease in catalyst activity caused by the loss of dechlorination sites. This kinetic model was investigated in a laboratory batch system consisting of a 400 [ml] batch reactor. The normalized reaction rate constant, k [$\text{m}^3/\text{s}\cdot\text{kg}_{\text{catalyst}}$], and the deactivation rate constant, k_d [1/s], are obtained over a range of pH (3-6) and catalyst weights for freely suspended Pd/Fe catalyst. The k and k_d values for the Pd/Fe catalyst (0.188 [w/w%] Pd) over the pH range (3-6) are given as follows:

$$k = -0.025 [\text{pH}] + 0.161 \quad [\text{m}^3/\text{s}\cdot\text{kg}_{\text{catalyst}}] \quad \text{pH range 3 to 6} \quad R^2 = 0.94 \quad (5.2)$$

$$k_d = 0.091 [H^+] \quad [1/\text{s}] \quad \text{pH range 3 to 6} \quad R^2 = 0.99 \quad (5.3)$$

The relationship describing the reaction rate coefficient, k^* [m^3/s], over a range of Pd catalyst weights, W , (Pd/Fe: 2-6 [g]; 0.188 [w/w%] Pd) at pH=5.8 is given as:

$$k^* = 0.0126 [W] \quad [\text{m}^3/\text{s}] \quad R^2 = 0.99 \quad (\text{Pd/Fe: 2-6 [g]; 0.188 [w/w\%] Pd}) \quad (5.4)$$

The normalized reaction rate constant is given as $k = 0.20 \pm 0.2$ [$\text{m}^3/\text{s}\cdot\text{kg}_{\text{catalyst}}$] at a $\text{pH}=5.8 \pm 0.087$. The deactivation rate constant remains independent of the amount of catalyst at a constant pH and is given as $k_d = 1.8 \times 10^{-4} \pm 2.1 \times 10^{-6}$ [1/s] ($\text{pH}= 5.8 \pm 0.087$)

The fluidization particles used in the MSFB are composite ferromagnetic particles which are prepared from the mixture of sodium alginate and the Pd/Fe catalyst powder. The alginate beads (nominal diameter: 2 [mm]) consist of 86% alginate (1.5% algin, 98.5% DI H_2O) and 14% catalyst with 0.188 Pd/Fe [w/w%]. The overall dechlorination process encompasses 5 steps: 1) desorption of chlorinated hydrocarbons from solid particles found in sludges, 2) bulk mixing, 3) convective transport of the chlorinated hydrocarbon to the alginate bead 4) diffusion through the alginate bead, and 5) reaction and deactivation on the Pd/Fe surface within the alginate bead. Steps 1-3 occur in series while steps 4 and 5 occur in parallel.

The system parameters including the diffusion coefficient, D_e , the mass transfer coefficient, k_t , the normalized reaction rate constant, k , and the deactivation rate constant, k_d were determined from two separate experimental approaches. First, the parameters were determined separately from independent, controlled experiments or from existing correlations. These parameters were found to be in very good agreement with those obtained from the second approach using experimental data in the MSFB. From this data, all four parameters, D_e , k_t , k , and k_d were evaluated with the help of an optimization routine (IMSL).

6.2 Recommendations

This study explored many aspects of the Pd/Fe catalyst which were previously not reported in literature. However, while some investigation of the importance of palladium/iron interface was explored, the exact nature of the crystalline structure of palladium for different Pd/Fe ratios should be investigated. Further understanding of the surface mechanism and the role the interface plays in it offers the advantage of optimizing the Pd/Fe structure for rapid dechlorination. Another concern here is to determine the ideal coverage which produces the maximum interfacial area for optimum dechlorination rates.

Besides focusing on developing an optimal Pd/Fe structure, it would be beneficial to alter the system to avoid the negative aspects of this catalyst including excess hydrogen evolution and iron dissolution. One possibility is to provide a new source of electrons besides zero-valent iron, Fe^0 . The use of a current source with palladium deposited on an inert substrate, such as copper or carbon, would allow for a more robust reaction system which could be visualized as a microreactor for dechlorinating chlorinated organics from aqueous solutions.

REFERENCES

- Alginate Products for Scientific Water Control, 3rd Edition* (1996), Kelco, Division of Merk and Company, Inc.
- Agrawal, A. (1997) Rapid and Complete Dechlorination of Chlorinated Phenols by Fe-Pd Bimetallic Reductants in Bench-Scale Reactors: Implications for Soil and Groundwater Remediation, *Preprinted Extended Abstract: American Chemical Society*, San Francisco, CA, April 13-17.
- Agrawal, A. and Tratnyek, P. G. (1996) Reduction of Nitro Aromatic Compounds by Zero-valent Iron Metal, *Environ. Sci. and Technol.*, **30** (1), 153-160.
- Al-Mulhim, M. (1995) Enhancement of Mass Transfer Coefficient in a Magnetically Stabilized Liquid-Solid Fluidized Bed, M. S. Thesis, Oregon State University (1995).
- Boronina, T., Klabunde, K., and Sergeev, G. (1995) Destruction of Organohalides in Water Using Metal Particles: Carbon Tetrachloride/Water Reactions with Magnesium, Tin and Zinc, *Environ. Sci. Technol.*, **29** (6), 1511-1517.
- Burns, M. A., and Graves, D. J. (1985) Continuous Affinity Chromatography Using a Magnetically Stabilized Fluidized Bed, *Biotechnol. Prog.*, **1** (2), 95.
- Chaiken, R. F. (1995) Diffusion of Cu^{2+} in Calcium Alginate Gel Beads: Further Analyses, *Biotechnol. and Bioeng.*, **45**, 454-457.
- Chaung, F., Larson, R. A., and Wessman, M. S. (1995) Zero-Valent Iron-Promoted Dechlorination of Polychlorinated Biphenyls, *Environ. Sci. Technol.*, **29** (9), 2460-2463.
- Cheng, I. F., Fernando, Q., and Korte, N. (1997) Electrochemical Dechlorination of 4-Chlorophenol to Phenol. *Environ. Sci. Technol.*, **31** (4), 1074-1078.
- Cussler, E. L. (1984) *Diffusion: Mass Transfer in Fluid Systems*, Cambridge University Press, N.Y.
- Estape, D., Godia, F., and Sola, C. (1992) Determination of Glucose and Ethanol Effective Diffusion Coefficients in Ca-Alginate Gel, *Enzyme and Microbial Technology*, **14** (5), 396-401.
- Farrell, J. and Reinhard, M. (1994) Desorption of Halogenated Organics from Model Solids, Sediments and Soil under Unsaturated Conditions. 2. Kinetics, *Environ. Sci. Technol.*, **28** (1), 63-72.

Furusawa, T., and Smith, J. M. (1973) Fluid-Particle and Intraparticle Mass Transport Rates in Slurries. *Ind. Eng. Chem. Fundam.*, **12** (2), 197-202.

Gillham, R. W. and O' Hannesin, S. F. (1994) Enhanced Degradation of Halogenated Aliphatics by Zero-Valent Iron, *Ground Water*, **32** (6), 958-967.

Graham, L. J. and Jovanovic G. (1998a) Catalytic Dechlorination of Chlorinated Hydrocarbons in Magnetically Stabilized Fluidized Bed (MSFB), *World Congress on Particle Technology Proceedings*, July 7-9, Brighton, UK. *In Preparation for Publication*.

Graham, L. J. and Jovanovic G. (1998b) Dechlorination of p-Chlorophenol on a Pd/Fe Catalyst in a Magnetically Stabilized Fluidized Bed; Implications for Sludge and Liquid Remediation, *ISCRE Conference*, Los Angeles, CA.

Graham, L. J, Pinto-Espinoza, J., and Jovanovic, G. (1998) Slurry Fluidization in a Magnetically Stabilized Fluidized Bed, *UBAMARI, Instituto Tecnológico de Durango*.

Graham, L. J. and Jovanovic G. (1996) Magnetically Stabilized Fluidized Bed: New Technology for the Remediation of Contaminated Soils, Sludges and Liquid Wastes, *Waste Management Symposium*, Tucson, Arizona.

Grittini C, Malcomsen, M., Fernando, Q., and Korte, N (1995) Rapid Dechlorination of Polychlorinated Biphenyls on the Surface of a Pd/Fe Bimetallic System, *Environ. Sci. and Technol.*, **29** (11), 2898-2900.

Gu, B., Liang, L., Cameron, P., West, O., and Korte, N. (1997) Degradation of Trichloroethylene (TCE) and Polychlorinated Biphenyl (PCB) by Fe and Fe-Pd Bimetals in the Presence of a Surfactant and a Cosolvent, *Proceedings of the 1997 International Containment Technology Conference and Exhibition*, St. Petersburg, FL.

Gu, B., Dickey, M. J., Yin, X, and Liang, L. (1997) Removal of Chlorinated Organic Compounds and Radionuclides from Contaminated Groundwater by Zero-Valent Iron, *Symposium on Emerging Technologies in Hazardous Waste Management, IX, I&EC Division, American Chemical Society*, Pittsburgh, PA, September 15-17.

Honorez, L. (1994) Fluid Dynamic Characteristics of a Magnetically Stabilized Liquid-Solid Fluidized Bed, M. S. Thesis, Oregon State University.

Johnson, T. L., Scherer, M. M., and Tratnyek, P. G. (1996) Kinetics of Halogenated Organic Compound Degradation by Iron Metal, *Environ. Sci. and Technol.*, **30**, 2634-2640.

- Jovanovic G. and Al-Mulhim M. (1995) Liquid-Solid Mass Transfer in Magnetically Stabilized Fluidized Beds, *AIChE 1995 Annual Meeting*, paper No. 127g, November 12-17, Miami Beach, CA.
- Jovanovic, G. and Honorez, L. (1994) Fluidization Regimes, Structure, and Porosity of Magnetically Stabilized Liquid-Solid Fluidized Bed, *AIChE Annual Meeting*, paper No. 157d, November 14-18, San Francisco, CA.
- Klein, J., Stock, J., and Vorlop, D.K. (1983) Pore Size and Properties of Spherical Calcium Biocatalysts, *Eur. J. Appl. Microbiol. Biotechnol.*, **18**, 86-91.
- Khudenko, B. M. (1991) Feasibility Evaluation of a Novel Method for Destruction of Organics, *Wat. Sci. Tech.*, **23**, 1873-1881.
- Kimura, S. (1998) Personal Communication, October 20.
- Klassen, K. T., Barton, J. W., Evans, B. S., and Reeves, M. E. (1996) Reductive Microbial Dechlorination of Indigenous Polychlorinated Biphenyls in Soil Using a Sediment-Free Inoculum, *Biotechnol. Prog.*, **12**, 310-315,
- Kovalick, Jr., W. W. (1995) Remediation Technologies for US Hazardous Waste Sites, *Chemistry and Industry*, 500-503.
- Kragten, J., *Atlas of Metal-Ligand Equilibria in Aqueous Solution*, Halsten Press Division of John Wiley and Sons, NY, 1978.
- Kunii, D., and Levenspiel, O. (1991) *Fluidization Engineering*, John Wiley and Sons, NY.
- Kwauk, M., Ma, X., Ouyang, F., Wu, Y., Weng, D. and Cheng, L. (1992) Magnetofluidized G/L/S Systems, *Chem. Eng. Sci.*, **47**, 3467-3472.
- Levenspiel, O. (1999) *Chemical Reaction Engineering 3rd Ed.*, John Wiley and Sons, NY.
- Liang, L., Korte, N., Goodlaxson, J. D., Clausen, J., Fernando, Q., and Muftikian, R. (1997) Byproduct Formation During the Reduction of TCE by Zero-Valence Iron and Palladized Iron, *Ground Water Monitoring and Remediation*, 122-127.
- Lide, D. R. (1993) *Handbook of Chemistry and Physics, 74th Edition*, CRC Press Inc., Boca Raton.
- Liu, Y, Schwartz, J., and Cavallaro, C. L. (1995) Catalytic Dechlorination of Polychlorinated Biphenyls. *Environ. Sci. Technol.*, **29** (3), 836-840.

Matheson, L. J. and Tratnyek, P. G. (1994) Reductive Dehalogenation of Chlorinated Methanes by Iron Metal, *Environ. Sci. Technol.*, **28** (12), 2045-2053.

McCann, M., Boersma, P., Danko, J. and Guerriero, M. (1994) Remediation of a VOC-Contaminated Superfund Site Using Soil Vapor Extraction, Groundwater Extraction, and Treatment: A Case Study. *Environmental Progress*. **13** (3), 209-213.

McKay, G., Bino, M. J., and Altamini, A. R. (1985) The Adsorption of Various Pollutants From Aqueous Solutions Onto Activated Carbon, *Wat. Res.*, **19** (4), 491-495.

Muftikian, R., Fernando, Q., and Korte, N. (1995) A Method for the Rapid Dechlorination of Low Molecular Weight Chlorinated Hydrocarbons in Water, *Wat. Res.*, **29** (10), 2434-2439.

Muftikian, R., Nebesny, K., Quintas, F. and Korte, N. (1996) X-Ray Photoelectron Spectra of the Palladium-Iron Bimetallic Surface Used for the Rapid Dechlorination of Chlorinated Organic Environmental Contaminants, *Environ. Sci. and Technol.*, **30**, 3593-3596.

Orth, S. and Gillham, R. W. (1996) Dechlorination of Trichloroethylene in Aqueous Solution Using Fe^0 , *Environ. Sci. Technol.*, **30**, 66-71.

Oyaas, J., Storre, I., Svendsen, H., and Levine, D. W. (1995) The Effective Diffusion Coefficient and the Distribution Constant for Small Molecules in Calcium-Alginate Gel Beads, *Biotechnol. Bioeng.*, **47**, 492-500.

Oyaas, J., Storre, I., Lysberg, M., Svendsen, H., and Levine, D. W. (1995) Communication to the Editor: Determination of Effective Diffusion Coefficients and Distribution Constants in Polysaccharide Gels with Non-Steady-State Measurements, *Biotechnol. Bioeng.*, **47**, 501-507.

Plonski, I. H. (1997) Kinetics of Active Iron Dissolution Inhibited by Adsorbed Hydrogen, *Int. J. Hydrogen Energy*, **22** (10/11), 1005-1020.

Radovic, L. R. (1996) Carbon Materials as Adsorbents, Reactants and Catalyst Supports: Some Examples of Remarkable Flexibility and a Suggestion of Macroscopic Complementarity, *Hem. ind.*, **50**(6), 225-234.

Raghaven R., Coles, E., and Dietz, D. (1996) Cleaning Excavated Soil Using Extraction Agents: A State of the Art Review, EPA/600/2-89/034.

Rhee, B. K. (1998) Enhancement of Mass Transfer Coefficient in a Three-phase Magnetically Stabilized Fluized Bed, M. S. Thesis, Oregon State University.

- Roberts, A.L., Totten, L. A., Arnold, W. A., Burris, D. R., and Campbell, T. J. (1996) Reductive Elimination of Chlorinated Ethylenes by Zero-Valent Metals, *Environ. Sci. and Technol.*, **30** (8), 2654-2658.
- Rosenblum, J. (1998), SEED Systems: Integrating TNS into a Small Business Consulting Firm, *the Natural Step Newsletter*, **1** (5), 6-7.
- Rosensweig, R.E. (1995) Process Concepts Using Field-Stabilized Two-Phase Fluidized Bed, *Journal of Electrostatics*, 163-187.
- Rosensweig, R. E. (1979a) Fluidization: Hydrodynamic Stabilization With a Magnetic Field, *Science*, **204** (6), 57.
- Rosensweig, R. E. (1979b) Magnetic Fluidization of the State of Uniform Fluidization, *Ind. Eng. Chem. Fundam.*, **18** (3), 260.
- Sada E., Katoh, S., Shiozawa, M., and Fukui, T. (1981) Performance of Fluidized Bed Reactors Utilizing Magnetic Fields, *Biotechnol. Bioeng.*, **23**, 2561.
- Scherer, M. M., Westall, J. C., Ziomek-Moroz, M., and Tratnyek, P. G. (1997) Kinetics of Carbon Tetrachloride Reduction at an Oxide- Free Iron Electrode, *Environ. Sci. and Technol.*, **31** (8), 2385-2391.
- Schlimm, C. and Heitz, E. (1996) Development of a Wastewater Treatment Process: Reductive Dehalogenation of Chlorinated Hydrocarbons by Metals, *Environmental Progress*, **15** (1), 38-47.
- Schwarzenbach, R. P., Gschwend, P. M., and Imboden, D. M. (1993) *Environmental Organic Chemistry*, Wiley-Interscience Publication, John Wiley & Sons Inc., New York.
- Shishido, M., Kojima, T., Araike, Y. K, and Toda, M. (1995) Biological Phenol Degradation by Immobilized Activated Sludge in Gel Bead with Three Phase Fluidized Bed Bioreactor, *Chemical Engineering Research and Design: Transactions of the Institution of Chemical Engineers*, **73** (6) 719-725.
- Shishido, M. and Toda, M. (1996) Simulation of Oxygen Concentration Profile in Calcium Alginate Gel Beads Entrapping Microbes During Biological Phenol Degradation, *Chemical Engineering Science*, **51** (6)
- Siegell, J.H., and Pirkle, Jr., J.C. (1984-5) Crossflow Magnetically Stabilized Fluidized Bed Chromatography, *Separation Science and Technology*, **19** (13-15), 977-993.

- Sivavec, T. M., Mackenzie, P. D., and Horney, D. P. (1997) Effect of Site Groundwater on Reactivity of Bimetallic Media: Deactivation of Nickel-Plated Granular Iron, *Preprint of the Americal Chemical Society, 213th National Meeting*, San Francisco.
- Tanaka, H., Matsumura, M., and Veliky, I. A. (1984) Diffusion Characteristics of Substrates in Ca-Alginate Gel Beads, *Biotechnol. and Bioeng.*, **26**, 53-58.
- Tang, L. (1990) A Mathematical Model for Adsorptive Bubble-Separation Processes, M. S. Thesis.
- Terranova B. E. and Burns, M. A. (1991) Continuous Cell Suspension Processing Using Magnetically Stabilized Fluidized Beds, *Biotechnol. Bioeng.*, **37**, 110.
- Tratnyek, P. G. (1996) Putting Corrosion to Use: Remediating Contaminated Groundwater with Zero Valent Metals, *Chemistry and Industry*, 499-503.
- Uzgiris, E. E., Edelstein, W. A., Philipp, H. R., and Iben, I. E. T. (1995) Complex Thermal Desorption of PCBs From Soil, *Chemosphere*, **30** (2), 377-387.
- Vinegar, H. J. (1998) Thermal Desorption Cleans Up PCB Sites, *Power Engineering*, 43-45.
- Wang, C. and Zhang, W. (1997) Synthesizing Nanoscale Iron Particles for Rapid and Complete Dechlorination of TCE and PCBs, *Environ. Sci. and Technol.*, **31** (7), 2154-2156.
- Westall, J. (1998) Personal Communication, September 10.
- Wheeler, J. M. and Middleman, S. (1970) Machine Computation of Transients in Fixed Beds With Intraparticle Diffusion and Nonlinear Kinetics, *Ind. Eng. Chem. Fundam.*, **9** (4), 624-627.
- Williams, P. T. (1990) The Formation and Control of Dioxins and Furans From the Incineration of Municipal Waste, *Effluent Treatment and Waste Disposal*, No. 116, 47-55, Institution of Chemical Engineers, Hemisphere Publishing Corp., New York.
- Zhang, S., and Rusling, J. F. (1993) Dechlorination of Polychlorinated Biphenyls by Electrochemical Catalysis in a Bicontinuous Microemulsion, *Environ. Sci. Technol.*, **27**, (7), 1375-1380.

APPENDICES

APPENDIX OF APPENDICES

Appendix A: Supplemental information for the dechlorination investigations

Appendix B: Analytical development for Model 1 and Model 2

Appendix C: HPLC Analysis: Standard curves for phenol and p-chlorophenol

Appendix D: Alginate bead production procedure

Appendix E: Determination of the fraction of organic carbon, f_{oc} , of Willamette Valley type soil

Appendix F: Determination of the K_{ow} and K_{om} values for K_d determination

Appendix G: MSFB flowrate calibration and field gradient

Appendix H: Calculation of p-chlorophenol aqueous diffusivity

Appendix I: Numerical solution for the partial differential equation for dechlorination of p-chlorophenol on alginate bead entrapped Pd/Fe catalyst.

Appendix J: FORTRAN/IMSL: Reaction/deactivation rate kinetics; k_r and k_d

Appendix K: FORTRAN/IMSL: D_e , k_r and k_d and k_l

Appendix L: Concentration in a solid-fluid network/mixture

APPENDIX A

SUPPLEMENTAL INFORMATION FOR DECHLORINATION INVESTIGATIONS

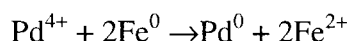
Pd/Fe, Pd/Ni and Zero-Valent Metals; Mg, Zn, Fe, Al

Agrawal, A. (1997) Rapid and Complete Dechlorination of Chlorinated Phenols by Fe-Pd Bimetallic Reductants in Bench-Scale Reactors: Implications for Soil and Groundwater Remediation, Preprinted Extended Abstract: American Chemical Society, San Francisco, CA, April 13-17.

Palladium doped iron metal was prepared through reduction of palladium salt on < 40 mesh iron (0.2% [w/w]). Using flow through aquifer model systems, the bimetallic catalyst was reacted with chlorinated phenols, dichlorobenzenes, and PCBs. Chlorophenols were first order in substrate concentration with k_{obs} found from slope of straight line on $\ln[CP]$ vs. time. Other factors investigated included variation of amount of palladium salt used to prepare the catalyst and cosolvent effect on dechlorination rate.

Grittini C, Malcomsen, M., Fernando, Q., and Korte, N (1995) Rapid Dechlorination of Polychlorinated Biphenyls on the Surface of a Pd/Fe Bimetallic System, *Environ. Sci. and Technol.*, 29 (11), 2898-2900.

Catalyst used included 2 [g] of iron particles (<10 [μm]) with 0.05 % [w/w] coverage of palladium. The deposition reaction was given by



A 1[ml] Aroclor 1260 or Aroclor 1254, 3[ml] of 20% aqueous methanol solution and 1[ml] acetone solution was prepared to give a completely solubilized 20 [ppm] PCB solution. Even at a fixed ambient temperature and with cosolvents present, both Aroclor mixtures were successfully dechlorinated in 5-10 minutes. Increased methanol concentration decreased the observed reaction rate while increased amount of catalyst and increased palladium content increase the observed reaction rate.

Further investigation into the condition of the surface demonstrated the presence of surface oxide layers with oxygen ratio varying as a function of depth into the iron. The chemistry hypothesis suggests PCB adsorption to the Pd or Pd/Fe where Pd acts as a collector of hydrogen gas produced on the Fe surface as a result of Fe dissolution. No comment was made on pH or oxygen content in solution

Cheng, I. F., Fernando, Q., and Korte, N. (1997) Electrochemical Dechlorination of 4-Chlorophenol to Phenol, *Environ. Sci. Technol.*, 31 (4), 1074-1078.

This study incorporated several reactive electrodes including iron wire and palladized carbon cloth, palladized graphite and platinized carbon cloth electrodes to determine the reduction mechanisms for dechlorination of 4-chlorophenol. Electrodes were prepared through exposure of graphite rod to 25 [mg] palladium salt in a 35 [ml] solution while a current of 5.6 [mA] was applied. Less than 0.1 [mg] Pd was detected on the rod after 4 hours. Reactions were performed at ambient temperature. Bare carbon cloth electrodes and platinized carbon cloth electrodes were not sufficient for dechlorination. Palladized carbon cloth electrodes had more favorable results with complete dechlorination occurring after 15 hours.

Electrode	% 4-Chlorophenol Dechlorinated	Observations
Bare Carbon Cloth	Nearly 0%; <10 ppm phenol	pH increased from 5.0 to 5.6 Vigorous hydrogen gas evolution Potential constant: $-1.10\text{V} \pm 10\text{mV}$
Palladized Carbon Cloth	100%	pH increased from 5.0 to 5.6 Vigorous hydrogen gas evolution Potential change: $-0.69\text{V} - 0.85\text{V}$
Platinized Carbon Cloth	5%	Vigorous hydrogen gas evolution
Bare Graphite Rod	Nearly 0%;	pH increased from 5.0 to 5.6 Vigorous hydrogen gas evolution
Palladized Graphite Rod	70%	pH increased from 5.0 to 5.6 Vigorous hydrogen gas evolution
Bare Iron Wire	0%	Potential constant: -0.95V
Palladized Iron Wire	Nearly 0%; <10 ppm phenol	Potential constant: -0.95V
Palladium Gauze	0%	Done at both constant current (5.6mA) and constant potential (-0.700V) H_2 fully saturated Pd lattice

Dissolved oxygen was not eliminated as it was found to have no effect on the reaction. Reaction mechanisms were discussed with the most probable being adsorption of 4-chlorophenol to the substrate surface which underwent reaction at the substrate-Pd island interface. Carbon surfaces were likely to facilitate the reaction due to favorable sorption of the organic.

Gu, B., Liang, L., Cameron, P., West, O., and Korte, N. (1997) Degradation of Trichloroethylene (TCE) and Polychlorinated Biphenyl (PCB) by Fe and Fe-Pd Bimetals in the Presence of a Surfactant and a Cosolvent, *Proceedings of the 1997 International Containment Technology Conference and Exhibition*, St. Petersburg, FL.

In addressing the limited solubility of many hydrophobic organics, the interest in utilizing cosolvents and surfactants has increased. This study was performed to determine if Fe and Pd-Fe catalysts could dechlorinate TCE and PCB in the presence of ethanol and isopropanol as cosolvents and dihexyl sulfosuccinate (Aerosol MA-1) as a surfactant. Surprisingly, the presence of 2% surfactants and 2% cosolvents had no effect on TCE dechlorination but did slow the reaction of PCB under flow through conditions.

Liang, L., Korte, N., Goodlaxson, J. D., Clausen, J., Fernando, Q., and Muftikian, R. (1997) Byproduct Formation During the Reduction of TCE by Zero-Valence Iron and Palladized Iron, *Ground Water Monitoring and Remediation*, 122-127.

Purpose of this study was to investigate both the dechlorination reaction of trichloroethylene (TCE) on Pd-Fe catalyst while demonstrating a batch scale experiment with no byproduct losses. Full elucidation of byproducts formed is important for understanding the nature of compounds resulting from the reaction. Batch reactors utilized zero-headspace extractors (ZHEs), 25 [g] of 40 mesh iron filings (0.05% [w/w] Pd), and 125 [ml] aqueous solution (pH=6.5; $C_{A,0}$ = 2 [mg/L] TCE) rotated at 30 [rpm].

Byproduct Persistence: Controls showed no loss of TCE; Reactions by both zero valent iron and Pd-Fe resulted in a persistence of vinyl chloride which was an order of magnitude less in the Pd-Fe system.

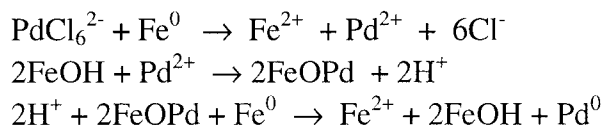
Mass balance: Due to inability to differentiate between ethane and ethene, mass balance was slightly above 100%.

Half Lives: TCE $t_{1/2}$ = 7.4 hours for Fe alone; TCE $t_{1/2}$ = 35 min for Pd-Fe

Muftikian, R., Nebesny, K., Quintas, F. and Korte, N. (1996) X-Ray Photoelectron Spectra of the Palladium-Iron Bimetallic Surface Used for the Rapid Dechlorination of Chlorinated Organic Environmental Contaminants, *Environ. Sci. and Technol.*, 30, 3593-3596.

X-ray photoelectron spectroscopy (XPS) was used to investigate the Pd/Fe surface. Specifically, the chemistry during the deposition reaction indicated stepwise reduction of solution Pd(IV) to Pd(II). The Pd(II) formed unstable Pd(II)-O-Fe bonds on the hydroxylated iron surface which collapsed spontaneously to yield Pd(0). A hydroxylated

iron-oxide film which could be removed by dilute acid then formed as a result of exposure to an aqueous solution. The chemistry was given by

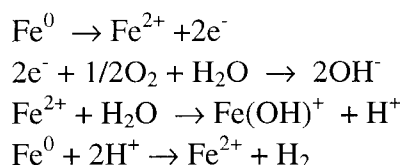


Important observations included:

- Rate of hydrodechlorination decreased with continued use of Pd-Fe surface
- Pd-Fe reactivity restored by washing with 3M HCl
- No loss of Pd during experiments

Muftikian, R., Fernando, Q., and Korte, N. (1995) A Method for the Rapid Dechlorination of Low Molecular Weight Chlorinated Hydrocarbons in Water, *Wat. Res.*, 29 (10), 2434-2439.

Compounds included in this study were 1,1,2-trichloroethylene (TCE), 1,1-dichloroethylene, cis and trans-1,2-dichloroethylene, and tetrachloroethylene (PCE) at initial concentrations of 20 [ppm]. Both iron filings (40 mesh) and iron powder (<10 [μm]) were used alone as well as with a 0.05% [w/w] palladium coating. With palladized iron, all TCE in 10 [ml] of a 20 [ppm] solution was dechlorinated to about 3 minutes but unpalladized iron had a much slower reaction rate. Similar results were obtained using 10 [μm] palladized and unpalladized iron. Palladium acted as a "promoter" metal which was not consumed in the reaction while the iron base was slowly removed through dissolution. pH increased from 6.68 to 8.51 with production of hydrogen gas with the following reactions:



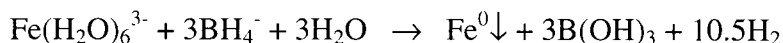
Sivavec, T. M., Mackenzie, P. D., and Horney, D. P. (1997) Effect of Site Groundwater on Reactivity of Bimetallic Media: Deactivation of Nickel-Plated Granular Iron, *Preprint of the American Chemical Society, 213th National Meeting, San Francisco.*

This investigation focused on the use of nickel plated iron filings for dechlorination of 2.1-3.3 mg/L trichloroethylene (TCE) solution using a flow through system. Nickel acted as a hydrogenation catalyst and was prepared as 0.50 mol% relative to Fe⁰. Initially, only ethane was observed but catalyst deactivation effects were seen after 76 pore volumes possibly due to mineral precipitation (FeCO₃, CaCO₃, Fe(OH)₂).

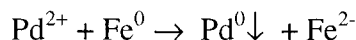
Wang, C. and Zhang, W. (1997) Synthesizing Nanoscale Iron Particles for Rapid and Complete Dechlorination of TCE and PCBs, *Environ. Sci. and Technol.*, 31 (7), 2154-2156.

Researchers compared the dechlorination of TCE and PCBs (Aroclor 1254) by various substrates including Fe powder or Pd/Fe powder (<10 [μm], Surface area = 0.9 [m^2/g]) and nano-size Fe or nano-size Pd/Fe (1-100 [nm], Surface area = 33.5 [m^2/g]).

Nano-size particles are prepared according to the following:



The iron precipitates from this reaction were coated by a thin layer of palladium by saturating the surface with an ethanol solution of $[\text{Pd}(\text{C}_2\text{H}_3\text{O}_2)_2]_3$ from Alfa Aesar. The reaction was given as follows:



Batch experiments with TCE:

Metal to solution ratio was 2 [g]/100 [ml] of a 20 [mg/l] solution. No dechlorination was observed for 10 [μm] Fe over 3 hours. Complete dechlorination was realized by 10 [μm] Pd/Fe within 2 hours, by nano-size Fe within 1.7 hours and by nano-size Pd/Fe within 0.25 hours. No chlorinated byproducts persistent in either nano-size system and final products included ethene, ethane, propene, propane, butene, butane and pentane.

Batch experiments with PCBs:

Metal to solution ratio was 5 [g]/100 [ml] of a 5 [mg/l] solution at ambient temperature. Complete dechlorination was observed when reacted within the nano-size Pd/Fe system within 17 hours. Only 25 % of the mass was dechlorinated by nano-size iron.

Main conclusions assert that freshly synthesized nano-size Fe was more highly reactive than commercially produces powders. Surface area normalized rate constants for the systems are reported as:

Nano Fe	$K_{SA} = 3.0 \times 10^{-3} \text{ L hr}^{-1} \text{ m}^{-2}$
10 [μm] Fe	$K_{SA} = 1.0 \times 10^{-3} \text{ L hr}^{-1} \text{ m}^{-2}$
Nano Pd/Fe	$K_{SA} = 0.1 \text{ L hr}^{-1} \text{ m}^{-2}$

Authors also suggest injection of the nano-size Pd/Fe particles directly into a contaminated well as an alternative to building an iron wall.

Zero-Valent Metals; Mg, Zn, Fe, Al

Boronina, T., Klabunde, K., and Sergeev, G. (1995) Destruction of Organohalides in Water Using Metal Particles: Carbon Tetrachloride/Water Reactions with Magnesium, Tin and Zinc. *Environ. Sci. Technol.*, 29 (6), 1511-1517.

An investigation into the reactivity of tin, magnesium, and zinc was performed in which carbon tetrachloride was the target compound. Experimental reactions were carried out in magnetically stirred batch systems at ambient temperature under an argon atmosphere. Magnesium ribbon, tin (mossy and granular), zinc (dust) and cryo- Zn and cryo- Sn particles were studied. Magnesium reactions were found to be overwhelmed by the metal's reaction with water. pH dropped down to 1-2 for the Sn/CCl₄/H₂O system and remained constant at about 6 for the Zn/CCl₄/H₂O system. The ability to dechlorinate CCl₄ to CHCl₃ and C₂H₄Cl₂ as byproducts was described as follows with surface area being deemed an important factor:

Sn (mossy) < Sn (granular) < Sn (cryo-particles) < Zn (dust) < Zn (cryoparticles)

Some attempt was made to determine the reaction intermediates with different final products given for the Zn/CCl₄/H₂O and the Sn/CCl₄/H₂O system.

Chaung, F., Larson, R. A., and Wessman, M. S. (1995) Zero-Valent Iron-Promoted Dechlorination of Polychlorinated Biphenyls, *Environ. Sci Technol.*, 29 (9), 2460-2463.

This paper demonstrated an alternate approach for utilizing bare iron surfaces for dechlorinating more difficult aromatic compounds like PCBs over a temperature range of 200-600°C. A high temperature environment (400-500°C) dechlorinated PCB to biphenyl within 10 min. Other side reactions of PCBs occurred above 500°C. More research must be done to examine the effects of moisture content and other process variables.

Gillham, R. W. and O' Hanesin, S. F. (1994) Enhanced Degradation of Halogenated Aliphatics by Zero-Valent Iron. *Ground Water*, 32 (6), 958-967.

10 [g] of 100 mesh electrolytic iron was utilized for dechlorination of 40 [ml] of 14 chlorinated methanes, ethanes, and ethenes. Both batch and column studies were performed. Rates of degradation decreased with a decrease in available surface area relative to solution volume and decreasing degree of chlorination. Reactions were expressed as pseudo-first order with "tailing" occurring in batch systems. The data

suggests that sequential dechlorination may not be necessary and that a compound may remain on the iron surface until complete dechlorination is achieved. Surface area ($1 \text{ m}^2/\text{ml}$ solution) normalized rate constants were reported with t_{50} values ranging from 0.013-20 hr for all compounds except DCM. DCM was persistent in all trials

Gu, B., Dickey, M. J., Yin, X, and Liang, L. (1997) Removal of Chlorinated Organic Compounds and Radionuclides from Contaminated Groundwater by Zero-Valent Iron, *Symposium on Emerging Technologies in Hazardous Waste Management, IX, I&EC Division, American Chemical Society, Pittsburgh, PA, September 15-17.*

The idea of utilizing reactive barrier materials to treat organics and uranium (U), technetium, nitrate, and other heavy metals released into groundwater stimulated this study to determine the removal efficiency and mechanisms of metal oxides, peat moss, and zero valence iron (ZVI) filings. Compounds investigated included trichloroethylene (TCE), perchloroethylene (PCE), and carbon tetrachloride (CT). Most compounds degraded quickly at first but large quantities of byproducts persisted. The use of ZVI was also highly effective towards removing 97% U within 30 min through reductive precipitation. Iron oxide only removed 15% U.

Johnson, T. L., Scherer, M. M., and Tratnyek, P. G. (1996) Kinetics of Halogenated Organic Compound Degradation by Iron Metal, *Environ. Sci. and Technol.*, 30, 2634-2640.

This investigation focused on normalization of literature reported data (18 studies) for dechlorination of chlorinated organics by zero valent iron. The normalized rate constant, k_{SA} , was determined to give a specific rate constant through which factors affecting reaction rate could be correlated. Highly chlorinated compounds and saturated compounds qualitatively dechlorinate more rapidly than less chlorinated or unsaturated organics. Primary substrate disappearance follows pseudo- first order in contaminant concentration with specific surface area and mass concentration of iron accounted for as separate constants in the model. Overall, k_{SA} values were within one order of magnitude but a more comprehensive study of the surface area characteristics under controlled conditions is necessary.

Liu, Y, Schwartz, J., and Cavallaro, C. L. (1995) Catalytic Dechlorination of Polychlorinated Biphenyls. *Environ. Sci. Technol.*, 29 (3), 836-840.

This approach to dechlorination of PCBs is based electron transfer from a titanium catalyst ($\text{Cp}_2\text{TiCl}_2\text{-NaBH}_4\text{-amine}$). Rates of reaction were coorelated with measured reduction potentials and a general mechanism wasproposed. Complete dechlorination of Aroclor 1248 was achieved in less than 24 hours.

Matheson, L. J. and Tratnyek, P. G. (1994) Reductive Dehalogenation of Chlorinated Methanes by Iron Metal, *Environ. Sci. Technol.*, 28 (12), 2045-2053.

This investigation looked into the chemistry behind zero valent iron dechlorination reactions of carbon tetrachloride. Well mixed, anaerobic batch systems were utilized to investigate effect of reaction rates, pH, temperature, mixing, and Fe surface area. CCl_4 decreased quickly to form chloroform which more slowly dechlorinated to methylene chloride which was persistent. Mechanism of dechlorination is different than with a hydrogenation catalyst such as palladium. Reaction possibly occurred at the Fe- H_2O interface and the net reaction was equivalent to the alkyl halide serving as the oxidizing agent during iron corrosion. It is important to note that organic reduction reactions and corrosion of metal surfaces can be inhibited by excessive H_2 accumulation. Also, iron hydroxide precipitates on the surface of the metal are favored by an increase in pH and directly inhibits further dissolution. Reaction rates were found to be pseudo first order in substrate and increased reaction rates were observed with a pH decrease, Fe substrate increase or mixing rate increase.

Roberts, A.L., Totten, L. A., Arnold, W. A., Burris, D. R., and Campbell, T. J. (1996) Reductive Elimination of Chlorinated Ethylenes by Zero-Valent Metals, *Environ. Sci. and Technol.*, 30 (8), 2654-2658.

This investigation focused on the determination of the pathway by which chlorinated ethylenes (*cis*-DCE and *trans*-DCE) are dechlorinated by zero-valent metals, Zn and Fe. The iron system involved 2 [g] Fe(0) (Surface area: $0.7 \text{ [m}^2\text{/g]}$) in a Teflon stoppered 25 [ml] serum bottle under deoxygenated conditions. The zinc system involved 200 [g] Zn(0) (Surface area: $0.035 \text{ [m}^2\text{/g]}$) in a 1 [L] container under deoxygenated conditions with a 0.1 M NaCl solution. pH in the zinc system remained fairly stable (7.1 ± 0.1 to 6.7 ± 0.1) without the presence of a buffer. Primary reactants for both systems included *trans*-DCE, *cis*-DCE, 1,1-DCE, and vinyl chloride.

Two possible reductive dehalogenation pathways both having a net transfer of $2 e^-$ are:

Hydrogenolysis: Replacement of a halogen by a hydrogen

Reductive Elimination: Replacement of two halide ions.

Reaction of PCE by Zn(0) resulted in TCE, *trans*-DCE, and acetylene as byproducts all of which were fit by a model for sequential dechlorination.

Scherer, M. M., Westall, J. C., Ziomek-Moroz, M., and Tratnyek, P. G. (1997) Kinetics of Carbon Tetrachloride Reduction at an Oxide-Free Iron Electrode, *Environ. Sci. and Technol.*, 31 (8), 2385-2391.

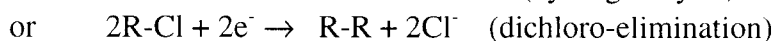
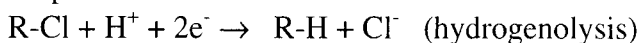
This investigation focused on the use of a rotating iron (Fe^0) disk electrode (RDE) in an electrochemical cell with emphasis placed on the effect of both mass transfer to the surface and subsequent dechlorination of CCl_4 . For the conditions of this study, the reaction appears limited by reaction at the metal surface (>900 rpm) and thus the first order heterogeneous rate constant was reported as $k_{CT} = 3.2 \times 10^{-5}$ cm/s. Preparation and conditioning of the surface influence the reaction rates as well as the reaction temperature. Reactions carried out in a well mixed batch reactor over a temperature range of 4-45 °C for CCl_4 gave an apparent activation energy, $E_{act} = 55.9 \pm 12.0$ and $E_{act} = 40.5 \pm 4.1$ kJ mol⁻¹ for hexachloroethane, which was large enough to reflect reaction rate control.

Schlimm, C. and Heitz, E. (1996) Development of a Wastewater Treatment Process: Reductive Dehalogenation of Chlorinated Hydrocarbons by Metals, *Environmental Progress*, 15 (1), 38-47.

Investigators studied the reaction of hexachlorocyclohexane (γ -BHC, lindane) with Mg/Cu, Fe/Cu, Al/Cu, and Zn (Particle size: 0.2-0.4 [mm]) surfaces over a pH range of 4-7 at ambient temperature. A fixed bed reactor was utilized under deoxygenated conditions. The dechlorination by metals was expressed as an electrochemical corrosion process as



with the electrons provided for the reduction as



with water, dissolved O_2 , and protons as competing electron acceptors.

Al/Cu: Required fluoride ions to remove oxide film (85% lindane conversion) in 105 min.;

Mg/Cu: 72% lindane conversion (40 min) but Mg reaction with water highly exothermic

Zn/Cu and Zn: Copper cementation was found not to be necessary. 97.4% lindane conversion was obtained within minutes at a pH=5. Main products included chloride and benzene with 5% chlorobenzene. Zn was most effective overall with best space-time yields.

Chloroform dechlorination by Zn was investigated and first order kinetics with a surface area dependence were developed.

APPENDIX B

ANALYTICAL DEVELOPMENT OF MODEL 1 AND MODEL 2

As described in Chapter 2, two different systems can be modeled (plug flow and completely mixed flow) for the change of bulk adsorbate concentration in a system containing alginate beads.

Analytical Solution for Model 1:

Model Assumptions:

1. The adsorbate concentration, C_b , within system boundary 1 is constant. No adsorption occurring in the bulk liquid.
2. The adsorbate concentration at the fluidized bed inlet is not changing substantially as it passes through the fluidized bed. Hence, it is a quasi-steady state assumption as used by other investigators (Al-Mulhim, 1995, Tang, 1990) in model development with short bed heights. Maximum bed height reached in our experiments is 37 [cm] with a fluid superficial velocity of 2 [cm/s] and a porosity of 0.45. This indicates that a maximum of 10 seconds is required for an element of fluid to pass once through the bead.
3. The fluid flows in plug flow through the fluidized bed.
4. The adsorbate equilibrium concentration above the particle surface, $C_l(R,t)$ is constant during one pass of the fluid through the fluidized bed. This is partially justified by previous assumptions and becomes negligible during model simplification.
5. The interparticle diffusion resistance is considered negligible as the particles are only 2 [w/w%] alginate and 10 [w/w%] active material with the remainder as water. Therefore, the internal volume is readily accessible to the adsorbate. Several investigators also neglected the interparticle diffusion in their model development (Furusawa and Smith, 1973, McKay, 1983, Silem *et. al*, 1993, Al-Mulhim, 1995).
6. The adsorption isotherm is assumed linear and is established as $N=K_b C_l$ (McKay *et. al*, 1985, Tang, 1990. Al-Mulhim, 1995).

System Boundary 1:

$$FC'_b - FC_b = V \frac{dC_b}{dt} \quad \Rightarrow \quad F(C'_b - C_b) = V \frac{dC_b}{dt} \quad (\text{B.1})$$

The initial condition to solve Equation B.1 is:

$$t=0 \quad C_b = C_{b,0} \quad (\text{B.2})$$

$$t=t \quad C_b = C_b \quad (\text{B.3})$$

System Boundary 2 (using quasi-steady state assumption):

$$(FC'_b)_x - (FC'_b)_{x+\Delta x} - k_l(C'_b - C_l(R, t))da = 0 \quad (\text{B.4})$$

where $a = a'V$ and a' is the area of particles per volume of column.

This gives:

$$F(C'_{b, x+\Delta x} - C'_{b, x}) = -k_l(C'_b - C_l(R, t))a' A \Delta x \quad (\text{B.5})$$

Taking the limit of Equation as $\Delta x \rightarrow 0$ leads to:

$$F \frac{dC'_b}{dx} = -k_l a' A (C'_b - C_l(R, t)) \quad \Rightarrow \quad F \frac{dC'_b}{(C'_b - C_l(R, t))} = -k_l a' A dx \quad (\text{B.6})$$

The boundary conditions to solve Equation B.6 are:

$$x=0 \quad C'_b = C'_b \quad (\text{B.7})$$

$$x=H \quad C'_b = C'_b \quad (\text{B.8})$$

By taking a differential balance of the adsorbate within the particle, we obtain:

$$D_e \left(\frac{\partial^2 C_l(r, t)}{\partial r^2} + \frac{2}{r} \frac{\partial C_l(r, t)}{\partial r} \right) - m \frac{\partial N_r}{\partial t} = \frac{\partial C_l(r, t)}{\partial t} \quad (\text{B.9})$$

The overall adsorbate concentration change within the system is represented by:

$$\frac{dC_b}{dt} = -k_l a' (C_b - C_l(R, t)) \quad (\text{B.10})$$

The boundary conditions used in solving Equations B.9-B.10 are:

$$D_e \frac{\partial C_l(R, t)}{\partial t} = k_l (C_b' - C_l(R, t)) \quad (\text{B.11})$$

$$\left(\frac{\partial C_l(r, t)}{\partial t} \right)_{r=0} = \text{finite} \quad (\text{B.12})$$

At this point, the model must be solved numerically. However, the model can be solved analytically if we incorporate the proposed assumptions.

By neglecting the interparticle diffusion resistance as proposed in assumption (5), we have the following consequences:

$$C_l(r, t) \text{ for all } r = C_l(R, t) \quad (\text{B.13})$$

$$N_r \text{ is uniform and } N_r = N \quad (\text{B.14})$$

By assuming a linear isotherm,

$$\frac{dN}{dt} = K_b \frac{dC_l(r, t)}{dt} \quad (\text{B.15})$$

As a result of these assumptions, Equations B.9-B.12 gives:

$$m \frac{dN}{dt} = k_l a (C_b - C_l(r, t)) \quad (\text{B.16})$$

Combining Equations B.15 and B.16, we obtain:

$$\frac{dC_l(r, t)}{dt} = -\frac{k_l a'}{mK_b} (C_b - C_l(r, t)) \quad (\text{B.17})$$

Dividing Equations B.10 by B.17 gives;

$$\frac{dC_b}{dC_l} = -mK_b \quad (\text{B.18})$$

Integration of Equation B.1 is given as:

$$\int_{C_{b,0}}^{C_b} dC_b = -mK_b \int_0^{C_l} dC_l \quad \Rightarrow \quad C_l(r, t) = C_l(R, t) = C_l = \frac{C_{b,0} - C_b}{mK_b} \quad (\text{B.19})$$

Utilizing the assumption that C_l is constant during one pass through the fluidized bed,

Equation B.6 can be integrated along the bed height (H) as:

$$\int_{C_b}^{C_b'} F \frac{dC_b}{C_b - C_l} = -k_l a' A \int_0^H dx \quad \Rightarrow \quad \text{Ln} \left\{ \frac{C_b' - C_l}{C_b - C_l} \right\} = -\frac{k_l a' A}{F} H \quad (\text{B.20})$$

Combining Equations B.19 and B.20, we obtain:

$$\text{Ln} \left\{ \frac{C_b' - \frac{C_0 - C_b}{mK_b}}{C_b - \frac{C_0 - C_b}{mK_b}} \right\} = -\frac{k_l a' A}{F} H \quad (\text{B.21})$$

Let $\alpha = \frac{a' AL}{F}$ and the previous equation can be rewritten as:

$$C_b' = \frac{C_{b,0} - C_b}{mK_b} + \left\{ C_b - \frac{C_{b,0} - C_b}{mK_b} \right\} e^{-\alpha k_l} \quad (\text{B.22})$$

Combining Equation B.21 with Equation B.1, we obtain:

$$F \left\{ C_b - \frac{C_{b,0} - C_b}{mK_b} \right\} \{ e^{-\alpha k_l} - 1 \} = V \frac{dC_b}{dt} \quad (\text{B.23})$$

Rearranging Equation B.23 gives:

$$C_b (1 + mK_b) - C_{b,0} = \left(\frac{V}{F} \right) \left\{ \frac{mK_b}{e^{-\alpha k_l} - 1} \right\} \frac{dC_b}{dt} \quad (\text{B.24})$$

Integration of Equation B.24 to account for the total adsorbate concentration change in the system gives:

$$\int_{C_{b,0}}^{C_b} \frac{dC_b}{C_b (1 + mK_b) - C_{b,0}} = \frac{F}{V} \left\{ \frac{e^{-\alpha k_l} - 1}{mK_b} \right\} \int_0^t dt \quad (\text{B.25})$$

$$\ln \left\{ \frac{C_b (1 + mK_b) - C_{b,0}}{C_{b,0} (1 + mK_b) - C_{b,0}} \right\} = \frac{1 + mK_b}{mK_b} \frac{F}{V} (e^{-\alpha k_l} - 1) t \quad (\text{B.26})$$

This solution can be checked:

As $t \rightarrow 0$, the right hand side of Equation B.26 $\rightarrow 0$ which leads to:

$$C_b (1 + mK_b) - C_{b,0} = C_{b,0} (1 + mK_b) - C_{b,0} \Rightarrow C_b = C_{b,0} \text{ which satisfies BC 3}$$

As $t \rightarrow \infty$, then the right hand side of Equation B.26 $\rightarrow \infty$ as well because k and α are always positive. This leads to:

$$C_b (1 + mK_b) - C_{b,0} = 0 \quad \Rightarrow \quad C_b = \frac{C_{b,0}}{1 + mK_b} = C_l$$

which is the expected result if the adsorption process proceeds to an infinite time period.

Analytical Solution for Model 2:

Model 2: This model presumes that the particles and the adsorbate are in contact with each other throughout the whole volume of the system as if the experimental system is a well mixed agitated tank. Model 2 has been used to measure liquid-particle mass transfer coefficients in well agitated vessels by many investigators including Al-Mulhim (1995), McKay (1983), and Furusawa and Smith (1973).

Equations B.1 and B.10 are combined to give:

$$\frac{dC_b}{dt} = -k_l a' \left(C_b + \frac{C_b - C_{b,0}}{mK_b} \right) = -k_l a' \frac{C_b mK_b + C_b - C_{b,0}}{mK_b} \quad (\text{B.27})$$

This equation is integrated as:

$$\int_{C_{b,0}}^{C_b} \frac{dC_b}{C_b(mK_b + 1) - C_{b,0}} = -\frac{k_l a'}{mK_b} \int_0^t dt \quad (\text{B.28})$$

which yields:

$$\text{Ln} \left\{ \frac{C_b(mK_b + 1) - C_{b,0}}{C_{b,0}(mK_b + 1) - C_{b,0}} \right\} = -\frac{mK_b + 1}{mK_b} k_l a' t \quad (\text{B.29})$$

Rearranging this equation gives:

$$\text{Ln} \left\{ \frac{\frac{C_b}{C_{b,0}}(mK_b + 1) - 1}{mK_b} \right\} = -\frac{mK_b + 1}{mK_b} k_l a' t \quad (\text{B.30})$$

or
$$\frac{C_b}{C_{b,0}} = \frac{1}{1 + mK_b} + \frac{mK_b}{1 + mK_b} \exp \left\{ -\left(\frac{1 + mK_b}{mK_b} \right) k_l a' t \right\} \quad (\text{B.31})$$

SIMPLIFICATIONS FOR MODEL 1 AND MODEL 2:

Model 1 Simplifications:

Model 1 can be simplified further if $C_l = 0$ at the beginning of the adsorption process.

Equation B.20 can be simplified to:

$$\ln \left\{ \frac{C_b' - C_l}{C_b - C_l} \right\} = -\frac{k_l a' A}{F} H \Rightarrow \ln \left\{ \frac{C_b'}{C_b} \right\} = -\frac{k_l a' A}{F} H \quad (\text{B.32})$$

which leads to:

$$C_b' = C_b e^{-\alpha k_l} \quad (\text{B.33})$$

Combining Equation B.1 with B.33 gives:

$$FC(e^{-\alpha k_l} - 1) = V \frac{dC_b}{dt} \quad (\text{B.34})$$

Equation B.34 is integrated as:

$$\int_{C_{b,0}}^{C_b} \frac{dC_b}{C_b} = \frac{F}{V} (e^{-\alpha k_l} - 1) \int_0^t dt \Rightarrow \ln \left(\frac{C_b}{C_{b,0}} \right) = \frac{F}{V} (e^{-\alpha k_l} - 1) t \quad (\text{B.35})$$

Model 2 Simplifications:

Model 2 also simplifies further if we incorporate the assumption that $C_l = 0$ into the overall adsorbate concentration change equation (B.10)

$$\frac{dC_b}{dt} = -k_l a' (C_b - C_l(R, t)) \Rightarrow \frac{dC_b}{dt} = -k_l a' (C_b - C_l(R, t)) \quad (\text{B.36})$$

The expression is integrated as:

$$\int_{C_{b,0}}^{C_b} \frac{dC_b}{C_b} = -k_l a' \int_0^t dt \Rightarrow \ln \left(\frac{C_b}{C_{b,0}} \right) = -k_l a' t \quad (\text{B.37})$$

APPENDIX C

HPLC ANALYSIS: STANDARD CURVES FOR PHENOL AND *p*-CHLOROPHENOL

Standard curves for absorbance vs concentration were determined for both *p*-chlorophenol and phenol. A series of solutions with known concentrations of either phenol or *p*-chlorophenol were prepared in distilled water and thoroughly mixed. These solutions were individually injected into the HPLC column and their respective absorbances were recorded by Visual Designer software. The solution concentration vs. peak absorbance readings were plotted in Figures C.1 and C.2, respectively for use in determining reaction concentrations. A sample chromatogram for the analysis of phenol and *p*-chlorophenol is also plotted in Figure C.3.

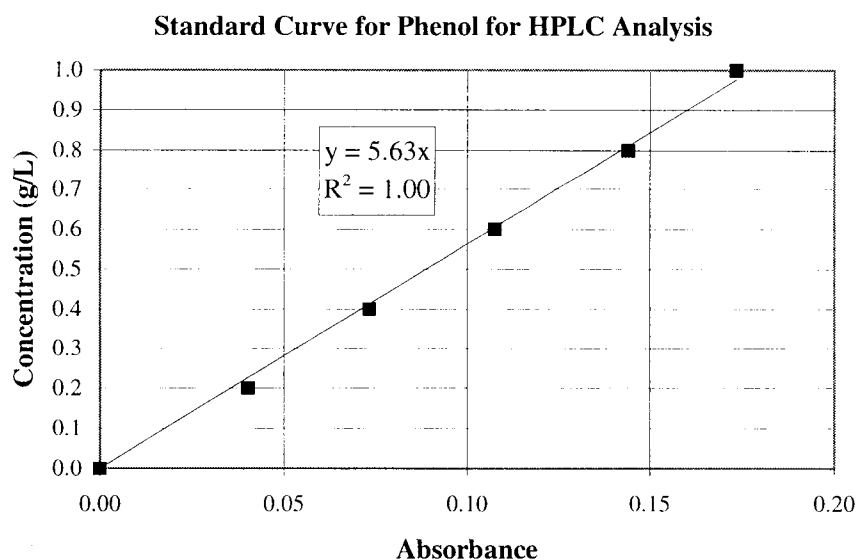


Figure C.1: Standard curve for HPLC analysis of phenol concentrations.

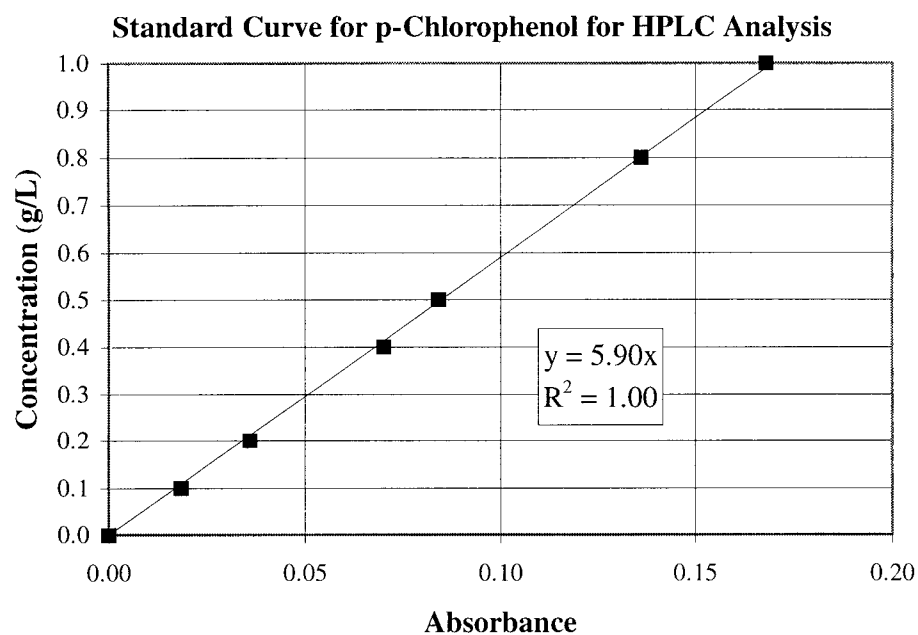


Figure C.2: Standard curve for HPLC analysis of *p*-chlorophenol concentrations.

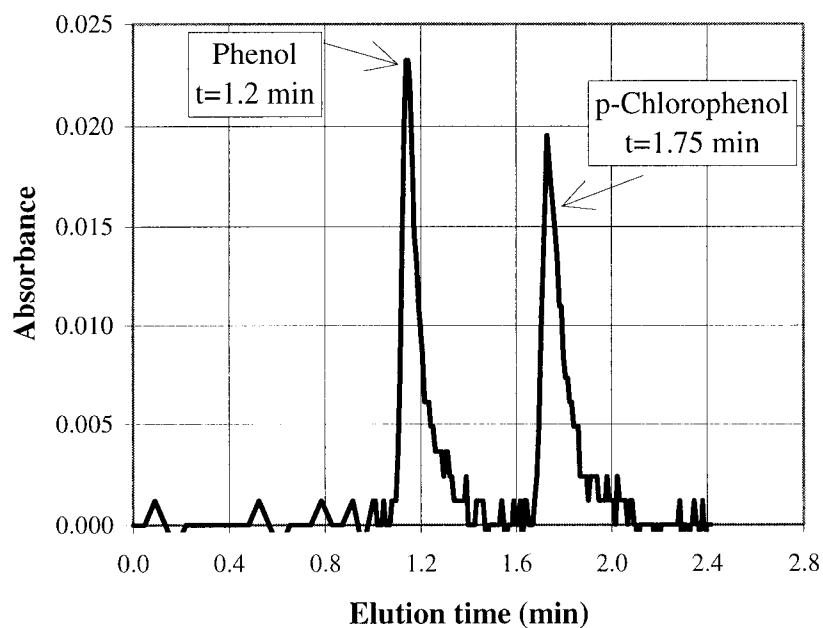


Figure C.3: Chromatogram of phenol and *p*-chlorophenol peaks..

APPENDIX D

ALGINATE BEAD PRODUCTION PROCEDURE

The particles used in this study are composite particles consisting of sodium alginate and Pd/Fe catalyst powder. The following instructions detail the preparation of the 1.5 [w/w %] sodium alginate solution used to produce alginate gel beads. The properties of the alginate and Pd/Fe powder are given in Table D-1.

1. Weigh 492.5 [g] of deionized water into a 600 [ml] beaker.
2. Weigh 7.5 [g] of Keltone HV sodium alginate into a weighing cup.
3. As deionized water is mixed, slowly add alginate powder to the 600 [ml] beaker.
4. Mix the solution for at least one hour to ensure a homogeneous solution. The mixer speed should be increased as the viscosity of the solution increases.
5. As the solution continues to mix, add 50 [g] of the freshly prepared Pd/Fe catalyst.
6. Mix for 5 minutes to evenly distribute the Pd/Fe catalyst within the alginate solution.

Table D-1: Alginate and Pd/Fe Properties

Material	Powder Size [μm]	Density [kg/m^3]
Alginate (Keltone HV)	1.8	1.59
Pd/Fe	5-8	7.87

Mechanism of Alginate Bead Formation

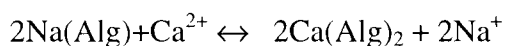
Besides the composition, the physical characteristics of the alginate beads depends upon incoming air flux rate in the particle generator, vessel pressure, surface tension, and viscosity of the alginate solution. Particle size is controlled through pressure regulation and air flow to the needle tip. Either an increase in the flux rate of the air inlet in the particle generator or pressure to the vessel results in smaller particles.

A single particle begins forming as a liquid meniscus at the needle tip which is inverted into a cone-like shape once pressure is supplied to the vessel. As the liquid moves downward it forms a filament strand which breaks and creates a spherical shape (Rhee, 1998).

It is important to maintain constant pressure and air flow to the inlet to ensure uniform particle size. The average particle size was determined through a series of measurements of the diameters of the particles with a calculated standard deviation of ± 0.04 [mm].

Once the droplets are introduced into the catch beaker of 1.5 [M] CaCl_2 , cross linking is initiated as calcium alginate forms on the surface of the sodium alginate beads.

Initially, the droplet center will remain unreacted until calcium has diffused to form a homogeneous alginate structure. The reaction between calcium ions and the alginate molecules is represented by the following (Kelco Company, 1998):



APPENDIX E

DETERMINATION OF ORGANIC CARBON FRACTION, f_{oc} , OF WILLAMETTE VALLEY TYPE SOIL

To determine the sorption equilibrium constant of *p*-chlorophenol, two soils from a government lab in Idaho and Western Oregon (Willamette Valley) were analyzed for their respective organic carbon content. This was performed on a Dohrmann DC-80 Total Carbon Analyzer (Dohrmann Instruments, Santa Clara, CA). The furnace temperature was 600-700 [°C] with an oxygen flowrate of 160-170 [ml/min].

The equipment was first calibrated using a known concentration of potassium hypophthalate (KHP) solution and the average standard output was 1250 ± 45 units (Table E.1). Samples from both the government lab soil and the Willamette Valley type soil were analyzed in triplicate using a small boat which held the soil sample with the following results shown Table E.2:

TABLE E.1: Calibration of Dohrmann DC-80 Total Carbon Analyzer

Standard	Output
Sample #1	1204
Sample #2	1284
Sample #2	1260
Average Value:	1250 ± 45

TABLE E.2: Raw Data From Dohrmann DC-80 Total Carbon Analyzer

Government lab soil	Mass of Sample [mg]	Analyzer Output Value
Sample #1	9.24	1597
Sample #2	7.87	1348
Sample #2	4.33	759.7
Willamette Valley type soil		
Sample #1	2.69	1432
Sample #2	2.57	1371
Sample #2	1.83	1035

The fraction of organic carbon was determined from the following formula and the results are given in Table E-3.

$$\%TOC = f_{oc} * 100 = \frac{(OutputValue) * (40 \times 10^{-6})}{SampleMass [mg]} * 100$$

TABLE E.3: Calculated Total Organic Carbon Fractions

Government lab soil	%TOC ($f_{oc} * 100$)
Sample #1	0.691
Sample #2	0.685
Sample #2	0.702
Average Value:	0.692 ± 0.009
Willamette Valley type soil	
Sample #1	2.13
Sample #2	2.134
Sample #2	2.262
Average Value:	2.18 ± 0.08

APPENDIX F

DETERMINATION OF K_{ow} AND K_{om} VALUES FOR K_d DETERMINATION

K_{ow} values for *p*-chlorophenol and phenol

$$K_{ow}(phenol) = 28.0 \frac{kg \text{ phenol} / L \text{ Octanol}}{kg \text{ phenol} / L \text{ H}_2\text{O}}$$

$$\log K_{ow} (phenol) = 1.447$$

To determine the K_{ow} value for *p*-chlorophenol, the following approximation was used as outlined in *Environmental Organic Chemistry* by Schwarzenbach (1993).

$$\log K_{ow}(p\text{-chlorophenol}) = \log K_{ow}(phenol) - f_H^\phi + f_{Cl}^\phi \quad (F.1)$$

$$f_H^\phi = 0.23$$

$$f_{Cl}^\phi = 0.94$$

$$\log K_{ow}(p\text{-chlorophenol}) = 1.447 - 0.23 + 0.94 \quad (F.2)$$

$$\log K_{ow}(p\text{-chlorophenol}) = 2.16$$

Determination of K_{om} values for *p*-chlorophenol:

K_{om} values are determined from a correlation reported in *Environmental Organic Chemistry* by Schwarzenbach (1993).

$$\log K_{om} = c * \log K_{ow} + d \quad (F.3)$$

p-Chlorophenol

$$c = 0.81$$

$$d = -0.25$$

$$\log K_{ow} = 2.16$$

$$\begin{aligned} \log K_{om}(p\text{-chlorophenol}) &= 0.81 * 2.16 - 0.25 \\ \log K_{om}(p\text{-chlorophenol}) &= 1.497 \end{aligned} \quad (F.4)$$

$$K_{om}(p\text{-chlorophenol}) = 31.43$$

APPENDIX G

MSFB FLOWRATE CALIBRATION AND FIELD GRADIENT

To determine the flowrate within the MSFB for experimental work, a series of measurements were taken which measured the volume of water pumped through the MSFB over a period of time vs. the pressure drop given by the flow. Table G.1 lists the data taken and Figure G.1 gives the plotted values. A linear portion of the curve over the range of flowrates used during experimental work can be seen in Figure G.2.

Table G.1: MSFB Flowrate Data

Pump Setting	Pressure Drop (cm H ₂ O)	Time (sec)	Volume of water (ml)	Flowrate (ml/sec)
1	1.25	46	1428.82	31.06
1	1.25	46.22	1432.45	30.99
2	2.5	21.12	1152.16	54.55
2	2.5	20.88	1135.13	54.36
2	2.5	12.21	669.79	54.86
3	3	11.47	804.93	70.18
3	3	14	974.78	69.63
3	3	12.75	885.51	69.45
4	4.5	14.41	1235.86	85.76
4	4.5	15.6	1337.51	85.74
4	4.5	12.66	1082.85	85.53
5	6.6	8.47	893.27	105.46
5	6.6	14.5	1529.63	105.49
5	6.7	12.4	1320.51	106.49
5.5	7.9	12.47	1423.21	114.13
5.5	7.9	12.37	1418.49	114.67
6	10.3	5.81	766.06	131.85
6	10.3	8.12	1065.93	131.27
6	10.4	9	1178.66	130.96
6.25	11.5	11.62	1587.45	136.61
6.25	11.6	8.44	1154.1	136.74
6.5	12.7	10.62	1519.79	143.11
6.75	13.5	11.16	1632.28	146.26
6.75	13.7	10.25	1531.76	149.44
7	14.2	9.5	1434.03	150.95
7	16.2	8.63	1384.96	160.48
7	16	8.15	1314.79	161.32
7	16	7.43	1197.22	161.13
8	17.9	6	1000.31	166.72
8	17	8.75	1447.97	165.48
8	16.6	8.78	1442.85	164.33

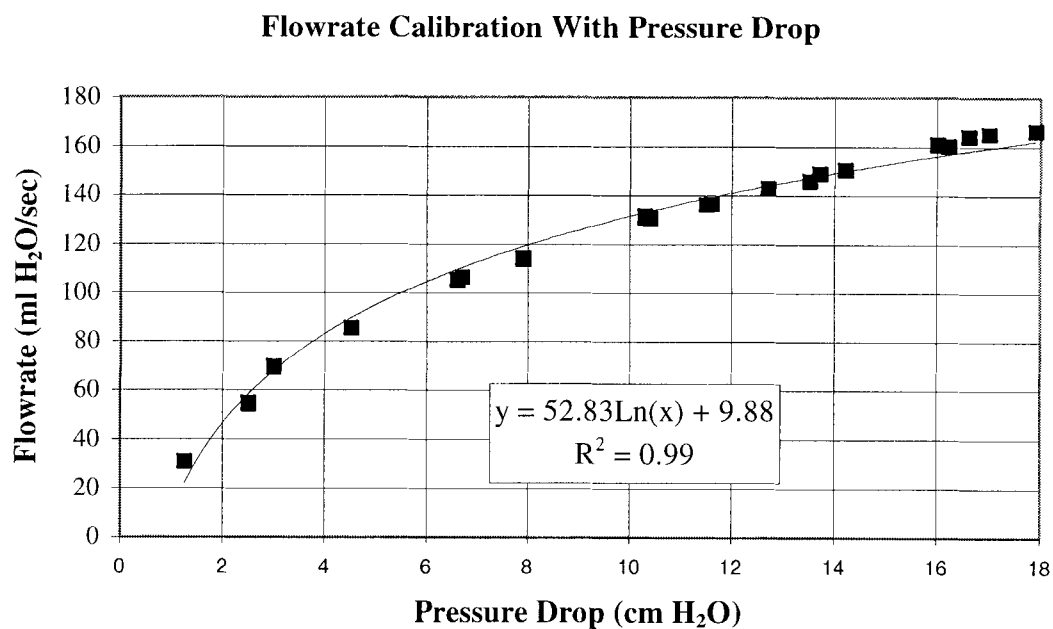


Figure G.1: Calibration curve for MSFB flowrate determination over full pumping range.

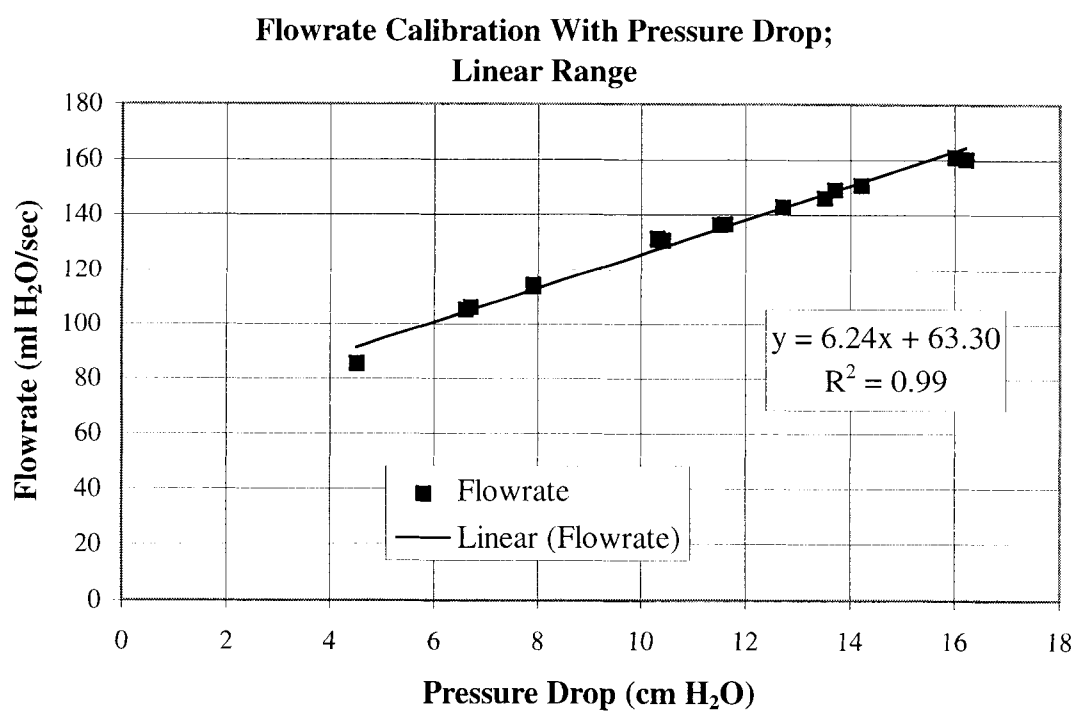


Figure G.2: Linear portion of calibration curve for flowrate determination in the MSFB.

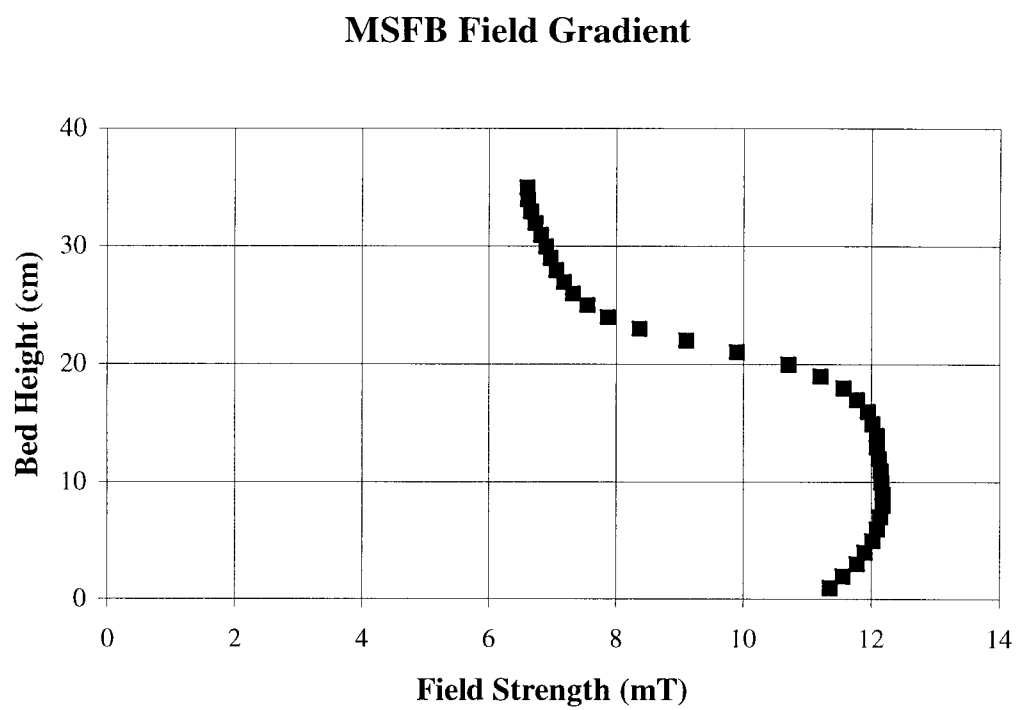


Figure G.3: MSFB applied magnetic field gradient.

APPENDIX H

CALCULATION OF *p*-CHLOROPHENOL AQUEOUS DIFFUSIVITY

D_{AB} for phenol in water at 20 [°C]:

$$\begin{aligned} D_{AB} &= 1.2 \times 10^{-9} \text{ m}^2/\text{s} && (\text{Schwarzenbach et. al, 1993}) \\ D_{AB} &\approx 1.1 \times 10^{-9} \text{ m}^2/\text{s} && (\text{Shishido et. al, 1995}) \end{aligned}$$

D_{AB} for *p*-chlorophenol in water at 20 [°C]:

Three correlations to determine the diffusion coefficient of *p*-chlorophenol in water are reported below with calculated values given in Table H-1:

1.) A semi-empirical method reported by Othmer and Thakar (1953) for organic molecules is given as (Schwarzenbach et. al, 1993):

$$D_{AB} = \frac{13.26 \times 10^{-5}}{(\mu)^{1.14} * (\bar{V})^{0.589}} \quad (\text{cm}^2/\text{s}) \quad (\text{H.1})$$

μ Solution viscosity in centipoise (10^{-2} g/cm*s)
 \bar{V} Molar (diffusion) volume of the chemical (cm^3/mol)

2.) An approximation using diffusion volumes given a known compound's D_{AB} and \bar{V} of similar structure is represented by (Schwarzenbach et. al, 1993):

$$\frac{D_{AB, \text{unknown}}}{D_{AB, \text{known}}} \approx \left(\frac{\text{diffusion volume}_{\text{known}}}{\text{diffusion volume}_{\text{unknown}}} \right)^{0.589} \quad (\text{H.2})$$

3.) An approximation given a known compound's D_{AB} and molecular weight of similar structure is given by (Schwarzenbach et. al, 1993):

$$\frac{D_{AB, \text{unknown}}}{D_{AB, \text{known}}} \approx \left(\frac{\text{molecular weight}_{\text{known}}}{\text{molecular weight}_{\text{unknown}}} \right)^{0.5} \quad (\text{H.3})$$

Unknown: *p*-Chlorophenol

Known: Phenol

Diffusion Volume Calculations:

$$\begin{aligned}\bar{V}_{(phenol)} &\approx 6*(C)+6*(H)+1*(O)+ \text{ring} \\ &= 6*(16.5) + 6*(2.0)+5.5-20.0=96.3 \text{ cm}^3/\text{mol}\end{aligned}\quad (\text{H.4})$$

$$\begin{aligned}\bar{V}_{(p\text{-Chlorophenol})} &\approx 6*(C)+6*(H)+1*(O)+ \text{ring} \\ &= 6*(16.5) + 6*(2.0)+5.5-20.0=113.8 \text{ cm}^3/\text{mol}\end{aligned}\quad (\text{H.5})$$

*Molecular Weight*_(phenol)=94 g/mol

*Molecular Weight*_(p-chlorophenol)=94 g/mol

Table H-1: Estimated D_{AB} Values for *p*-Chlorophenol

$D_{AB} [\text{m}^2/\text{s}]$	Correlation
8.2×10^{-10}	H.1
1.09×10^{-9}	H.2
1.3×10^{-9}	H.3

A: *p*-Chlorophenol

B: Water at 20 [°C]

APPENDIX I

NUMERICAL SOLUTION FOR THE PARTIAL DIFFERENTIAL EQUATION FOR DECHLORINATION OF *p*-CHLOROPHENOL ON ALGINATE BEAD ENTRAPPED Pd/Fe CATALYST

Numerical approximation of the partial differential equations for *p*-chlorophenol diffusion through alginate beads with entrapped Pd/Fe catalyst and the respective boundary conditions is described below (Wheeler and Middleman, 1970).

Bead Diffusion With Reaction Including External Mass Transfer Resistance
(Chapter 2: Equations 2.34-2.39)

Equation 2.34:
$$\frac{\partial C_I(r,t)}{\partial t} = D_e \left(\frac{\partial^2 C_I(r,t)}{\partial r^2} + \frac{2}{r} \frac{\partial C_I(r,t)}{\partial r} \right) - \frac{k^*}{V} C_I(r,t) a^n$$

$$C_I(I, J+1) = C_I(I, J) + (D_e * \Delta t) \left[\left(\frac{C_I(I+1, J) - 2 * C_I(I, J) + C_I(I-1, J)}{\Delta r} \right) \right] + \\ (D_e * \Delta t) \frac{2}{R} * \left(\frac{C_I(I+1, J) + C_I(I-1, J)}{2 * \Delta r} \right) - \left(\frac{k^* a \Delta t}{V} \right) \left(\frac{C_I(I+1, J) + C_I(I-1, J)}{2} \right) \quad (I.5)$$

with $a = \exp^{-k_d t}$

Equation 2.35:
$$D_e \frac{\partial C_I(R, t)}{\partial r} = k_l \left[C_b(t) - \frac{C_I(R, t)}{K_b} \right]$$

$$C_I(R+1, J) = C_I(R, J) + \frac{k_l \Delta r}{D_e} \left(C_b(J) - \frac{C_I(R, J)}{K_b} \right) \quad (I.6)$$

Equation 2.36: $\varepsilon V \frac{dC_b(t)}{dt} = -Vk_l a \left[C_b(t) - \frac{C_l(R, t)}{K_b} \right]$

$$C_b(J+I) = C_b(J) - k_l \Delta t \frac{(1-\varepsilon)(1-\phi)}{\varepsilon} \left(C_b(J) - \frac{C_l(R, J)}{K_b} \right) \quad (I.7)$$

Equation 2.39: $\left. \frac{\partial C_l(r, t)}{\partial r} \right|_{r=0} = \textit{finite}$

$$C_l(I, J) = C_l(I+I, J) \quad (I.8)$$

APPENDIX J

FORTRAN/IMSL: REACTION/DEACTIVATION RATE KINETICS; k_r and k_d

FORTRAN program for solving the ordinary differential equation and respective boundary conditions in Equations 2.15-2.16, Chapter 2.

$$-\frac{d(vC_A)}{dt} = (Wk)C_A = k^* C_A a \quad (2.15)$$

$$-\frac{da}{dt} = k_d a^n \quad n = 1 \quad (\text{Modeled as a first order deactivation process}) \quad (2.16)$$

Numerical Approach: IMSL-IVPRK/DIVPRK

Uses the Runge-Kutta-Verner fifth-order and sixth-order method to solve the ordinary differential equation representing reaction and deactivation kinetics.

Optimization Routine: IMSL-UMCGF

$$F = \sum \left(C(t)_{model} - C(t)_{expt} \right)^2 \quad (J.1)$$

APPENDIX K

FORTRAN/IMSL ROUTINE TO DETERMINE D_e , k_r , k_d and k_l

Fortran programs for optimizing the numerical approach for the partial differential equation and respective boundary conditions in Equations K.1-K7:

Numerical Approach: Euler's finite divided difference

Optimization Routine: IMSL Routine- BCONF; Minimization with Simple Bounds

Uses a quasi-Newton method and a finite difference gradient to minimize the objective function:

$$F = \sum \left(C_b(t)_{model} - C_b(t)_{expt} \right)^2 \quad (K.1)$$

Alginate Gel Bead Balance:

$$\frac{\partial C_l(r, t)}{\partial t} = D_e \left(\frac{\partial^2 C_l(r, t)}{\partial r^2} + \frac{2}{r} \frac{\partial C_l(r, t)}{\partial r} \right) - \frac{k^*}{V} C_l(r, t) a^n \quad (K.2)$$

$$\text{Initial Conditions: } C_l(r, t = 0) = C_{l,0} \quad (K.3)$$

$$\text{and } C_b(t = 0) = C_{b,0} \quad (K.4)$$

$$\text{Boundary Conditions: } \left. \frac{\partial C_l(r, t)}{\partial r} \right|_{r=0} = 0 \quad (K.5)$$

$$\text{and } D_e \left. \frac{\partial C_l(r, t)}{\partial r} \right|_{r=R} = k_l \left[C_b(t) - \frac{C_l(R, t)}{K_b} \right] \quad (K.6)$$

Variable Parameters:

- Effective diffusion coefficient, D_e [m^2/s^2], for *p*-chlorophenol in alginate beads
- Bulk liquid-particle mass transfer coefficient, k_l [m/s]
- Reaction rate constant, k^* [m^3/min], for dechlorination on entrapped Pd/Fe catalyst
- Deactivation rate constant, k_d [$1/\text{s}$] for deactivation on entrapped Pd/Fe catalyst

$$\text{Bulk Liquid Concentration: } \varepsilon V \frac{dC_b(t)}{dt} = -V k_l a \left[C_b(t) - \frac{C_l(R, t)}{K_b} \right] \quad (K.7)$$

APPENDIX L

CONCENTRATION IN A SOLID-FLUID NETWORK/MIXTURE

The general form of the mass conservation equation for species i in a solid-fluid network is represented by:

$$\begin{aligned}\frac{\partial C_i}{\partial t} &= D_e \nabla^2 C_i - r_i \\ D_e &= \frac{D_i}{\tau}\end{aligned}\tag{L.1}$$

The tortuosity factor, τ , represents the complexity of the diffusion path and the concentration of species i , C_i is defined as moles of species i per unit **fluid volume**.

To account for the void fraction, ε , of fluid in the solid liquid network yields:

$$\varepsilon \frac{\partial C_i}{\partial t} = \varepsilon D_e \nabla^2 C_i - \varepsilon r_i\tag{L.2}$$

When ε is uniform throughout the network and time-independent, the apparent concentration is defined as:

$$C_i^* = \varepsilon \times C_i\tag{L.3}$$

with C_i^* representing the moles of species i per unit **volume of solid fluid complex**.

Rewriting the mass conservation equation in terms of apparent concentration gives:

$$\frac{\partial C_i^*}{\partial t} = D_e \nabla^2 C_i^* - r_i^*\tag{L.4}$$

where r_i^* represents the moles of species i consumed per unit **volume of solid fluid complex**.

Applying the mass conservation equation to the system involving bulk liquid with alginate beads provides the following expressions:

Alginate beads

For spherical coordinates with symmetrical conditions, the mass conservation equation for species i in alginate beads reduces to:

$$\frac{\partial C_{i,l}}{\partial t} = D_e \left[\frac{\partial^2 C_{i,l}}{\partial r^2} + \frac{2}{r} \frac{\partial C_{i,l}}{\partial r} \right] - r_{i,l} \quad (\text{L.5})$$

or

$$\frac{\partial C_{i,l}^*}{\partial t} = D_e \left[\frac{\partial^2 C_{i,l}^*}{\partial r^2} + \frac{2}{r} \frac{\partial C_{i,l}^*}{\partial r} \right] - r_{i,l}^* \quad (\text{L.6})$$

$$\text{where } C_{i,l}^* = C_{i,l} \times (\text{fraction of fluid in a bead}) \quad (\text{L.7})$$

$$r_{i,l}^* = r_{i,l} \times (\text{fraction of fluid in a bead}) \quad (\text{L.8})$$

and $C_{i,l}$ is moles of species i per unit **fluid volume** in a bead
 $C_{i,l}^*$ is moles of species i per unit **bead volume**, i.e. a mixture of gel and fluid

Reactor

The mass balance on the reactor is given by a simplification of the mass conservation equation (The bulk fluid is uniform within the reactor):

$$\frac{\partial C_{i,b}}{\partial t} = -r_{i,b} \quad (\text{L.9})$$

where $C_{i,b}$ represents the moles of species i per unit **reactor volume** and
 $r_{i,b}$ is the moles of species i consumed per unit volume of **fluid** in the reactor.

In terms of apparent concentration,

$$\frac{\partial C_{i,b}^*}{\partial t} = -r_{i,b} \quad (\text{L.10})$$

$$\text{where } r_{i,b}^* = r_{i,b} \times (\text{fraction of fluid in the reactor}) \quad (\text{L.11})$$

Boundary Conditions:

Since the boundary conditions are set at the external surface of the bead, the concentration must be defined based on a common physical space, i.e. the fluid. Thus, both concentrations must be based on unit **fluid** volume

A: Intra-bead diffusion control; No external mass transfer resistance exists at the bead surface

$$C_{i,l} = C_{i,b} \quad \text{at} \quad r=R \quad (\text{L.12})$$

or

$$\frac{C_{i,l}^*}{(\text{fraction of fluid in a bead})} = \frac{C_{i,b}^*}{(\text{fraction of fluid in the reactor})} \quad (\text{L.13})$$

B: Film resistance control; External mass transfer resistance exists at the bead surface

The boundary condition at the external surface of the bead is expressed as:

$$\begin{aligned} \left[-D_e \frac{\partial C_{i,l}}{\partial r} \right]_{r=R} \times (\text{Surface area available for diffusion}) \\ = k_l (C_{i,b} - C_{i,l}) \times (\text{Surface area available for mass transfer}) \end{aligned} \quad (\text{L.14})$$

The following approximates the bead external surface:

$$\text{Fraction of fluid in a bead} = \frac{(\text{Surface area available for diffusion})}{(\text{Surface area available for mass transfer})} \quad (\text{L.15})$$

Thus,

$$\left[-D_e \frac{\partial C_{i,l}}{\partial r} \right]_{r=R} \times (\text{fraction of fluid in a bead}) = k_l (C_{i,b} - C_{i,l}) \quad (\text{L.16})$$